Masters
Program
in **Geospatial**
Technologies

EVALUATION OF THERMAL REMOTE SENSING FOR DETECTION OF THERMAL ANOMALIES AS EARTHQUAKE PRECURSORS

A Case Study for Malatya-Pütürge-Doğanyol (Turkey) Earthquake, July 13, 2003

Ünal OKYAY

Dissertation submitted in partial fulfilment of the requirements
for the Degree of *Master of Science in Geospatial Technologies*

EVALUATION OF THERMAL REMOTE SENSING FOR DETECTION OF THERMAL ANOMALIES AS EARTHQUAKE PRECURSORS

A Case Study for Malatya-Pütürge-Doğanyol (Turkey) Earthquake, July 13, 2003

Dissertation supervised by

Professor Mário Caetano, PhD.

Instituto Superior de Estatística e Gestão de Informação
Universidade Nova de Lisboa
Lisbon, Portugal

Dissertation co-supervised by

Professor Filiberto Pla, PhD.

Departamento de Lenguajes y Sistemas Informatícos
Universitat Jaume I
Castellón, Spain

Torsten Prinz, PhD.

IVV Geowissenschaften
University of Münster
Münster, Germany

February 2012

ACKNOWLEDGEMENTS

I would like to express my special thanks to my supervisor Assoc. Prof. Marío Caetano, for his support and for his guidance throughout my research. I would like to also thank to Prof. Filiberto Pla and Dr. Torsten Prinz for their co-supervision of this study.

I would like to thank to Prof. Marco Painho for his valuable suggestions and comments during the progress meetings and his support for us throughout the entire Geospatial Technologies Master's Program.

I would like to express my gratitude to Assoc. Prof. M. Lütfi Süzen for his continuous support, invaluable guidance and trust, unbelievable patience and motivation provided me to overcome all the problems not only at every stage of the study but also at every stage of my life since I met him.

I would also like to thank to Lisboa Navigators American Football Team for accepting me as a brother more than a team member and for their help whenever I need for the last 18 months of my life. It was a pleasure and an honor to be a part of the Navigators family.

I am grateful to my family for their unbelievable support, continuous motivation, patience and endless trust; to my "piches" brothers for their eternal friendship and support; to my geo-friends for their trust, ideas and suggestions.

Last, but most importantly, I would like to show my very special thanks and appreciation to my Gözde for being always there for me even suffered from my often irritating moods and always more believed me than I do.

EVALUATION OF THERMAL REMOTE SENSING FOR DETECTION OF THERMAL ANOMALIES AS EARTHQUAKE PRECURSORS

A Case Study for Malatya-Pütürge-Doğanyol (Turkey) Earthquake, July 13, 2003

ABSTRACT

Several studies in last two decades indicated that presence of positive thermal anomalies associated with seismic activities can be detected by satellite thermal sensing methods. This study evaluates the potential of thermal remote sensing for detection of thermal anomalies prior to Malatya-Pütürge-Doğanyol (Turkey) earthquake using MODIS/Terra V5 LST/E (MOD11A1) data. In the previous studies, different methods based on different approaches have been suggested. In this particular study, four of the suggested methods were selected for evaluation as well as for comparison of different approaches. The analyses were carried out for fortnight before and after the earthquake. Depending on the method 4 to 7 years of daily daytime and nighttime MOD11A1 data were utilized. Furthermore, same set of analyses carried out for non-earthquake years as well as the earthquake year for the area. The results show that when only the earthquake year considered, all the methods used for the analyses detected the LST changes successfully and consistently not only before but also after the earthquake. However, thermal anomalies were not unique for the earthquake year and were also observed in the absence of seismic activity within defined time interval. Therefore, there exist no coherent evidence that indicates a direct link between the occurrence of seismic activity and the land surface temperature anomaly for Malatya-Pütürge-Doğanyol earthquake. Based on the information extracted, it can be said that, the reason for observing LST changes even in the absence of the seismic activity is the effect of environmental factors which have considerable influence on the methods and thus the detection of LST anomalies. Therefore, it can be said that since the effect of the Sun's irradiation is minimal during night nighttime images would be more appropriate for thermal anomaly detection purpose. The findings support the argument that not every earthquake is preceded by detectable thermal precursor (Freund 2007; Saraf et al. 2009). On the other hand, not every LST anomaly is followed by an earthquake. Additionally, since the mechanism is not very well understood yet, it is not possible to identify earthquakes which would have thermal precursor prior to the incident. Therefore, it is concluded that utilizing LST anomalies based on satellite imagery for monitoring impending earthquake would not be adequate and feasible unless the mechanism of thermal precursors are very well understood.

KEYWORDS

Earthquake Precursor

Land Surface Temperature

LST

MODIS

RST

Satellite Thermal Image

Thermal Anomaly

ACRONYMS

ASTER	Advanced Spaceborne Thermal Emission and Reflection Radiometer
AVHRR	Advanced Very High Resolution Radiometer
EAFZ	East Anatolian Fault Zone
EMS	Electro Magnetic Spectrum
EOS	Earth Observation System
ESDT	Earth Science Data Type
EV	Earth View
GEOTIFF	Geo-Tagged Image File Format
HDF	Hierarchical Data Format
HDR	Header /Raw Binary
IR	Infrared
LP DAAC	Land Processes Distributed Active Archive Center
LST/E	Land Surface Temperature/Emissivity
MODIS	Moderate Resolution Imaging Spectroradiometer
MRT	MODIS Reprojection Tool
NASA	National Aeronautics and Space Administration
NOAA	National Oceanic and Atmospheric Administration
QA	Quality Assessment
QC	Quality Control
RS	Remote Sensing
RST	Robust Satellite Technique
TIR	Thermal Infrared

TABLE OF CONTENTS

ACKNOWLEDGEMENTS iii
ABSTRACT iv
KEYWORDS v
ACRONYMS vi
TABLE OF CONTENTS vii
INDEX OF TABLES ix
INDEX OF FIGURES x
1. Introduction 1
  1.1. Research Objectives 2
  1.2. Basic Assumptions 2
  1.3. Research Questions 2
2. Literature Review 3
  2.1. Malatya-Pütürge-Doğanyol earthquake 3
  2.2. Physical basis of thermal anomalies as earthquake precursors 3
  2.3 Detection of thermal anomalies as earthquake precursors using thermal remote sensing 5
3. Data and Methods 11
  3.1. Data 11
    3.1.1. Algorithm Description 11
    3.1.2. Scientific Data Sets 13
  3.2. Software used for the study 13
  3.3. Methods 14
    3.3.1. Preprocessing 14
      3.3.1.1. Reprojection and Mosaicking 14
      3.3.1.2. Preprocessing of QC Images 15
      3.3.1.3. Preprocessing of LST Images 17
    3.3.2. LST differencing of spatial averages based on two years 17
    3.3.3. LST differencing of spatial averages based on multiple years 19
    3.3.4. LST differencing of pixels based on multiple years 19
    3.3.5. Robust Satellite Technique (RST) 20
4. Results 23
    4.1. Preprocessing 23

4.2. LST Differencing of spatial averages based on two years 23
4.3. LST Differencing of spatial averages based on multiple years.............................. 31
4.4. LST Differencing of pixels based on multiple years... 37
4.5. Robust Satellite Technique (RST)... 44
5. Discussions and Conclusions 52
5.1 Discussion on research questions... 57
5.2 Discussion on basic assumptions 58
5.3. Limitations 59
5.4. Recommendation for future studies 60
Bibliography... 61
APPENDICES 66
A.1 Daytime results of LST differencing of pixels for non-earthquake year (2000)......... 67
A.2 Nighttime results of LST differencing of pixels for non-earthquake year (2000)....... 70
A.3 Nighttime reference images for Robust Satellite Technique...................................... 73
A.4 Results of daytime RETIRA index computation for non-earthquake year (2000)...... 74
A.5 Results of nighttime RETIRA index computation for non-earthquake year (2000) ... 77
A.6 Comparison of temporal means calculated including and excluding earthquake year. 79

INDEX OF TABLES

Table 1: MODIS data products inputs and data used for generalized split-window algorithm to generate MOD11_L2 product 12

Table 2: The Scientific Data Sets in the MOD11A1 product 13

Table 3: Defined bit flags for quality assurance scientific data sets QC Day/Night (adapted from Wan, 2009) 16

Table 4: Acceptable bit flag combinations for Quality Control Images 16

INDEX OF FIGURES

Figure 1: Simplified Tectonic map of Turkey showing the epicenter of the earthquake (adopted from Özacar et al. 2010)........ 3

Figure 2: MODIS Integerized Sinusoidal (ISIN) Tiling System showing the tiles used in this study........ 15

Figure 3: Preprocessing Workflow........ 17

Figure 4: Areas defined and used for spatial averaging........ 19

Figure 5: Distribution of spatially averaged daytime LST differences comparing 2003 (earthquake year) and 2002(non-earthquake year) [μLST_{2003} - μLST_{2002}]........ 24

Figure 6: Distribution of spatially averaged nighttime LST differences comparing 2003 (earthquake year) and 2002(non-earthquake year) [μLST_{2003} - μLST_{2002}]........ 24

Figure 7: Distribution of spatially averaged daytime LST differences comparing 2003 (earthquake year) and 2001(non-earthquake year) [μLST_{2003} - μLST_{2001}]........ 25

Figure 8: Distribution of spatially averaged nighttime LST differences comparing 2003 (earthquake year) and 2001(non-earthquake year) [μLST_{2003} - μLST_{2001}]........ 26

Figure 9: Distribution of spatially averaged daytime LST differences comparing 2003 (earthquake year) and 2000(non-earthquake year) [μLST_{2003} - μLST_{2000}]........ 27

Figure 10: Distribution of spatially averaged nighttime LST differences comparing 2003 (earthquake year) and 2000(non-earthquake year) [μLST_{2003} - μLST_{2000}]........ 27

Figure 11: Distribution of spatially averaged daytime LST differences comparing 2002 and 2001(two non-earthquake year) [μLST_{2002} - μLST_{2001}]........ 28

Figure 12: Distribution of spatially averaged nighttime LST differences comparing 2002 and 2001(two non-earthquake year) [μLST_{2002} - μLST_{2001}]........ 29

Figure 13: Distribution of spatially averaged daytime LST differences comparing 2002 and 2000(two non-earthquake year) [μLST_{2002} - μLST_{2000}]........ 30

Figure 14: Distribution of spatially averaged nighttime LST differences comparing 2002 and 2000(two non-earthquake year) [μLST_{2002} - μLST_{2000}]........ 30

Figure 15: Distribution of spatially averaged daytime LST differences comparing 2001 and 2000(two non-earthquake year) [μLST_{2001} - μLST_{2000}]........ 31

Figure 16: Distribution of spatially averaged nighttime LST differences comparing 2001 and 2000(two non-earthquake year) [μLST_{2001} - μLST_{2000}]........ 31

Figure 17: Distribution of spatially averaged daytime LST differences comparing 2003 and temporal mean [μLST_{2003} - $\mu\overline{LST}_{(2000\rightarrow 2003)}$]........ 32

Figure 18: Distribution of spatially averaged nighttime LST differences comparing 2003 and temporal mean [μLST_{2003} - $\mu\overline{LST}_{(2000\rightarrow 2003)}$]........ 33

Figure 19: Distribution of spatially averaged daytime LST differences comparing 2002 and temporal mean [μLST_{2002} - $\mu\overline{LST}_{(2000\rightarrow 2003)}$]........ 34

Figure 20: Distribution of spatially averaged nighttime LST differences comparing 2002 and temporal mean [μLST_{2002} - $\mu\overline{LST}_{(2000\rightarrow 2003)}$]........ 34

Figure 21: Distribution of spatially averaged daytime LST differences comparing 2001 and temporal mean [μLST_{2001} - $\mu\overline{LST}_{(2000\rightarrow2003)}$] 35

Figure 22: Distribution of spatially averaged nighttime LST differences comparing 2001 and temporal mean [μLST_{2001} - $\mu\overline{LST}_{(2000\rightarrow2003)}$] 35

Figure 23: Distribution of spatially averaged daytime LST differences comparing 2000 and temporal mean [μLST_{2000} - $\mu\overline{LST}_{(2000\rightarrow2003)}$] 36

Figure 24: Distribution of spatially averaged nighttime LST differences comparing 2000 and temporal mean [μLST_{2000} - $\mu\overline{LST}_{(2000\rightarrow2003)}$] 36

Figure 25: Spatial distribution of daytime LST differences comparing 2003 with the historical mean based on pixel values [June 29 – July 10] *Star icon indicates the epicenter of July 13, 2003 earthquake* 38

Figure 26: Spatial distribution of daytime LST differences comparing 2003 with the historical mean based on pixel values [July 11 – July 22] *Star icon indicates the epicenter of July 13, 2003 earthquake. Note that the red box indicates the day of the earthquake* 39

Figure 27: Spatial distribution of daytime LST differences comparing 2003 with the historical mean based on pixel values [July 23 – July 27] *Star icon indicates the epicenter of July 13, 2003 earthquake* 40

Figure 28: Spatial distribution of nighttime LST differences comparing 2003 with the historical mean based on pixel values [June 29 – July 10] *Star icon indicates the epicenter of July 13, 2003 earthquake* 41

Figure 29: Spatial distribution of nighttime LST differences comparing 2003 with the historical mean based on pixel values [July 11 – July 22] *Star icon indicates the epicenter of July 13, 2003 earthquake. Note that the red box indicates the day of the earthquake* 42

Figure 30: Spatial distribution of nighttime LST differences comparing 2003 with the historical mean based on pixel values [July 23 – July 27] *Star icon indicates the epicenter of July 13, 2003 earthquake* 43

Figure 31: Daytime reference images (a) $\mu\Delta LST(r)$ time average for month June and (b) $\sigma\Delta LST(r)$ standard deviation for month June computed over years (2000-2006) 44

Figure 32: Daytime reference images (a) $\mu\Delta LST(r)$ time average for month July and (b) $\sigma\Delta LST(r)$ standard deviation for month July computed over years (2000-2006) 45

Figure 33: Results of daytime RETIRA index computation for earthquake year (2003) [June 29 – July 10] *Star icon indicates the epicenter of July 13, 2003 earthquake* 46

Figure 34: Results of daytime RETIRA index computation for earthquake year (2003) [July 11 – July 22] *Star icon indicates the epicenter of July 13, 2003 earthquake. Note that the red box indicates the day of the earthquake* 47

Figure 35: Results of daytime RETIRA index computation for earthquake year (2003) [July 23 – July 27] *Star icon indicates the epicenter of July 13, 2003 earthquake* 48

Figure 36: Results of nighttime RETIRA index computation for earthquake year (2003) [June 29 – July 10] *Star icon indicates the epicenter of July 13, 2003 earthquake* 49

Figure 37: Results of nighttime RETIRA index computation for earthquake year (2003) [July 11 – July 22] *Star icon indicates the epicenter of July 13, 2003 earthquake. Note that the red box indicates the day of the earthquake* 50

Figure 38: Results of nighttime RETIRA index computation for earthquake year (2003) [July 23 – July 27] *Star icon indicates the epicenter of July 13, 2003 earthquake* 51

Figure A 1: Spatial distribution of daytime LST differences comparing 2000 with the historical mean based on pixel values [June 29 – July 10] 67

Figure A 2: Spatial distribution of daytime LST differences comparing 2000 with the historical mean based on pixel values [July 11 – July 22] 68

Figure A 3: Spatial distribution of daytime LST differences comparing 2000 with the historical mean based on pixel values [July 23 – July 27] 69

Figure A 4: Spatial distribution of nighttime LST differences comparing 2000 with the historical mean based on pixel values [June 29 – July 10] 70

Figure A 5: Spatial distribution of nighttime LST differences comparing 2000 with the historical mean based on pixel values. [July 11 – July 22] *Note that on July 13, 2000 LST nighttime image is not available* 71

Figure A 6: Spatial distribution of nighttime LST differences comparing 2000 with the historical mean based on pixel values [July 23 – July 27] 72

Figure A 7: Nighttime reference images (a) $\mu\Delta LST(r)$ time average for month June and (b) $\sigma\Delta LST(r)$ standard deviation for month June computed over years (2000-2006) 73

Figure A 8: Nighttime reference images (a) $\mu\Delta LST(r)$ time average for month July and (b) $\sigma\Delta LST(r)$ standard deviation for month June computed over years (2000-2006) 73

Figure A 9: Results of daytime RETIRA index computation for non-earthquake year (2000) [June 29 – July 10] 74

Figure A 10: Results of daytime RETIRA index computation for non-earthquake year (2000) [July 11 – July 22] 75

Figure A 11: Results of daytime RETIRA index computation for non-earthquake year (2000) [July 23 – July 27] 76

Figure A 12: Results of nighttime RETIRA index computation for non-earthquake year (2000) [June 29 – July 10] 77

Figure A 13: Results of nighttime RETIRA index computation for non-earthquake year (2000) [July 11 – July 22] *Note that on July 13, 2000 LST nighttime image is not available* 78

Figure A 14: Results of nighttime RETIRA index computation for non-earthquake year (2000) [July 23 – July 27] 79

Figure A 15: Daytime and Nighttime temporal means calculated including and excluding earthquake years over the area r=400km around epicenter 79

1. Introduction

Using remote sensing techniques for earthquake monitoring is not altogether new and discussions have been made upon. Yet there exist no single versatile and operational solution, to monitor or to forecast any seismic activity. Although the physical mechanism is quite well studied, the changes caused by earthquakes to environmental parameters are not well documented.

One of the remote sensing technique has been used recently is the thermal remote sensing. The relation between satellite based Land surface Temperature (LST) measurements and seismic activity can be used for earthquake monitoring however, in spite of the number of previous studies no comprehensive explanation for the possible links between the earthquake precursors and the seismo-tectonic processes on the surface of the Earth and the lower atmosphere is accepted by the science community (Ouzounov 2006; Saraf et al. 2009). Several studies have been carried out regarding the relationship between the thermal anomaly and occurrence of earthquakes or more precisely seismic activities. These studies showed that not every earthquake studied was preceded by LST anomalies as precursors just like foreshocks which might or might not precede an earthquake (Freund 2007). The reason for these diverse results could be the complex and dynamic nature of thermal anomalies as earthquake precursors which requires spatial, spectral and temporal coverage as well as local attributes such as local air temperature, humidity, and soil and/or rock type of the area, focal mechanism of the earthquake, etc. Furthermore, different earthquakes can belong to different tectonic regimes with different deformation patterns which will directly affect the results as well.

The objective of this particular study is to evaluate the already suggested thermal remote sensing methods for detection of thermal anomalies as earthquake precursors for July 13, 2003 Malatya-Pütürge-Doğanyol (Turkey) earthquake. The suggested methods in the literature have different approaches for the thermal anomaly detection. Therefore, this study also aimed to compare the effects of different approaches on thermal anomaly detection.

1.1. Research Objectives

1. Evaluate the already suggested remote sensing methods for detection of land-surface temperature anomaly prior to the Malatya-Pütürge-Doğanyol earthquake.
2. Compare the different approaches of already suggested remote sensing methods for LST anomaly detection.

1.2. Basic Assumptions

1. There exist LST anomalies prior to Malatya-Pütürge-Doğanyol earthquake which can be detected by suggested remote sensing methods.
2. LST anomalies detected by suggested remote sensing methods are due to stress accumulation before Malatya-Pütürge-Doğanyol earthquake.
3. Different approaches of suggested remote sensing methods do not affect the detection of LST anomalies.

1.3. Research Questions

1. Is there any LST anomaly prior to the Malatya-Pütürge-Doğanyol earthquake that can be detected by suggested remote sensing methods?
2. Can the LST anomalies detected by the suggested remote sensing methods be due to the occurrence of Malatya-Pütürge-Doğanyol earthquake?
3. How do different approaches of the suggested remote sensing methods affect the detection of LST anomalies?
4. What are the strengths weaknesses of the suggested methods?

2. Literature Review

2.1. Malatya-Pütürge-Doğanyol earthquake

Malatya-Pütürge-Doğanyol Earthquake is one of the largest earthquake occurred on East Anatolian Fault Zone (EAFZ) in the last decade. It is reported that the earthquake occurred on July 13, 2003 at 04:48 a.m. local time. The magnitude reported for the earthquake is M_w 5.7 where the focus depth is 11.30km (AFAD 2003). The epicenter coordinates are 38.25N and 38.85E. (Figure 1)

The earthquake occurred on 85km long Hazar-Sincik fault segment which is a part of EAFZ. The first movement direction readings of 34 P-waves clustered in three disjunct group shows that the earthquake bears the same characteristics of the fault zone as left lateral strike slip fault. The faulting due to the earthquake has 55^o strike and 75^o dipping angle (Tan 2004).

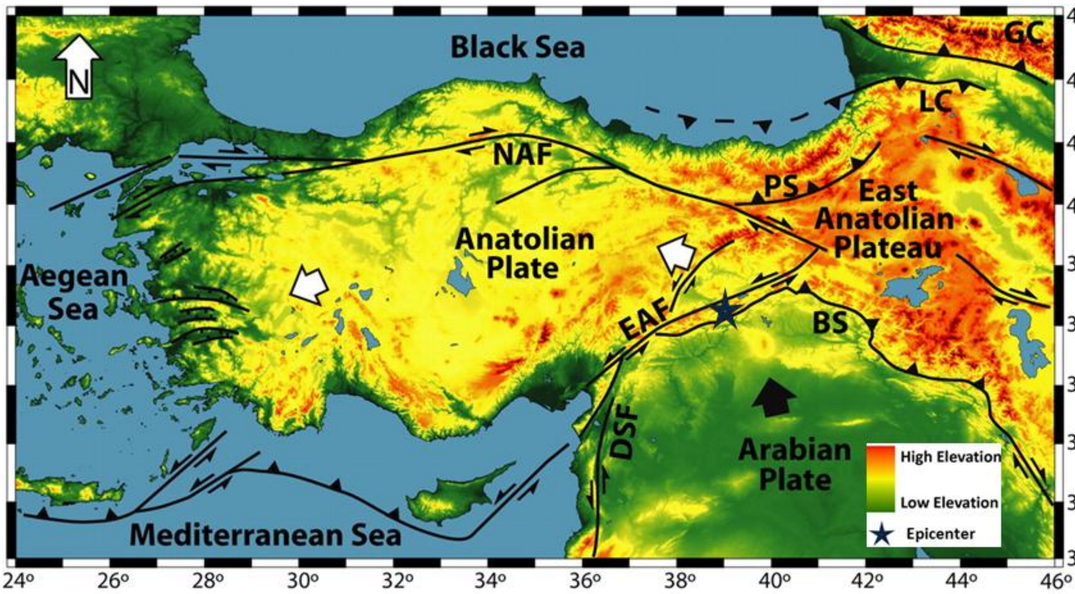

Figure 1: Simplified Tectonic map of Turkey showing the epicenter of the earthquake (adopted from Özacar et al. 2010)

2.2. Physical basis of thermal anomalies as earthquake precursors

An earthquake shock is the peak point of some preparation process which is also called earthquake sequence. This sequence starts some time before the earthquake and lasts for some time after the earthquake (Hayakawa et al. 2000). Recognition of this property of the sequence let satellite monitoring of seismic hazard (Saraf et al. 2009). The stress accumulation in this sequence might manifest itself as increased Land Surface Temperature

(LST) hence, enhanced Thermal Infrared (TIR) signal. This enhanced TIR emission originated from earth surface prior to seismic activity and detected by remote sensors is defined as thermal anomaly (Freund et al. 2005). Recently, identification of thermal anomalies (i.e. LST increases) as earthquake precursor has gained wide support around the world. The patterns and properties (i.e. intensity, spatial extent, etc.) of TIR anomalies vary depending on the internal characteristics of the earthquake such as magnitude, focal mechanism, focal depth as well as the terrain conditions where the earthquake happens. The verification of observed TIR anomalies as precursors requires a well-explained physical mechanism of their appearance (Pulinets 2006). Different explanations regarding the physical basis of thermal anomaly generation have been propounded.

Saraf et al. (2009) compiled several propounded reasons behind the thermal anomalies and categorized based on governing theories as **(1)** Earth degassing theory and gas-thermal theory, **(2)** Seismo-ionosphere coupling theory and **(3)** p-hole activation theory.

Earth gassing theory stated that as the stress conditions strengthens around the location of earthquake initiation of microcracks allows release of gases like H_2, He, CH_4, CO_2, O_3, H_2S and water vapor with associated heat into the lower atmosphere (Qiang et al. 1991). Furthermore, increase of the stress and the expansion of the area of degassing lead the enhancement the greenhouse effect which eventually increases the temperature to its maximum. Later, gas-thermal theory was proclaimed which states that paroxysmal releasing of crustal gas and sudden change of electrostatic field in lower atmosphere may be the reason of lower atmosphere thermal anomaly (Qiang et al. 1997). In this theory, piezoelectric effect of the rocks and earthquake lightening are considered to be the cause of the change in lower atmospheric electrostatic field.

The seismo-ionosphere coupling theory states that at least two processes (i) the action of ionization source and (ii) the strong electric fields can change the thermodynamics of lower atmosphere (Pulinets 2004). The purpose of the theory is to explain the physical phenomena behind the thermal anomaly and surface latent heat flux variations. The primary source of air ionization is considered to be the radon emanation from active faults and cracks in the seismically active areas. The ions, subsequently, form cluster in varying sizes. Then, water condenses on existing ions which leads heat condensation. The entire process leads air humidity and air temperature changes. When the radon ionization increases to anomalous values detectable contribution in the surface latent heat flux which can be detected by satellites is provided (Pulinets et al. 2006). The drawback of this theory is that the described chemical processes considered are not unique for earthquakes. In other words, these processes take place continuously which makes this theory unsustainable (Saraf et al. 2009).

The p-hole (positive-hole) activation theory was described based on a mechanism of strong low frequency electromagnetic emission through solid state physics point of view (Freund 2002, 2003, 2007; Freund et al. 2005). This mechanism is experimented on under stressed rock masses in tectonic locations. The p-holes (where the that electron deficiencies happen) become activated from pre-existing however inactive positive hole pairs (PHP). In other words, normally stabilized pre-existing PHPs split under mechanical deformation or passage of seismic waves and become activated. Subsequently, split PHPs recombine at rock-air interface which leads LST increase (Freund 2003).

Unlike Saraf et al. (2009), Ouzounov and Freund (2004) summarized the five possible explanations regarding the physical basis of thermal anomaly generation as (i) Piezoelectric and elastic strain dilatation forces, (ii) Rising fluids leading to gas seepage rise therefore emanation of warm gases, (iii) A transient high in the thermal conductivity profile of subsurface rocks, (iv) Rising water levels (Gorny et al. 1988; Salman et al. 1992; Tronin et al. 2002) and (v) CO_2 spreading laterally which cause a local greenhouse effect. It is also stated that although variety of explanations have been propounded no comprehensive model has been offered that science community found acceptable (Ouzounov and Freund 2004).

2.3 Detection of thermal anomalies as earthquake precursors using thermal remote sensing

The thermal field of the earth is originated from its temperature and formed by the re-emission of the absorbed solar energy and to lesser extent by geothermal fluxes. The basic parameters define the characteristics of TIR signal are **(1)** emissivity, **(2)** albedo and **(3)** thermo-physical properties of the rocks (Saraf et al. 2009). The thermal emission and the changes upon it can be monitored by several satellite systems on board using TIR sensors.

Temperature changes which slowly affect the Earth’s surface prior to large earthquakes reported long before remote sensing technology (Milne 1913; Ouzounov and Freund 2004). Scientists recognized temperature increase before strong earthquakes and conducted several studies upon (Milne 1913; Wu 1980; Wu et al. 1982; Geng, 1985). Using satellite imaging systems, however, started by late 80's. Gorny et al. (1988) is the first study to document the pre-earthquake temperature increase using satellite images. Along with the use of satellite images long-term thermal fields associated with the presence of large linear structures and fault systems have been detected (Carreno et al. 2001). Furthermore, prior to the major earthquakes short-term anomalies on the thermal field can also been detected by satellite imaging and TIR remote sensing techniques (Tronin et al. 2002). It is stated that short-term thermal anomalies are sensitive to the crustal earthquakes having magnitude more than 4.7 (Tronin et al. 2002; Ouzounov and Freund 2004; Tronin 2006). The short-term anomalies can be observed typically a few days to a few weeks before and lasts a few days after the earthquake with 2-4^{o}C intensity. However, since the short-term anomalies appear within a narrow timespan they might be overlooked (Ouzounov and Freund 2004).

Through the last two decades studies from all over the world showed that some major earthquake were preceded by pre-earthquake thermal anomalies (Tronin 1996, 2000a, b ; Tronin et al. 2002; Qiang et al. 1991, Qiang et al. 1997, Qiang et al. 1999; Tramutoli et al. 2001, Tramutoli et al. 2005, Lisi et al. 2010; Pergola et al. 2010; Filizzola et al. 2004, Genzano et al. 2007, 2009; Aliano et al. 2008a, 2008b; Ouzounov and Freund 2004; Ouzounov et al. 2006; Saraf and Choudhury 2005a, b ,c; d; Saraf et al. 2007, Saraf et al. 2008, Saraf et al. 2011; Panda et al. 2007; Choudhury et al. 2006; Rawat et al. 2011). However, based on the observations it is also stated that not every earthquake is preceded by thermal anomalies (Freund 2007; Saraf et al. 2009).Through these studies different data sets and methods were utilized. Among the studies mentioned two distinct group of researchers stand out: Indian group (Saraf, Choudhury, Panda, Rawat, et al.) and Italian group (Tramutoli, Genzano, Filizzola, Pergola, et al.) however several other scientists used different approaches for detection of thermal anomalies as well.

Incipiently, Tronin et al. (2002) focused on the earthquakes in Japan and China. The analysis for China was based on 7 years of nighttime NOAA/AVHRR (NOAA-14) satellite thermal images. The ground temperature was retrieved based on Becker's algorithm using band 4 and 5 (Becker and Li 1990). For each image thermal background of the area (temporal mean and standard deviation) was calculated. Subsequently, pixels shows plus or minus two standard deviation from the average considered to be anomalous. The results showed that the anomaly was observed 6-24 days before the earthquake and lasts for 7 days after the earthquake with around 3^{o}C amplitude. Note that different periods of 2-3 months were investigated between Oct 1997 and Feb 1999. During this period more than 13 earthquakes magnitude more than 3 were reported in North-east China with varying magnitudes between 3.6 and 5.9. Out of these earthquakes 4 of them showed positive thermal anomaly response. The observed time-dependent pattern of the anomaly was said not to be associated with meteorological and topographical factors (Tronin et al 2002). It is concluded that thermal anomalies are sensitive to the crustal earthquakes magnitude more than 4.7 and can be observed within 200km-1000km from the epicenter location (Tronin et al. 2002).

Ouzounov and Freund (2004) were the first who suggested the differentiation of spatially averaged LST. The focus of their study was the Bhuj earthquake [M_w 7.7] in Gujarat/Western India (Jan 26th, 2001). For the analysis nighttime MODIS mid-IR data set was used. Based on split-window algorithm daily LST was calculated within 100x100km around the epicenter. The daily spatially average LST of the earthquake year and the same of the non-earthquake year subsequently differentiated. Note that since MODIS data is available only after Mar 5th, 2000, non-earthquake was selected as 2002. Therefore spatially averaged LST in 2002 was subtracted from spatially averaged LST in 2001. The daily analysis of the images covers 90 days between December 1st, 2000 and March 1st, 2001. Results showed that a positive anomaly with amplitude of 3-4^{o}C was observed 5 days before the earthquake and disappeared shortly before the earthquake. It is stated that the rapidity of the thermal anomaly suggested that the reason for such an anomaly cannot be due to the LST variation caused by a heat pulse from Earth's subsurface (Ouzounov and Freund 2004).

As mentioned before the Indian group has several studies regarding the detection of LST anomalies prior to earthquakes. Saraf et al. (2005a) focused on Bhuj, Gujarat earthquake in Jan 26, 2001 with magnitude M_w 7.7. The analysis carried out in two steps. For the first step analysis daily NOAA-AVHRR images of three months (Dec 1st, 2000 to Feb 15th, 2001) were visually studied then subsequently the images of the days between Jan 12th and Jan 29th 2001 were analyzed in detail. In order to obtain background of thermal regime the images of the same period in 2003 were studied visually. Note that the time of acquisition of the images of 2001 is around 17:00 -18:30 while it is around 22:00-23:00 for the images of 2003. All the images are visualized based on a continuous color ramp between -40 and 35^{o}C interval. The comparison between the images was done visually and the absolute difference between the observed LST is reported as 5-7^{o}C at its peak (Saraf et al. 2005a).

Saraf et al. (2005b) focused on the earthquakes of Algeria in May 2003. Between May 21st and May 29th occurrences of 22 earthquakes were reported with varying magnitudes (M 2.5-6.8). Nighttime NOAA-AVHRR images of the period May 12th to June 5th were obtained and studied for the first step of the analysis where the LST is retrieved base on Becker's split-window algorithm. Afterwards, the period of May 13th to May 30th was studies in detail (Saraf et al. 2005b). Note that spatio-temporal analysis of LST changes was done only based on the images of the earthquake year and no historical or background information was used. The anomalous pixels were identified based on the comparison of the pixel values at hand and surrounding pixels. The LST difference was reported as 5-10^{o}C at its peak for the anomalous pixels. On the other hand, Panda et al (2007) focused on Oct 8th 2005 Kashmir Pakistan earthquake (M_w 7.6) and followed a different approach. Daily daytime MODIS LST products between Sept 26th, 2005 and Oct 27th, 2005 were used for the analysis. First of all, in order to retrieve historical thermal background thermal regime the images of same period between 2000 and 2004 were analyzed. The calculation of the background thermal regime was through averaging of daily pixel values through 2000-2004. Calculated daily averages, subsequently, was subtracted from corresponding days in 2005. The results showed that LST anomaly reaches 5-10^{o}C at its peak around the epicenter. Note that other studies Indian group carried out follow similar approaches and show similar characteristics with the studies mentioned above. Through their studies Indian group benefited from NOAA-AVHRR and MODIS (Terra/Aqua) data sets.

Regarding the studies of Italian group the method (Robust Satellite Technique - RST) is the same for different studies focusing on different earthquakes [2009 Abruzzo earthquake/Italy: EOS-MODIS Terra and Aqua (Pergola et al. 2010), 2001 Bhuj-Gujarat earthquake/India: Meteosat-5 TIR (Genzano et al. 2007), 1999 Kocaeli earthquake/Turkey: Meteosat TIR (Tramutoli et al. 2005), etc.]. The numbers of the years utilized for the analysis, however, vary based on the availability of data. Even though there is no specific number for the years and as the number of years increases the accuracy and reliability increases, it is stated that RST applicable for 4-10 years of data (Lisi et al. 2000). Note that detailed information about this RST will be provided in the methods section.

All the studies mentioned above revealed thermal anomalies prior to the corresponding earthquakes. A recent study however challenged that argument for Bhuj-Gujarat/India earthquake (Blackett et al. 2011). In the study two areas were defined around the epicenter as 200kmx200km and 1500kmx1500km for utilization of three methods [(i) Differencing of spatial LST averages based on two years (Ouzounov and Freund 2004), (ii) Extended version of differencing of spatial averages based on multiple years and (iii) RST]. The first two methods were utilized for the smaller area where the third method is utilized for both small and large areas. The analysis was based on 6 years of daily MODIS LST/E products between Jan 5th and Fen 16th. For the first method LST differences pairs of years including both earthquake and non-earthquake years were calculated and the results were plotted. Moreover, for the second method temporal mean of the spatial averages were calculated and subsequently subtracted from every year used for the analysis (2000-2006). The results of the first two methods showed that for the time interval LST changes were observed but these changes do not have unique pattern which means LST changes observed in the absence of seismic activity (Blackett et al. 2011). It is concluded that LST differencing based on two years or multiple years cannot be confirmed since both the year of interest and the baseline year or temporal mean of the years have considerable effect on the calculations. Additionally, variability of long-term data series can also affect the calculations On the other hand; it is also shown that existence of missing data (cloud cover, mosaicking gap, etc.) particularly over normally warmer and normally cooler locations can affect RST calculations by positive or negative biases (Blackett et al. 2011).

Throughout the literature review is it found that most of the studies focus only on the earthquake years. In other words, suggested methods were only utilized for the years where the earthquake exists which lack a comparative analysis between the results of the methods for presence and absence of earthquakes. For instance, Ouzounov and Freund (2004), as mentioned above, used the earthquake year (2001) and only one non-earthquake year (2002) as reference year for differentiation. Unlike the majority of the previous studies Blackett et al. (2011) utilized methods not only for earthquake year but also for non-earthquake years. In other words, the reference year for LST differentiation were changed which leads them to make a comparative analysis between the results for presence and absence of earthquake. Additionally, Italian group used earthquake years and also non-earthquake years in their studies where RST is utilized. The earthquake years were used for validation purpose where non-earthquake year were used for confutation purpose. The results of the confutation analysis (for non-earthquake years) also showed anomalous pixels, however, it is concluded that the anomalies are not time persistent spatially extensive as in the validation analysis (for earthquake year) (Pergola et al 2010; Lisi et al. 2010; Tramutoli et al. 2005). It is stated that the presence of such anomalous pixels denounces the limitation of RETIRA index in its nature which is vulnerable to the abrupt occurrence of signal outliers due to local/observational conditions (Tramutoli et al 2005; Filizzola et al. 2004). During the literature review it is also found that for the analysis only one set of data (either daytime or nighttime) was used for the suggested methods where no comparison between the effects of daytime and nighttime observations was made.

The literature review showed that no study was carried out for earthquakes in Turkey except the one for Izmit (August 17th, 1999) earthquake which was carried out by Italian group based on RST (Tramutoli et al. 2005). Moreover, it is also found that except Blackett et al. (2011) there is no comparative analysis of different methods used for one earthquake. Therefore, in this particular project it is aimed to make a comparative analysis of already suggested methods for one earthquake in Turkey while comparing the effects of daytime and nighttime observations.

3. Data and Methods

3.1. Data

The MODIS/Terra V5 Land Surface Temperature and Emissivity (LST/E) L3 Global 1km Grid SIN (short name: MOD11A1) product has been used in order conduct time-series land surface temperature analysis and downloaded directly from LP DAAC Data Pool where selected MODIS and ASTER holdings are freely available.

MOD11A1 product is tile-based and gridded in Integerized Sinusoidal (ISIN) projection which provides daily per-pixel temperature and emissivity values at 1km (precisely 0.928km) spatial resolution. Data characteristics for MOD11A1 product can be summarized as follows:

Temporal Coverage	: March 5th, 2000 – Current
Area	: ~1100 km x 1100 km (Latitude/Longitude)
Image Dimensions	: 1200 x1200 (Rows/Columns)
Spatial Resolution	: 1km (precisely 0.928km)
Map Projection	: Integerized Sinusoidal
Data Format	: HDF-EOS
Number of Scientific Data Sets	: 12

3.1.1. Algorithm Description

The daily MOD11A1 LST product is generated based on the results of the MOD11_L2 LST product. This process is simply based on mapping the SDSs of all pixels in MOD11_L2 LST product onto grids in the ISIN or SIN projection for one day and averaging the values in each grid.

The MOD11_L2 product is generated by a generalized split-window algorithm (Wan and Dozier, 1996) using several MODIS products such as the MODIS Sensor Radiance data product (MOD021KM), the MODIS Geolocation product (MOD03), the cloud mask product (MOD35_L2), the MODIS Atmospheric Profile (MOD07_L2), the quarterly Land cover (MOD12Q1), and MODIS snow product (MOD10_L2) Detailed information about the MODIS data products and data used is available in Table1. The algorithm is optimally used to separate ranges of atmospheric column water vapor and lower boundary air surface temperatures in to tractable sub-ranges (Wan, 2009). The output file of MOD11_L2 includes scientific data sets of LST, QC, error in LST, Band 31 and 32 emissivities, viewing zenith angle and time, latitude and longitude, local attributes and global attributes.

<table>
<tr><th>ESDT</th><th>Long Name</th><th colspan="2">Data Used</th></tr>
<tr><td rowspan="4">MOD021KM</td><td rowspan="4">MODIS Level 1B Calibrated and Geolocated Radiances</td><td rowspan="2">EV_1km_Emissive for MODIS bands:</td><td>31 (11.03 μm)</td></tr>
<tr><td>32 (12.02 μm)</td></tr>
<tr><td colspan="2">Latitude (every 5 lines)</td></tr>
<tr><td colspan="2">Longitude (every 5 pixels)</td></tr>
<tr><td rowspan="6">MOD03</td><td rowspan="6">MODIS Geolocation</td><td colspan="2">Land/Water Mask</td></tr>
<tr><td colspan="2">Height</td></tr>
<tr><td colspan="2">Sensor Zenith Angles</td></tr>
<tr><td colspan="2">Solar Zenith Angles</td></tr>
<tr><td colspan="2">Latitude</td></tr>
<tr><td colspan="2">Longitude</td></tr>
<tr><td>MOD35_L2</td><td>MODIS Cloud Mask</td><td colspan="2">Cloud Mask</td></tr>
<tr><td rowspan="2">MOD07_L2</td><td rowspan="2">MODIS Atmospheric Profile</td><td colspan="2">Retrieved Temperature Profile</td></tr>
<tr><td colspan="2">Water Vapor</td></tr>
<tr><td>MOD12Q1</td><td>Land Cover</td><td colspan="2">Land Cover Type 1</td></tr>
<tr><td>MOD10L2</td><td>MODIS Snow Cover</td><td colspan="2">Snow Cover</td></tr>
</table>

Table 1: MODIS data products inputs and data used for generalized split-window algorithm to generate MOD11_L2 product

The algorithm assumes LST retrieval is constrained for the pixels that **(1)** have nominal L1B radiance data in bands 31 and 32, **(2)** are in clear-sky conditions of ≥95% confidence over land ≤2000m; ≥66% confidence over land > 2000m and ≥66% confidence over lakes defined in MOD35_L2 product and **(3)** are on land or inland water. Basically, clouds are masked with the MOD35_L2 (MODIS Cloud Mask) product and the oceans are masked with the MOD03 (MODIS Geolocation) product. Emissivities for band 31 and 32, on the other hand, are estimated by the classification-based emissivity method (Snyder et al., 1998; Snyder and Wan, 1998) for which the land cover types for each pixel is determined by the MOD12Q1 (MODIS Quarterly Land Cover) product and MOD10_L2 (MODIS Daily Snow Cover) products.

The LST products produced by using the generalized split-window algorithm have been validated in most cases to have ± 1 K accuracy in clear-sky conditions when compared with the in-situ measurements (Coll et al. 2005; Wan et al. 2002b; Wan et al. 2004 and Wan 2008).

3.1.2. Scientific Data Sets

The Scientific Data Sets in the MOD11A1 product include LST 1km Day/Night, QC Day/Night, View Time Day/Night, View Angle Day/Night, Emissivity Band 31/Band 32, Clear Sky Coverage Day/Night. The following table summarizes the Scientific Data Sets of MOD11A1 product and their characteristics (Table 2).

SDS Name	Long Name	Number type	Unit	Valid Range	Fill Value	Scale Factor	Add Offset
LST_Day_1km	Daily daytime 1km grid Land-surface Temperature	uint16	K	7500-65535	0	0.02	0.0
QC_Day	Quality control for daytime LST and emissivity	uint8	none	0-255	0	N/A	N/A
Day_view_time	(local solar) Time of daytime Land-surface Temperature observation	uint8	hrs	0-240	255	0.1	0
Day_view_angle	View zenith angle of daytime Land-surface Temperature	uint8	deg	0-130	255	1.0	-65.0
LST_Night_1km	Daily nighttime 1km grid Land-surface Temperature	uint16	K	7500-65535	0	0.02	0.0
QC_Night	Quality control for nighttime LST and emissivity	uint8	none	0-255	0	N/A	N/A
Night_view_time	(local solar) Time of nighttime Land-surface Temperature observation	uint8	hrs	0-240	255	0.1	0
Night_view_angle	View zenith angle of nighttime Land-surface Temperature	uint8	deg	0-130	255	1.0	-65.0
Emis_31	Band 31 Emissivity	uint8	none	1-255	0	0.002	0.49
Emis_32	Band 32 Emissivity	uint8	none	1-255	0	0.002	0.49
Clear_day_cov	Day clear-sky coverage	uint16	none	0-65535	0	0.0005	0
Clear_night_cov	Night clear-sky coverage	uint16	none	0-65535	0	0.0005	0

Table 2: The Scientific Data Sets in the MOD11A1 product

3.2. Software used for the study

As mentioned in the previous section MOD11A1 LST product are provided in intergerized sinusoidal projection. MODIS Reprojection Tool MRT was used in order to reproject and mosaic the tiles of MOD11A1 product, in other words, for a part of pre-processing. Image analysis and all kinds of GIS analyses were conducted mostly in ArcGIS 9.3.1. Additionally, for some of analyses not available in the previous version ArcGIS 10 was used. In order to meet the spreadsheet necessities throughout the study and for drafting the dissertation Microsoft Office Suite 2010 was used.

3.3. Methods

3.3.1. Preprocessing

Satellite images usually need preprocessing such as atmospheric, geometric or radiometric corrections prior to the main image analysis. As the images used for this study are L3 MODIS LST/E products mentioned in the previous sections, all the necessary corrections has been done and the images are provided ready for image analysis. Nevertheless, preprocessing for the MOD11A1 products was needed for **(1)** reprojection and mosaicking, **(2)** quality assessment of the pixels and **(3)** extracting information in meaningful data ranges and unit.

3.3.1.1. Reprojection and Mosaicking

As mentioned in the previous sections, the MOD11A1 products are provided in ISIN projection in default. ISIN projection is data specific and has no compatibility with any other data sets which makes reprojection essential. Additionally, Turkey is covered by four adjacent MOD11A1 tiles which need to be combined in order to display the whole country and hence the area of interest in one image. Both reprojection and mosaicking have been done on MODIS Reprojection Tool (MRT) provided by LP DAAC. MRT accepts HDF files as input while the output format can be HDF, HDR or GEOTIFF. Information about the input file is displayed on the interface as well as the SDSs which lets user select data layers to be processed. A wide range of output projection types are available in MRT where different datums can be selected. MRT also provides three different resampling methods for reprojection as *"Nearest Neighbor (NN)", "Bilinear"* and *"Cubic Convolution (CC)"*. It is reported that NN resampling does not interpolate between existing bit values therefore it is the only resampling method which preserves bit-pattern encoded structure of the quality maps during resampling. Moreover, in CC and Bilinear resampling methods introduce artifacts to the resulting images such as excessively high values due to the numerical instability in the underlying MRT algorithm (Neteler 2010). As the adjacent tiles are provided as input files MRT creates the mosaic output image automatically according to the selected reprojection parameters. Therefore, reprojection and mosaicking are done in MRT simultaneously. For this study, daily LST daytime and LST nighttime data sets and corresponding QC layers were reprojected using Geographic Projection with WGS84 datum based on nearest neighbor resampling method where the output file format was GEOTIFF.

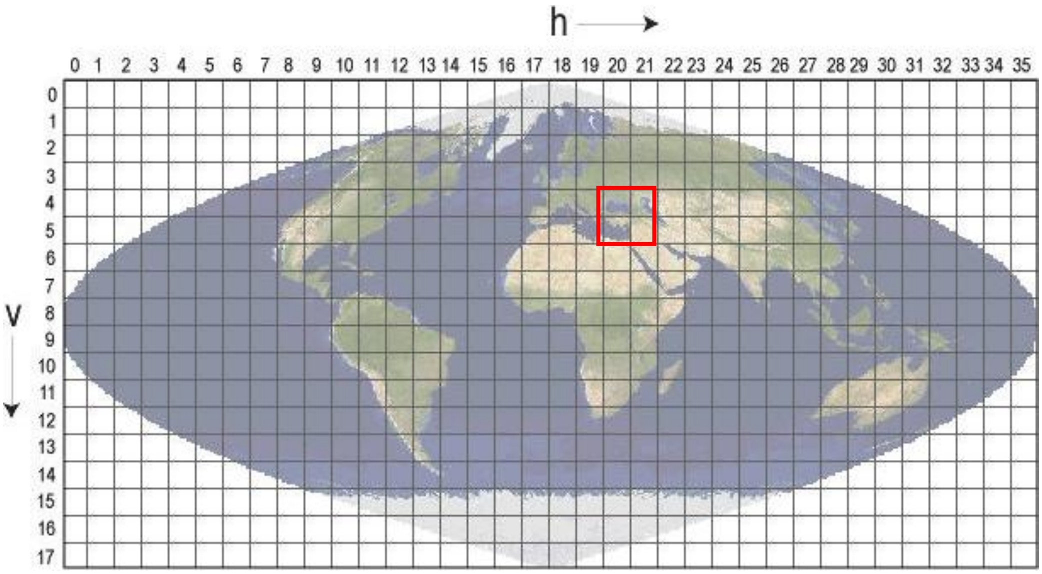

Figure 2: MODIS Integerized Sinusoidal (ISIN) Tiling System showing the tiles used in this study

3.3.1.2. Preprocessing of QC Images

The Quality Control (QC) data sets for day- and nighttime use unsigned 8 bit integer with a valid range of (0-255). These pixel values represent various permutations and combinations of bit flag parameters defined in MODIS LST Products Users Guideline (Wan, 2009) (Table 3).

Based on the criteria defined in Table 3 a number of permutations and combinations were calculated in order to determine the pixel values in the QC image to be retrained as good quality pixels. Different combinations and permutations of bit flags compose an 8-bit binary number which has a decimal equivalent in QC image within (0-255) range.

The bit flag values used for the analysis for each of the rows in the Table 3 are as follows:

- Mandatory QA flag values : 00 and 01;
- Data Quality flag values : 00 and 01;
- Emissivity Error flag : 00, 01 and 10;
- LST Error flag : 00 and 01;

According to the calculated permutations and combinations using the bit flag values defined above the QC image pixel values represent the good quality data are {0, 1, 16, 17, 32, 33, 64, 65, 80, 81, 96, 97} – a detailed information regarding the calculations is available in Table 4. Pixels in the QC image with these values were assigned as “1” where the remaining pixels were assigned as “0”. The resultant image is a binary image which was used to retain only the good quality LST image pixels to for further image analysis.

bits	Long Name	Key
1&0	Mandatory QA Flags	00: LST produced, good quality not necessary to examine more detailed QA 01: LST produced, other quality, recommend examination of more detailed QA 10: LST not produced due to cloud effects 11: LST not produced primarily due to reasons other than cloud
3&2	Data Quality Flag	00: good quality data 01: other quality data 10: TBD 11: TBD
5&4	Emissivity Error Flag	00:average emissivity error ≤ 0.01 01:average emissivity error ≤ 0.02 10:average emissivity error ≤ 0.04 11:average emissivity error > 0.04
7&6	LST Error Flag	00: average LST error ≤ 1K 01: average LST error ≤ 2K 10: average LST error ≤ 3K 11: average LST error > 3K

Table 3: Defined bit flags for quality assurance scientific data sets QC Day/Night (adapted from Wan, 2009)

Pixel Value	**LST Error**		**Emissivity Error**		**Data Quality Flag**		**QA Flag**	
	2^7	**2^6**	**2^5**	**2^4**	**2^3**	**2^2**	**2^1**	**2^0**
0	0	0	0	0	0	0	0	0
1	0	0	0	0	0	0	0	1
16	0	0	0	1	0	0	0	0
17	0	0	0	1	0	0	0	1
32	0	0	1	0	0	0	0	0
33	0	0	1	0	0	0	0	1
64	0	1	0	0	0	0	0	0
65	0	1	0	0	0	0	0	1
80	0	1	0	1	0	0	0	0
81	0	1	0	1	0	0	0	1
96	0	1	1	0	0	0	0	0
97	0	1	1	0	0	0	0	1

Table 4: Acceptable bit flag combinations for Quality Control Images

3.3.1.3. Preprocessing of LST Images

Primarily, the binary QC image derived in the previous section was used to identify good and poor pixels of day- and nighttime LST images. Only the good quality pixels in the Land-surface temperature data sets were used. The LST data sets for day- and nighttime use 16-bit unsigned integer with a valid range of (7500-65535). The scale factor for the LST data sets is defined as (0.02) in MODIS Users Guideline (Wan, 2009) which means the original values were exaggerated 50 times. Therefore, in order to get the original values in ^{o}K the pixel values on the LST images were multiplied by (0.02). The resultant images provided per-pixel temperature in degree Kelvin. Furthermore, in order to get pixel values in degree Celsius, Kelvin to Celsius conversion was made. The final images are LST daytime and LST nighttime images only with high quality pixels that provide per-pixel temperature in degree Celsius ready-to-use for further image analysis.

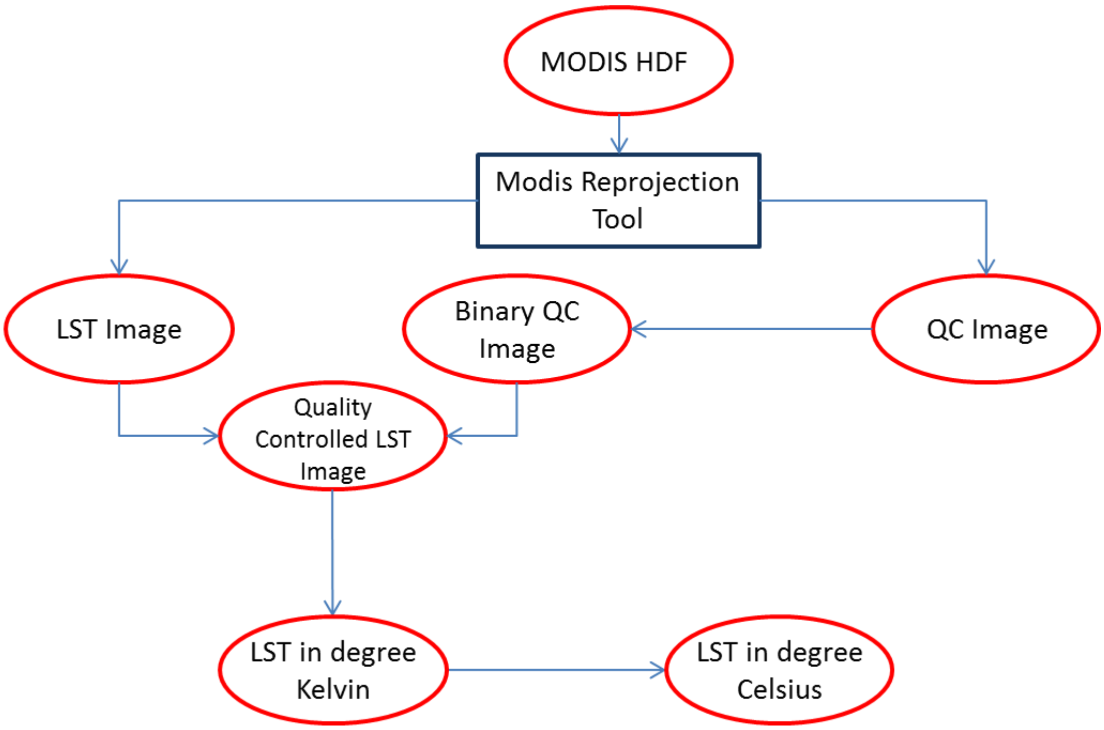

Figure 3: Preprocessing Workflow

3.3.2. LST differencing of spatial averages based on two years

The LST differencing of spatial averages based on two years was first suggested by Ouzounov and Freund (2004) in order to test the potential LST anomalies related with the 2001 Gujarat earthquake. Spatially averaged daily nighttime LST were calculated using MODIS LST/E data of an area equivalent to 100kmx100km for a number of weeks before and after the earthquake. Additionally, the same calculation was made for the equivalent days of the year 2002. Subsequently, the daily LST difference between 2001 and 2002 (μLST_{2001}-μLST_{2002}) were calculated for the same time-span. The results were used to identify what they termed as “thermal anomaly pattern” for the area (Ouzounov and Freund 2004).

In this study, LST differencing of spatial averages method based on two years was adopted for Malatya-Pütürge-Doğanyol earthquake. Spatially averaged daily daytime and nighttime LSTs were calculated using the preprocessed MOD11A1 LST images for fortnight before and after the earthquake in 2003. The calculations were extended to all previous years that MODIS LST data is available – note that MODIS data is available after Mar 5th, 2000 – and the LST differences were calculated for all pairs or years between 2000 and 2003 (μLST_x-μLST_y where x, y={2000,2001,2002,2003} and x>y). Note that pairs including two non-earthquake years were also used for analysis. Unlike only one rectangular area of interest defined in the original method, in this study five circular areas are defined where the epicenter is the center of the circles with radii of 25km, 50km 100km, 200km and 400kms (Figure 4). The purpose of having different areas is to assess the influence of the size of the study area for the method. In total, LST differences for six pairs of years over five circular areas were calculated. Note that in the same time interval defined for the analysis (June 29th – July 27th) no other earthquake having magnitude more than 5 is reported in the region between 2000 and 2003. Therefore, none of the defined areas in Figure 4 is affected by any other earthquake having magnitude more than 5 rather than Malatya-Pütürge-Doğanyol earthquake.

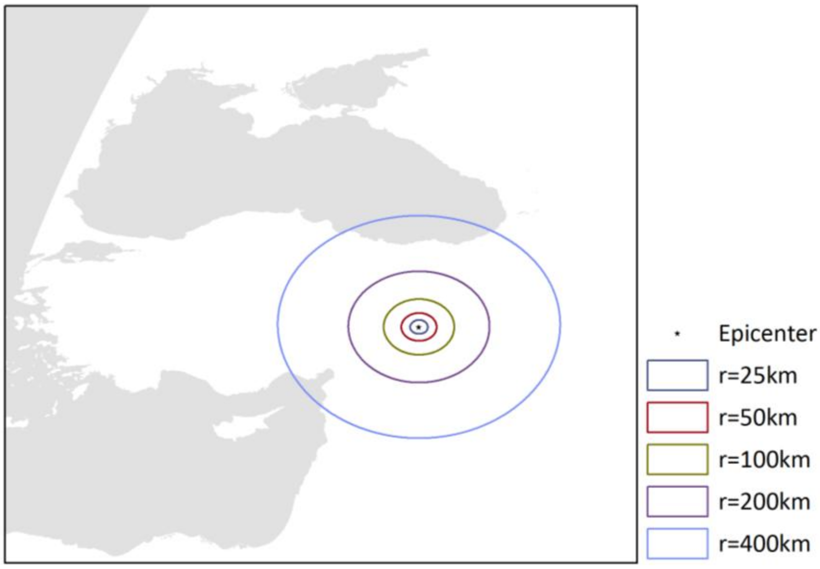

Figure 4: Areas defined and used for spatial averaging

3.3.3. LST differencing of spatial averages based on multiple years

The LST differencing of spatial averages based on multiple years is basically a modified version of LST differencing of spatial averages based on two years mentioned in the previous section. Instead of utilizing only two distinct years for differencing, a temporal mean of spatially averaged daily day- and nighttime LST of four years ($\overline{\mu LST}_{2000\rightarrow 2003}$) including the year of the earthquake and all previous years where MODIS data is available were calculated based on the preprocessed MOD11A1 LST images for fortnight before and after the earthquake over the area of interest. Then the daily difference between the earthquake year and the temporal mean (μLST_{2003}-$\overline{\mu LST}_{2000\rightarrow 2003}$) was calculated in order to get the LST change pattern of the area. Moreover, calculations were extended for all previous years. In other words, the daily difference between all non-earthquake years and the temporal mean were also calculated (μLST_x-$\overline{\mu LST}_{2000\rightarrow 2003,}$ where x= {2000, 2001, 2002}). In a similar manner with the previous method the analysis was conducted over five circular areas of where the epicenter is the center of the circles with radii 25km, 50km, 100km, 200km and 400km (Figure 4).

3.3.4. LST differencing of pixels based on multiple years

In contrast to the previously mentioned methods, instead of averaging LSTs over defined areas, pixel LST values were directly utilized for analysis of thermal changes in the area of interest. For LST differencing, first the daily day- and nighttime spatio-temporal historical averages of the pixels were calculated for the equivalent days mentioned in the previous methods (i.e. fortnight before and after the earthquake). Note that MODIS LST data is available after Mar 5th, 2000 which means that LST images are available only for three years before the earthquake. Therefore, including the earthquake year the number of years for calculation is limited to four years. In order to increase the accuracy LST images of following three years after 2003 were used for daily spatio-temporal historical average calculations. The preprocessed MOD11A1 LST images of 7 years (2000 – 2006) including the year of earthquake were used for daytime and nighttime calculations except (June 29th – July 4th) interval in 2001 where there is no data available. For this interval 6 years of daily LST images were used for calculations. Subsequently, the calculated historical averages were subtracted from the LST images of the corresponding dates of 2003 representing the earthquake year and 2000 representing non-earthquake year to retain the LST difference on pixel basis. Note that due to time limitations of the study only one non-earthquake year selected and used for the analysis. In order to discern the thermal differences in space and time the resultant difference images divided into classes. Basically, pixels with negative LST difference were assigned into the same class while pixels with positive LST difference further divided into six classes with 2°C intervals.

3.3.5. Robust Satellite Technique (RST)

Robust Satellite Technique (RST) is a general approach of satellite analysis used for monitoring major natural and environmental hazards which is independent from specific sensor/satellite. Therefore, RST can be utilized on different satellite data and applied for different events such as earthquakes, volcanoes, floods, forest fires, etc. (Pergola et al., 2010). RST requires a multi-temporal analysis of homogeneous satellite TIR records of several years co-located in time and space domain. Each pixel of the satellite image is processed within the characteristics of the TIR signal in other words in terms of expected and natural variability range of the TIR signal for each pixel in the satellite image. Anomalous TIR signal, therefore an anomalous pixel, is identified as a deviation from its normal or expected value using a unitless index called Robust Estimator of TIR Anomalies (RETIRA) index (Tramutoli et al. 2001; Tramutoli et al. 2005 ; Filizzola et al. 2004; Genzano et al. 2007; Pergola et al. 2010). The RETIRA (R_I) index is computed for the associated image by the following equation.

$$\otimes_{\Delta LST}(r,t) = \frac{\Delta LST(r,t) - \mu_{\Delta LST}(r)}{\sigma_{\Delta LST}(r)}$$

where ***r≡ (x,y)*** is the location coordinates of the pixel center on a satellite image;

t is the time of image acquisition with t ϵ τ. Note that τ defines the homogenous time domain of satellite image acquisition in the same time-slot of the day and period (month) of the year;

ΔLST(r,t) is the difference between the LST value on the associated image *LST(r,t)* at the location *r≡(x,y)* and at acquisition time (t ϵ τ) and its spatial average of the image *T(t)* (i.e. *ΔLST(r,t)= LST(r,t)-LST(t)*). Note that only cloud-free pixels belonging to the same class (i.e. land or sea class) are considered for computation purposes over the area of interest. As MOD11A1 LST image provides LST only for land and inland water pixels, all the cloud-free pixels were considered to be in land class and were used for the analysis. The use of such a differential variable *ΔLST(r,t)* instead of *LST(r,t)* is expected to reduce possible contributions of daily and/or annual climatological changes such as occasional warming (Tramutoli et al. 2001, Tramutoli et al. 2005; Filizzola et al. 2004; Genzano et al. 2007; Pergola et al. 2010).

μΔLST(r) time average of *ΔLST(r,t)* at the location *r≡(x,y)* calculated on cloud free pixels of homogenous time domain (t ϵ τ). Note that time average image is a reference image that shows the normal or expected behavior of *ΔLST* for location *r*;

σΔLST(r) standard deviation of *ΔLST(r,t)* at the location *r≡(x,y)* calculated on cloud free pixels of homogenous time domain (t ϵ τ). Note that standard deviation image is a reference image that shows the variability of *ΔLST* for location *r*.

Time average μΔLST(r) and σΔLST(r) are calculated once for all by processing several years of historical satellite images acquired by the same sensor in the same homogeneous time domain (i.e. same time-slot of the day and the same period(month) of the year) for each location *r*. The number of years for multi-temporal analysis of historical satellite images varies from 4 to 10 years depending on the availability of satellite data (Lisi et al. 2010).

The difference between *ΔLST(r,t)* and μΔLST(r) represents the Signal (S) to be investigated for its possible relation with seismic activity while σΔLST(r) represents the corresponding Noise (N) due to natural and/or observational causes. In other words, RETIRA index is computed based on the comparison of the Signal and its local variability Noise both of which are observed historically for location *r* in similar observational conditions (i.e. sensor, time domain, etc.).

In this study the RST is applied to preprocessed MOD11A1 LST images, therefore pixel values are LST and directly utilized in the RETIRA equation. Note that since the images are already quality controlled only good quality pixels (i.e. cloud-free pixels) were used for the analysis. In a similar manner with the previous methods daily day- and nighttime images fortnight before and after the earthquake were used for RST. For the equivalent days of 7 years (2000-2006), daily ΔLST(r,t) values were calculated. Moreover, based on the obtained daily ΔLST(r,t) values μΔLST(r) time average and σΔLST(r) standard deviation calculations were made for the whole scene utilized for the analysis. Although the timespan defined for the study covers only 2 days in June and 27 days in July μΔLST(r) time average and σΔLST(r) standard deviation calculations have been done separately for June and July – for the same period (month) of the year as it is mentioned before. Subsequently, RETIRA equation was utilized for the associated images in 2003 representing the earthquake year and in 2000 representing the non-earthquake year in order to retain the index on a daily basis. Note that due to time limitations only one non-earthquake year was selected and used for the analysis. The resultant images were identified and divided into classes based on R_l values. In the previous studies various intervals were used for the classification and identification of anomalous pixels [R_l>2, >2.5, >3, >3.5 (Tramutoli et al. 2005); R_l≥2, ≥3 (Genzano et al. 2007); R_l≥2, ≥2.5, ≥3 (Pergola et al. 2010); R_l≥2.5 (Blackett et al. 2011)]. In this study, the intervals for R index values are defined as R_l≤-3.5, ≤-3.0, ≤-2.5, ≤2, -2<R_l<2, ≥2, ≥2.5, ≥3 and ≥3.5 in order not only to see the positive variability but also the negative variability of LST over space and time.

4. Results

4.1. Preprocessing

The entire image analysis began with preprocessing of MOD11A1 products as it was described earlier. The area of interest is covered by 4 adjacent tiles of MODIS data which needed to be combined in order to have one image at hand. Associated tiles were combined and reprojected through MRT. Amongst 12 SDSs provided in MOD11A1 product only daytime/nighttime LST images and corresponding QC images were extracted for further analysis. In summary, 58 LST and 58 QC images (29 daytime/29 nighttime each) were extracted per year. The same process was applied to 7 years of satellite data from 2000 to 2006. Note that MOD11A1 product is not available for five days in 2001 (June 29 – July 3) and for one day in 2000 (Jul 14) nighttime LST image is also not available. Therefore, 198 daytime LST images and corresponding QC images; and 197 nighttime LST images and corresponding QC images were extracted.

Extracted QC images were used for generating binary maps in order to use quality assessment of LST images. Quality controlled LST images then subjected to a final process in order to convert the exaggerated values of LST first into degree Kelvin and eventually into degree Celsius. Resultant 395 quality controlled LST images (198 daytime/197 nighttime) were used for further image analysis.

4.2. LST Differencing of spatial averages based on two years

As mentioned earlier daily spatial averages of daytime and nighttime LSTs were calculated for 4 years over the predefined circular areas where radii vary from 25km to 400km. Then differences between earthquake year and three non-earthquake years were calculated. Moreover, calculation extended only for two non-earthquake years. In order to investigate the thermal anomaly pattern for the area of interest daily LST differences were plotted on graphs for each and every year combination used for the analysis (Figure 5-16). Note that the days which have less than 70% of good quality pixels in the defined areas were excluded for the analysis and graphs were generated accordingly.

In order to see the influence of the extent of the areas used for spatial averaging the plots of the same combination of years but different areal radii were shown on the same graph. As a preliminary conclusion, it can be claimed that the radius and hence the extent of the area for spatial averaging has a slight effects on the results.

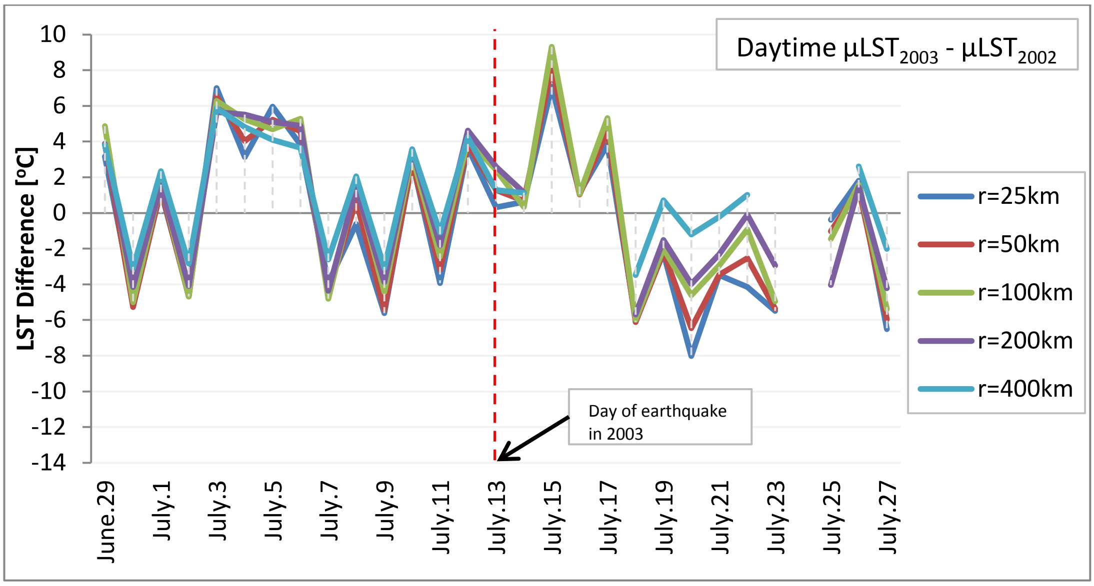

Figure 5: Distribution of spatially averaged daytime LST differences comparing 2003 (earthquake year) and 2002(non-earthquake year) [μLST_{2003} - μLST_{2002}]

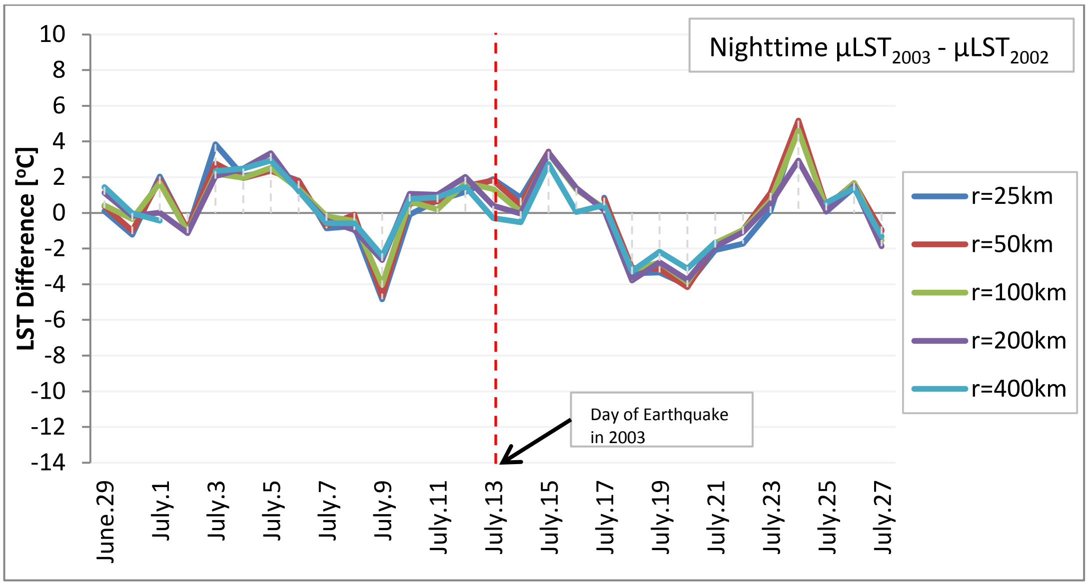

Figure 6: Distribution of spatially averaged nighttime LST differences comparing 2003 (earthquake year) and 2002(non-earthquake year) [μLST_{2003} - μLST_{2002}]

In the first graph which shows the daytime distributions of LST differences for 2003 and 2002 positive thermal LST anomaly can be seen before and also after the earthquake (Figure 5). The differences can vary from 4 up to 8^{o}C for the daytime values. The positive LST anomaly concentrates in July 3rd – July 6th interval. In this time interval daily variability of LST differences (peaks and dips) are more visible for smaller radius where for larger radius the graphs become smoother and less variability is observed. Other significant positive LST anomalies are observed on July 10th and July 12th three days and one day before the earthquake respectively, the highest peak, however, is observed after the earthquake on July 15th. Soon after on July 17th another positive LST anomaly is observed as well. Furthermore, when the nighttime distributions of LST differences are examined (Figure 6) it is observed that positive LST anomaly was also occurred for the same time interval (July 3rd – July 6th) but with less intensity when its compared with the daytime measurements. Similarly, after the day of earthquake on July 15th another peak is observed again with less intensity compared with daytime observation. On the other hand, the peak observed in daytime on July 17th is absent for nighttime. The highest peak observed in nighttime analysis is also after the earthquake but the day of the peak (July 24th) is different from the one observed previously in daytime distribution.

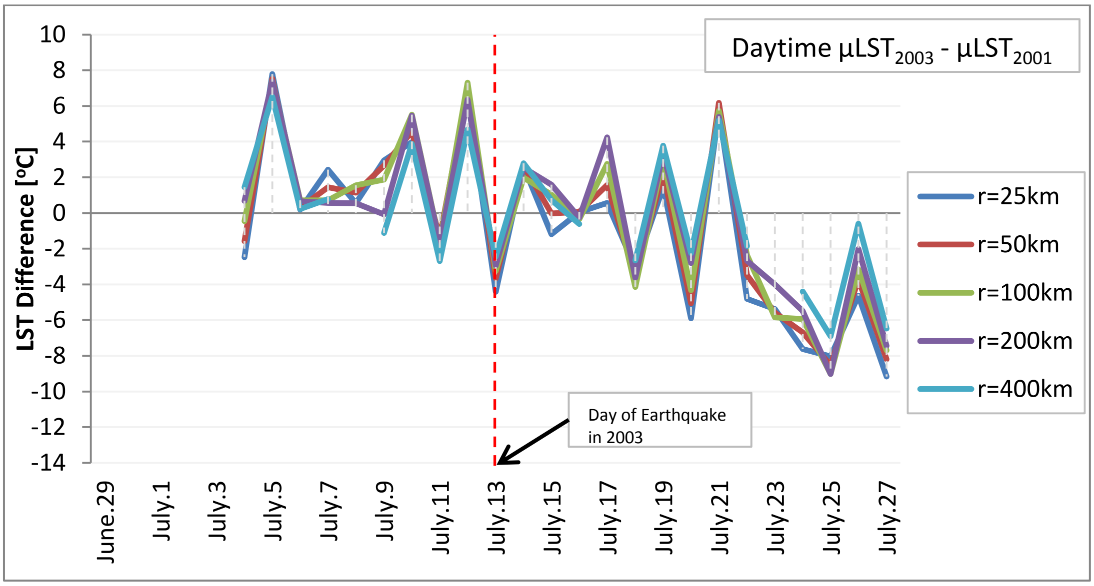

Figure 7: Distribution of spatially averaged daytime LST differences comparing 2003 (earthquake year) and 2001(non-earthquake year) [μLST_{2003} - μLST_{2001}]

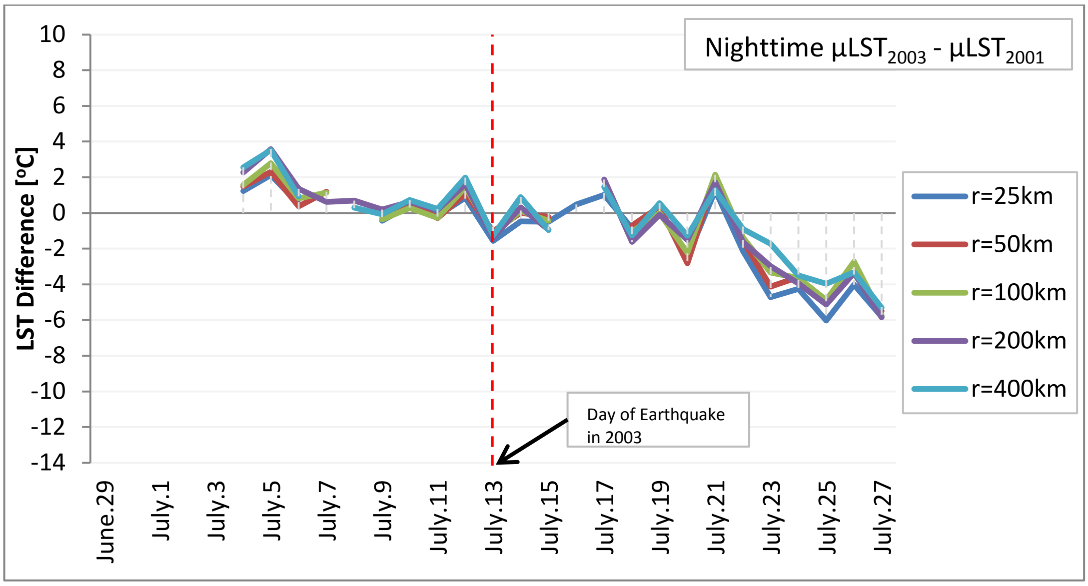

Figure 8: Distribution of spatially averaged nighttime LST differences comparing 2003 (earthquake year) and 2001(non-earthquake year) [μLST_{2003} - μLST_{2001}]

For the graph produced for the daytime distributions of daily LST differences comparing 2003 and 2001 the positive LST anomalies can be seen before and also after the earthquake which means it does not have a unique pattern (Figure 7). Moreover, the intensities of the LST anomalies before and after the earthquake are almost the same. The LST differences before the earthquake reaches to approx. 7°C on July 5th and on July 12th while it reaches to approx. 5°C on July 10th. After the earthquake there are three significant peaks two of which are observed on July 17th and July 19th with approx. 4°C while the last peak is observed on July 21st with approx. 6°C. Nighttime distributions show totally different pattern than daytime distributions like the previous pair of years 2003-2002 (Figure 8). The only significant LST difference is observed before the earthquake on July 5th with approx. 4°C for the area with radius 25 km. However, the intensity fades away as the radius increases. For the area with radius 400km the LST difference is around 2°C and it loses significance.

When the distributions of daytime and nighttime LST differences comparing 2003 and 2000 are examined the results are quite same with the previous observations (Figure 9 and 10). In general, a negative trend is observed for both daytime and nighttime averages. This shows that the regional LST in 2000 (non-earthquake year) is higher than regional LST in 2003 (earthquake year). However, like the previous pairs of years LST differences increase between July 3rd and July 6th, for this interval LST differences rise just above zero yet less than approx. 1°C. Moreover, the nighttime distributions show smoother pattern than the same of daytime.

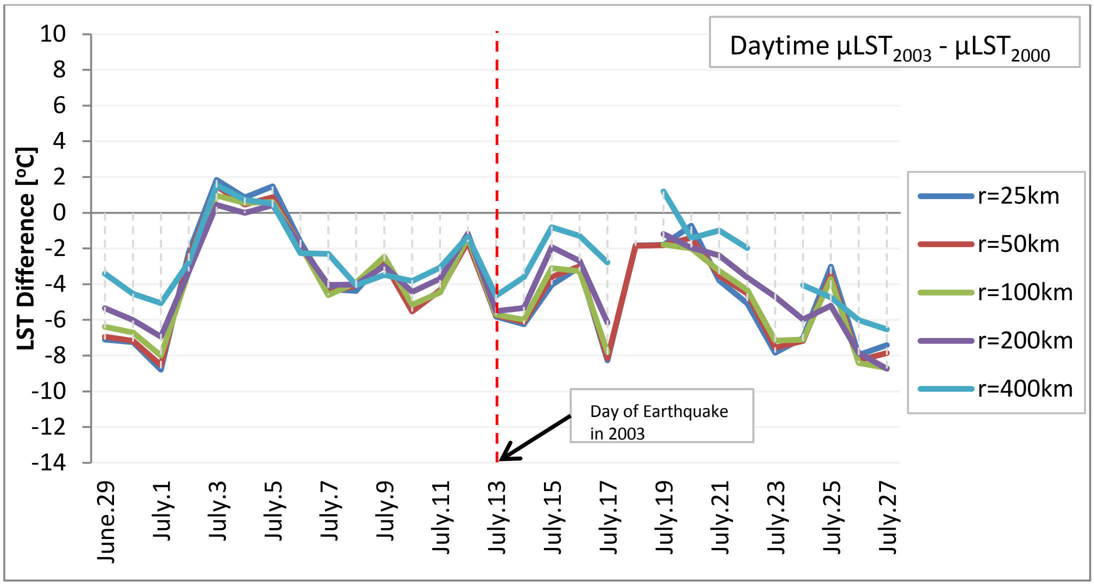

Figure 9: Distribution of spatially averaged daytime LST differences comparing 2003 (earthquake year) and 2000(non-earthquake year) [μLST_{2003} - μLST_{2000}]

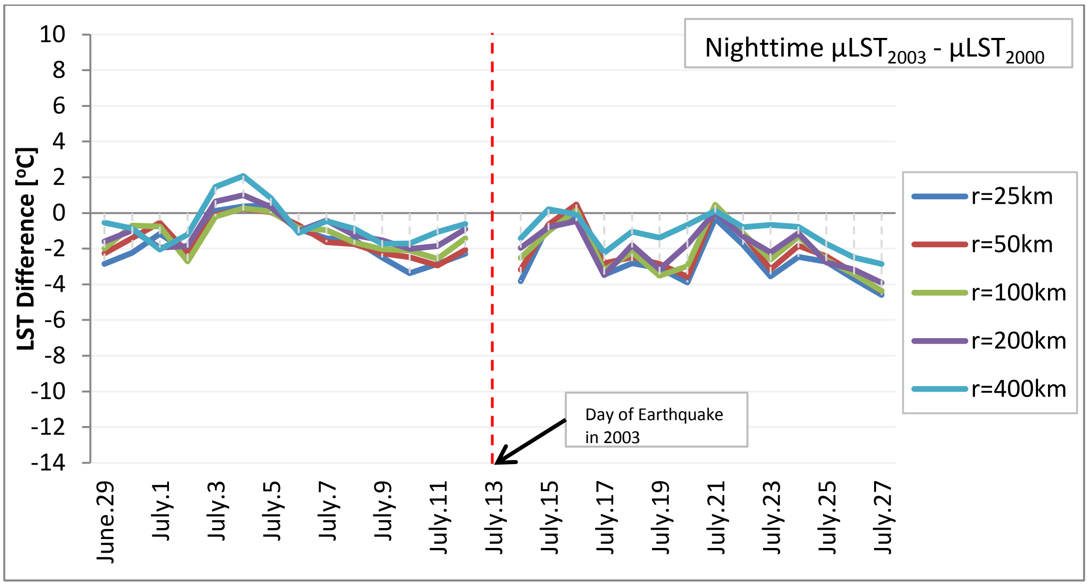

Figure 10: Distribution of spatially averaged nighttime LST differences comparing 2003 (earthquake year) and 2000(non-earthquake year) [μLST_{2003} - μLST_{2000}]

Abrupt LST differences are observed after the earthquake in a similar manner with the previous plots yet again in different days. In Figure 9 on July 17th and in Figure 10 on July 16th and 21st increases of LST difference are observed which depart from the general pattern of the distribution.

Even though the differentiations up to now consider one earthquake year and one non-earthquake year the results are quite diverse. The positive LST anomalies can be seen before and after the earthquake however the days that show positive LST anomaly are not consistent. Furthermore, albeit the days that show positive LST anomaly before the earthquake are consistent the intensity of the differences vary for daytime and nighttime averages. Therefore, it is concluded that the Sun's irradiation has considerable effect on LST changes which may suppress the effect of stress accumulation.

For the first pair of non-earthquake years (2002 and 2001) comparing daytime averages, it is observed that LST anomaly is present although there is no earthquake occurrence in the area. The intensity of the anomaly observed is the highest so far including the pairs of years the earthquake occurred (Figure 11). As seen on Figure 11, on July 7th and July 9th the LST differences between the 2002 and 2001 reach 6^{o}C and 8^{o}C respectively. Furthermore, on July 21st the LST difference climbs up to approx. 9^{o}C. Note that there is no earthquake occurrence in neither of the years in the specified time interval. Similarly, in the nighttime analysis positive LST anomalies are observed between July 7th and July 9th; and July 16th and July 20th with around 4^{o}C (Figure 12).

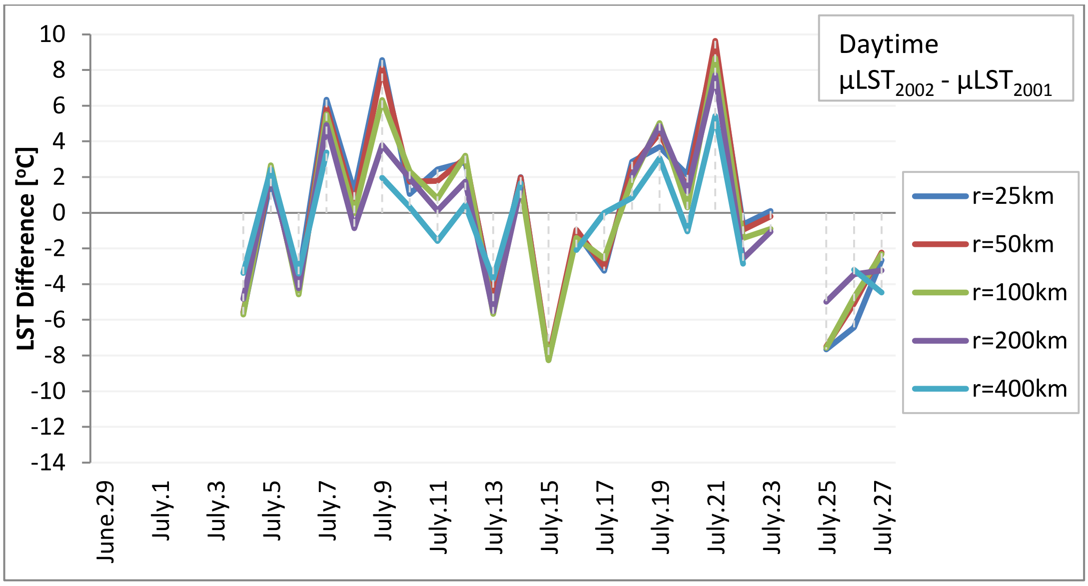

Figure 11: Distribution of spatially averaged daytime LST differences comparing 2002 and 2001(two non-earthquake year) [μLST_{2002} - μLST_{2001}]

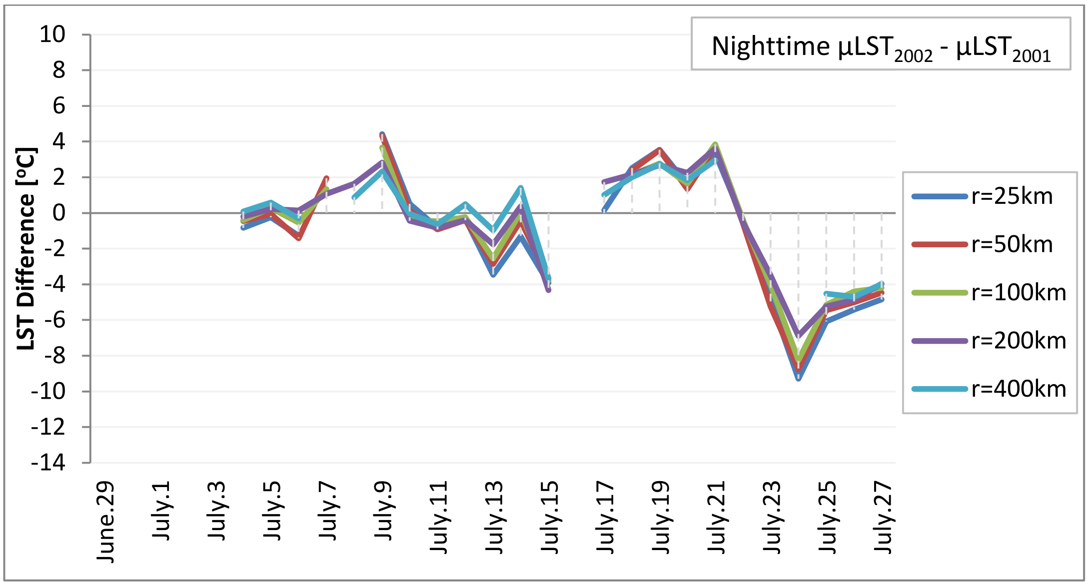

Figure 12: Distribution of spatially averaged nighttime LST differences comparing 2002 and 2001(two non-earthquake year) [μLST_{2002} - μLST_{2001}]

The graph showing the distribution of daytime LST differences comparing 2002 and 2000 also shows similar results. There is no earthquake but there is thermal anomaly observed. For instance, until July 17th the plot follows a negative trend around -8^{o}C and on July 18th the LST difference reaches up to 4^{o}C which means an absolute difference of around 12^{o}C between two days (Figure 13).

On the other hand, on July 20th the LST difference reaches its maximum with around 5^{o}C. Again as the radius increases the variation of LST difference is smoothed out and shows less intensity for the same day of observation. In the nighttime analysis for the same day (July 17th) an increase is also observed however this time the increase is not as drastic as daytime analysis which is again related with the lack of the Sun's radiation (Figure 14).

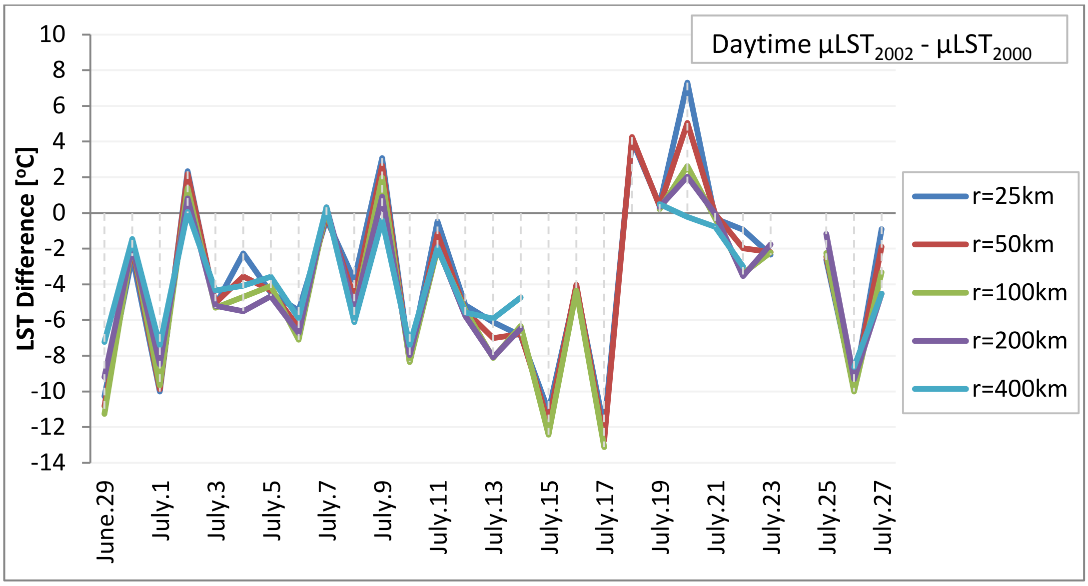

Figure 13: Distribution of spatially averaged daytime LST differences comparing 2002 and 2000(two non-earthquake year) [μLST_{2002} - μLST_{2000}]

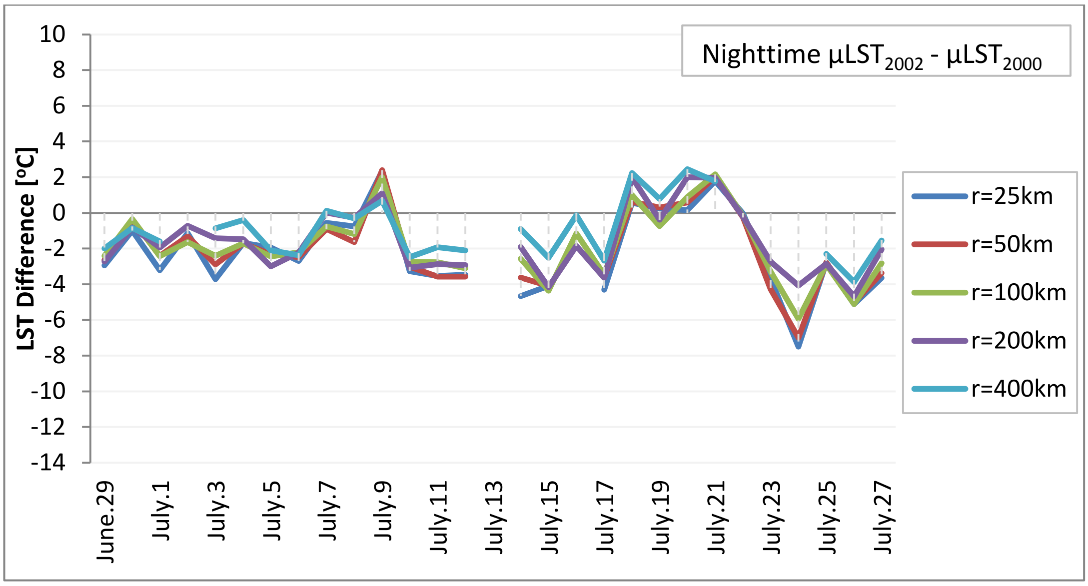

Figure 14: Distribution of spatially averaged nighttime LST differences comparing 2002 and 2000(two non-earthquake year) [μLST_{2002} - μLST_{2000}]

The last pair of non-earthquake years (2001 and 2000) used for the analysis show similar trends and albeit there is no earthquake LST anomalies are successfully observed (Figure 15 and 16). On July 20th and July 25th LST differences are observed to be around 5^{o}C for daytime analysis (Figure 15). In the nighttime analysis on the other hand LST difference around 3^{o}C is observed on the days July 24th and July 25th (Figure 16).

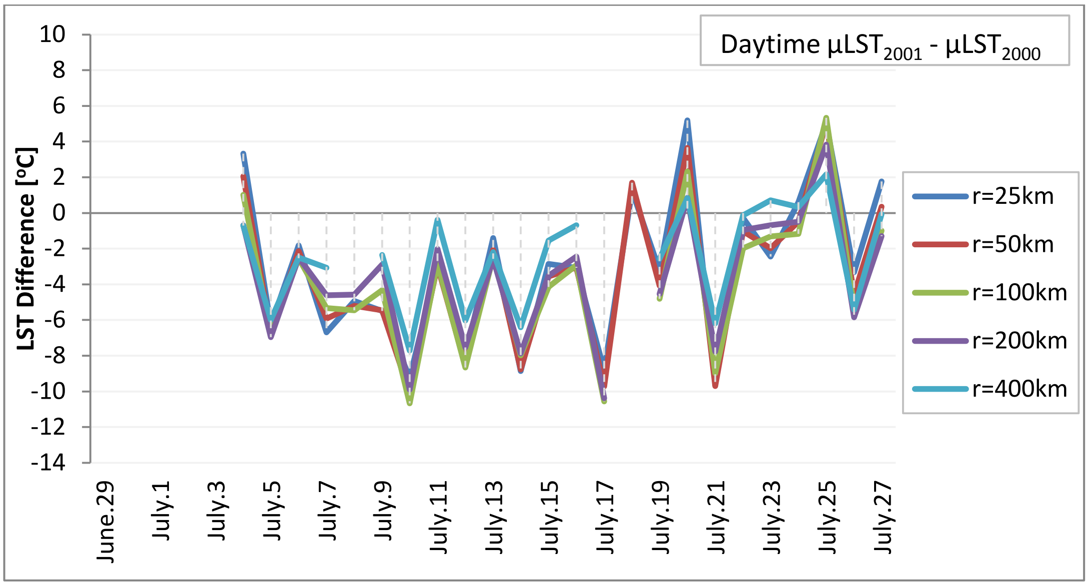

Figure 15: Distribution of spatially averaged daytime LST differences comparing 2001 and 2000(two non-earthquake year) [μLST_{2001} - μLST_{2000}]

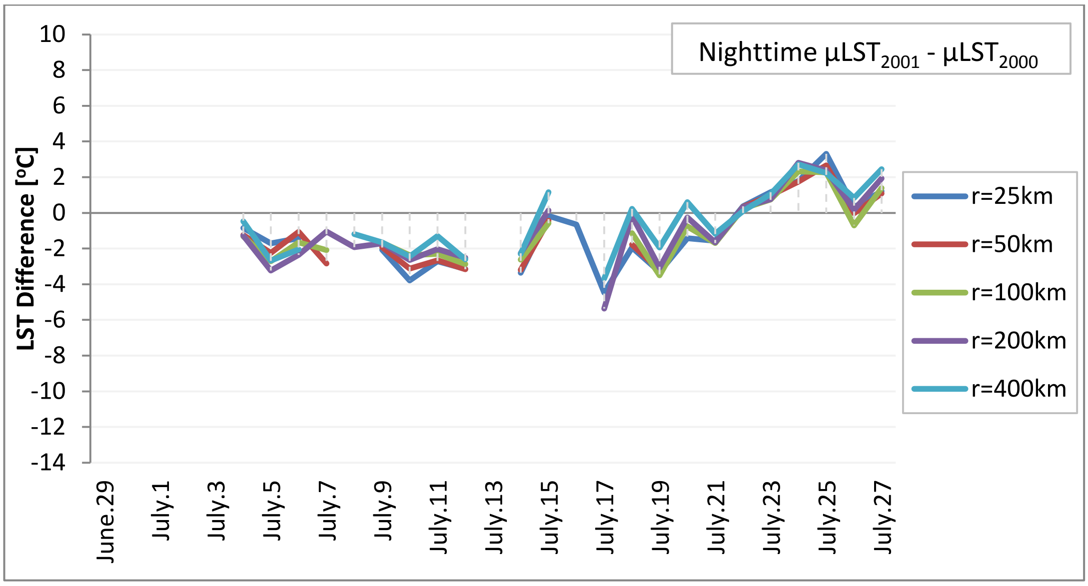

Figure 16: Distribution of spatially averaged nighttime LST differences comparing 2001 and 2000(two non-earthquake year) [μLST_{2001} - μLST_{2000}]

4.3. LST Differencing of spatial averages based on multiple years

Primarily, temporal means of spatially averaged daily daytime and nighttime LSTs of four years ($\overline{\mu LST}_{2000\rightarrow 2003}$) including the year of the earthquake and all previous years that MODIS data is available were calculated. Then the calculated temporal means of daytime and nighttime images were subtracted from equivalent days of the earthquake year and three non-earthquake years as well. Similar to LST differencing spatial averages based on two years distribution of daytime and nighttime average spatially averaged LST differences based on multiple years were plotted (Figure 17 – 24).

In the first two graphs the comparison of earthquake year and the temporal mean is shown for daytime and nighttime respectfully (Figure 17 and 18). In a similar manner with the previous method (LST differencing based on two years) thermal anomaly is observed between July 3rd and July 6th with 2 to 4°C intensity. When the absolute LST difference is considered between July 2nd and July 3rd it is observed to be around 6°C. Another temperature rise can be seen on July 12th just one day before the earthquake however when the general variability of the plot is taken in to account this LST difference loses its significance (Figure 17).

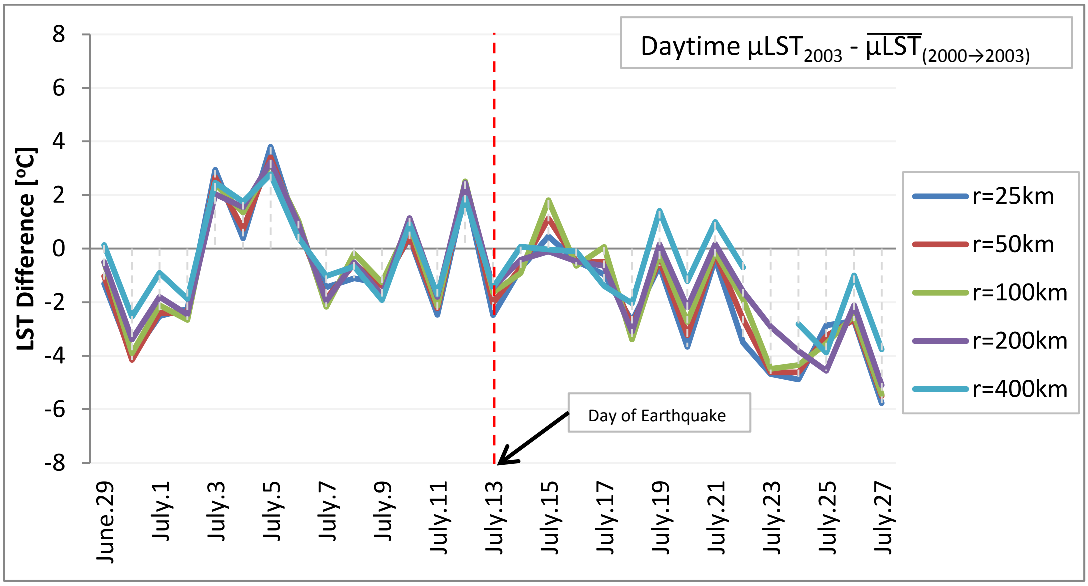

Figure 17: Distribution of spatially averaged daytime LST differences comparing 2003 and temporal mean [μLST_{2003} - $\overline{\mu LST}_{(2000 \rightarrow 2003)}$]

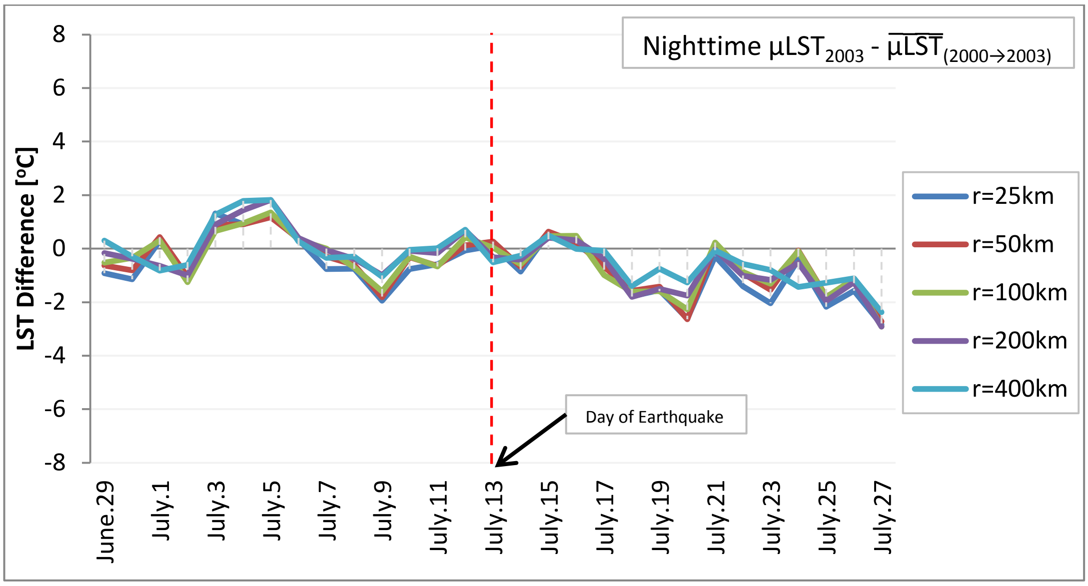

Figure 18: Distribution of spatially averaged nighttime LST differences comparing 2003 and temporal mean [μLST_{2003} - $\overline{\mu LST}_{(2000\rightarrow2003)}$]

The nighttime distribution graph shows a slight increase for the equivalent days mentioned (July 3rd – July 6th) yet again when the variability of the plot is taken into account the LST rise in these days does not seem to be anomalous (Figure 18).

As the method is extended for non-earthquake years it is also observed that the LST anomaly is seen even in the absence of earthquake. On Figure 19 which shows the comparison between 2002 and the temporal mean, for July 9th, July 18th and July 20th the LST difference is observed to be around 3°C. Moreover, the absolute LST difference between July 17th and July 18th is observed to be around 8°C (Figure 19). In the nighttime distribution, on the other hand, slight LST differences can be seen for July 9th and the days between July 18th and July 21st. Apart from those days no positive LST difference is observed. However, between July 21st and July 24th there is a negative LST difference observed with around 7°C (Figure 20).

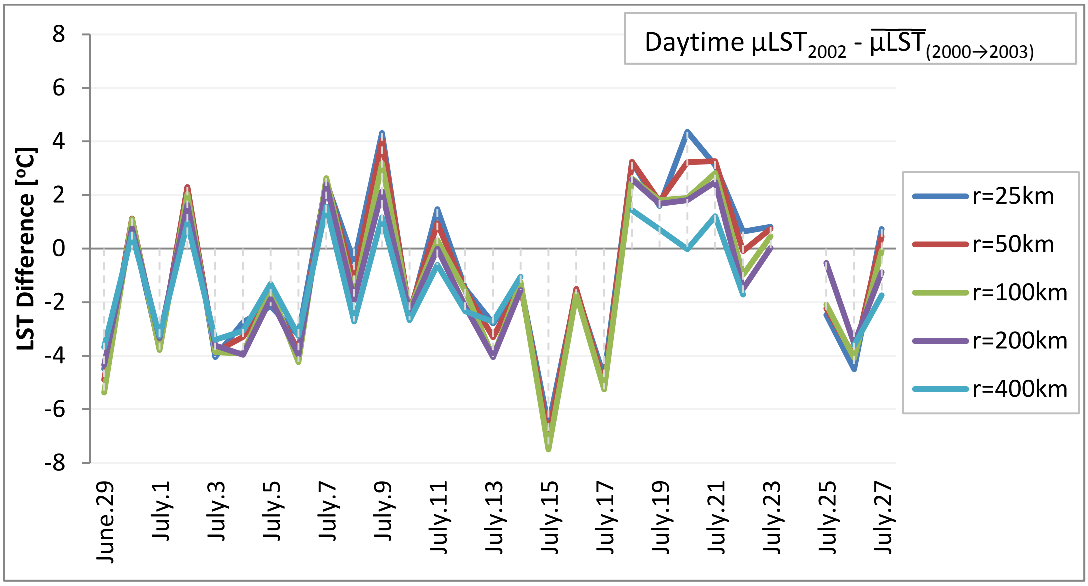

Figure 19: Distribution of spatially averaged daytime LST differences comparing 2002 and temporal mean [μLST_{2002} - $\overline{\mu LST}_{(2000\rightarrow 2003)}$]

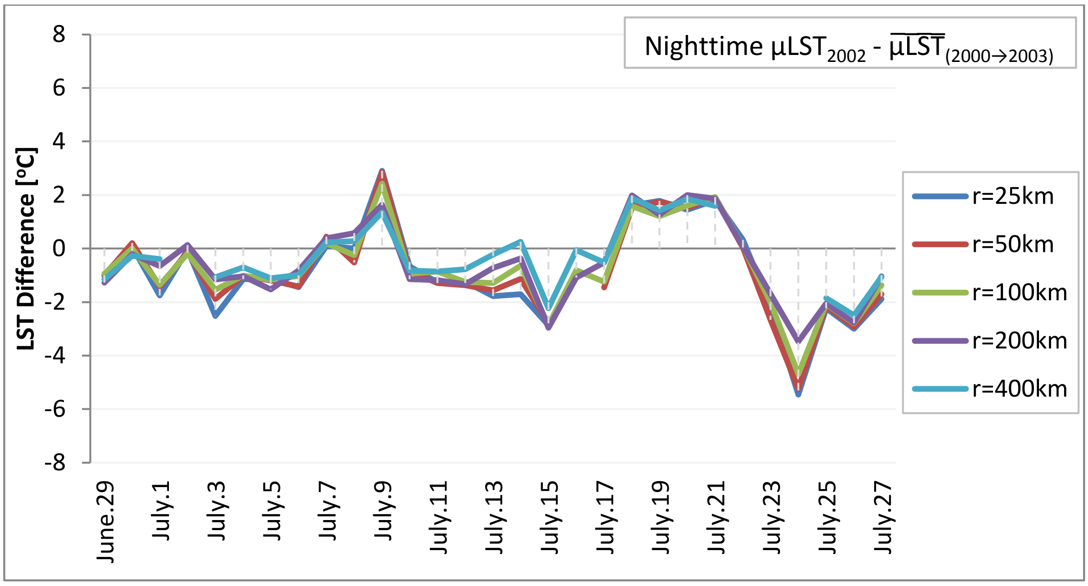

Figure 20: Distribution of spatially averaged nighttime LST differences comparing 2002 and temporal mean [μLST_{2002} - $\overline{\mu LST}_{(2000\rightarrow 2003)}$]

The daytime LST differences of 2001 and the temporal mean are highly variable as seen on Figure 21. It can be said that the LST difference is negative in general which means for most of the days the average daily LST is higher than the same in 2001. However, starting from July 21st LST rise is observed which reaches its maximum on July 25th with around 6^{o}C (Figure 21). Similarly, in the nighttime for the equivalent days mentioned there is also a positive LST difference with 4^{o}C (Figure 22).

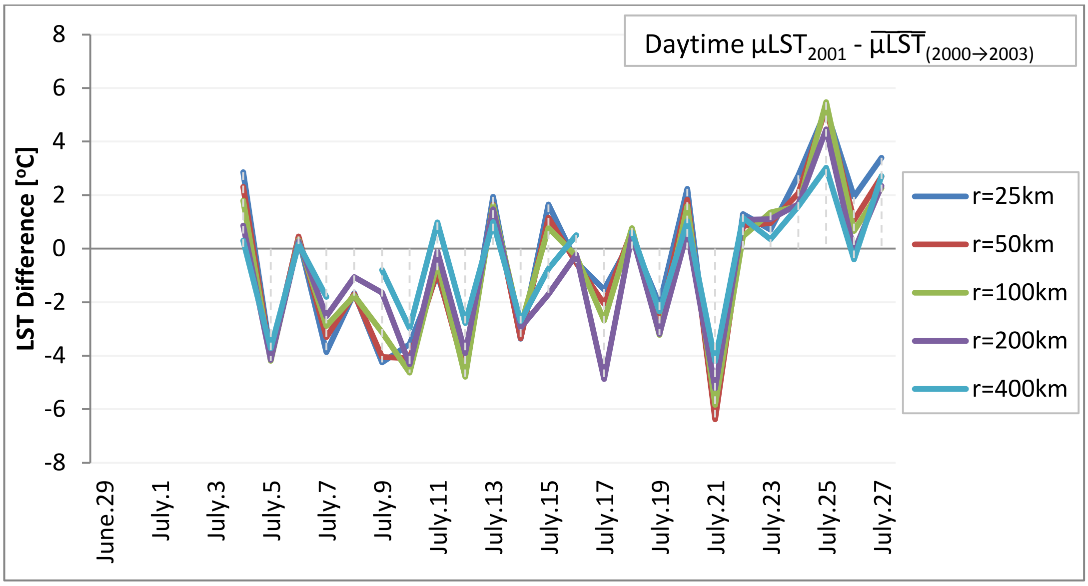

Figure 21: Distribution of spatially averaged daytime LST differences comparing 2001 and temporal mean [μLST_{2001} - $\overline{\mu LST}_{(2000 \rightarrow 2003)}$]

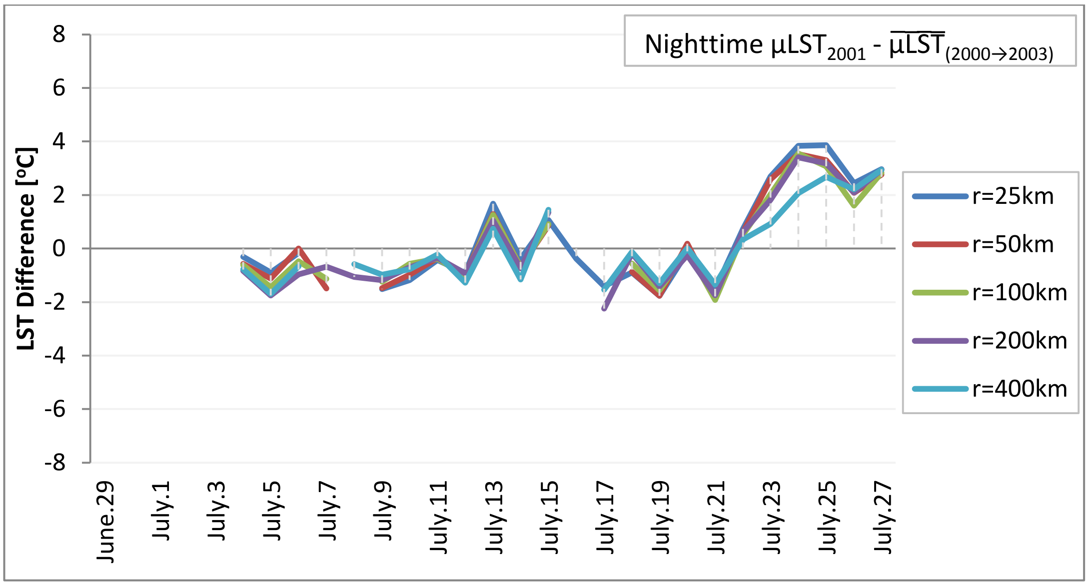

Figure 22: Distribution of spatially averaged nighttime LST differences comparing 2001 and temporal mean [μLST_{2001} - $\overline{\mu LST}_{(2000 \rightarrow 2003)}$]

The last pair of graphs shows the distribution of spatially averaged LST differences comparing 2000 and the temporal mean (Figure 23 and 24). The plot of the daytime averages shows a positive LST difference for the most of the days which means the LST for the region is higher than the temporal mean. A drastic fall, however, is seen on the plot between the days July 17th and July 18th with around 9°C (Figure 23). Furthermore, when the nighttime distribution graph is examined there is no significant positive or negative LST difference is observed which means in 2000 the nighttime LSTs are almost the same with the temporal mean (Figure 24).

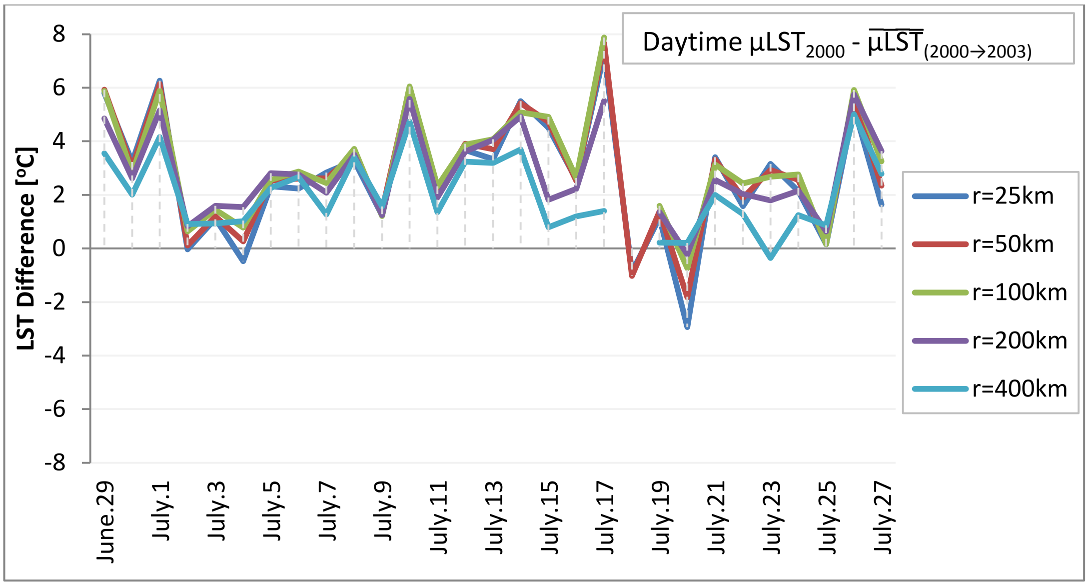

Figure 23: Distribution of spatially averaged daytime LST differences comparing 2000 and temporal mean [μLST_{2000} - $\overline{\mu LST}_{(2000\rightarrow2003)}$]

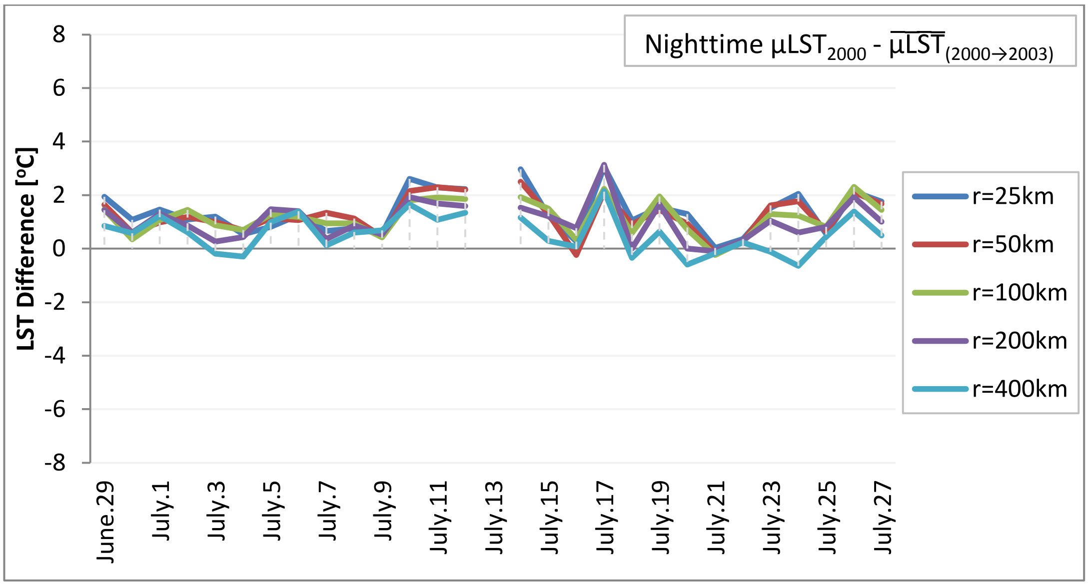

Figure 24: Distribution of spatially averaged nighttime LST differences comparing 2000 and temporal mean [μLST_{2000} - $\overline{\mu LST}_{(2000\rightarrow2003)}$]

4.4. LST Differencing of pixels based on multiple years

Spatial distributions of daytime and nighttime LST differences representing the earthquake year are shown in the following figures (Figure 25-30). As described before pixel values (LST differences) less than $0^{o}C$ are classified in the same class while the rest of the pixel values are further divided into $2^{o}C$ intervals. Analysis of daytime images shows that LST rises for several days in 2003 and therefore positive thermal anomaly can be seen in the resultant images. The thermal anomaly is first seen on June 29th mainly Central and Central Northern Turkey however the next day the presence of the anomaly fades away. Again, starting with July 2nd the thermal anomaly can be seen in Western and Central Turkey as well as Eastern Balkans. On the following days until July 6th anomalous pixels can be seen mainly over Central Turkey, Syria, Iraq, Georgia and Russia. In this interval the largest spatial extent of anomalous pixels is observed on July 3rd however the highest intensity is observed on July 4th. The anomalous pixels with the highest intensities first appear over Central Turkey and then move towards Russia (Figure 25, July 3rd to July 6th). In the analysis of daytime images on July 12th one day before the earthquake strikes LST anomaly is also observed mainly over Georgia, Russia and Eastern Turkey. Additionally, after the earthquake on July 15th, July 19th, July 17th and July 21st in the daytime images anomalous pixels are also observed over Central Turkey and Syria respectfully (Figure 26). After July 21st until July 27th the last day of the analysis anomalous pixels with low intensities and very limited spatial extent if not no anomalous pixels are observed (Figure 27).

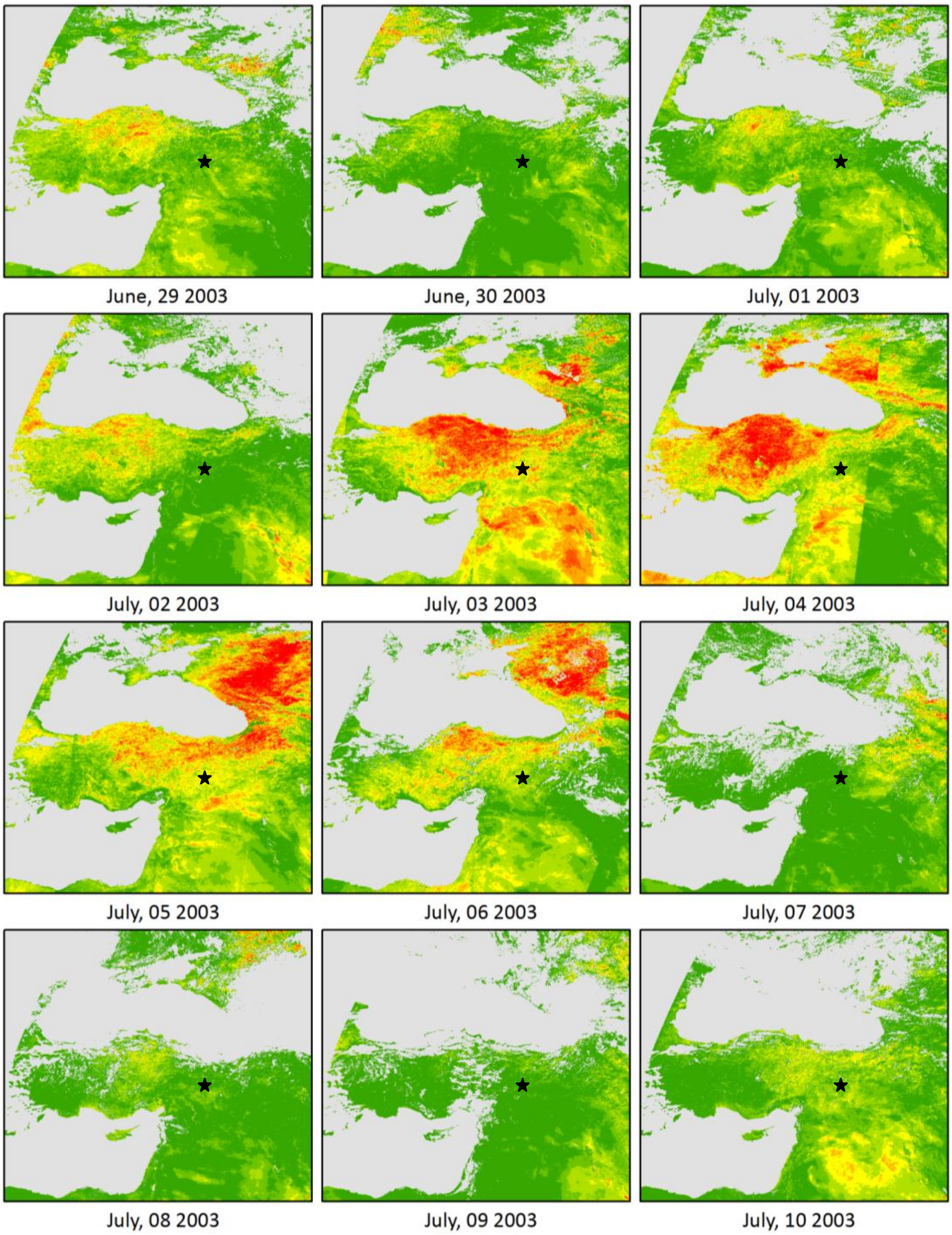

Figure 25: Spatial distribution of daytime LST differences comparing 2003 with the historical mean based on pixel values [June 29 – July 10] *Star icon indicates the epicenter of July 13, 2003 earthquake*

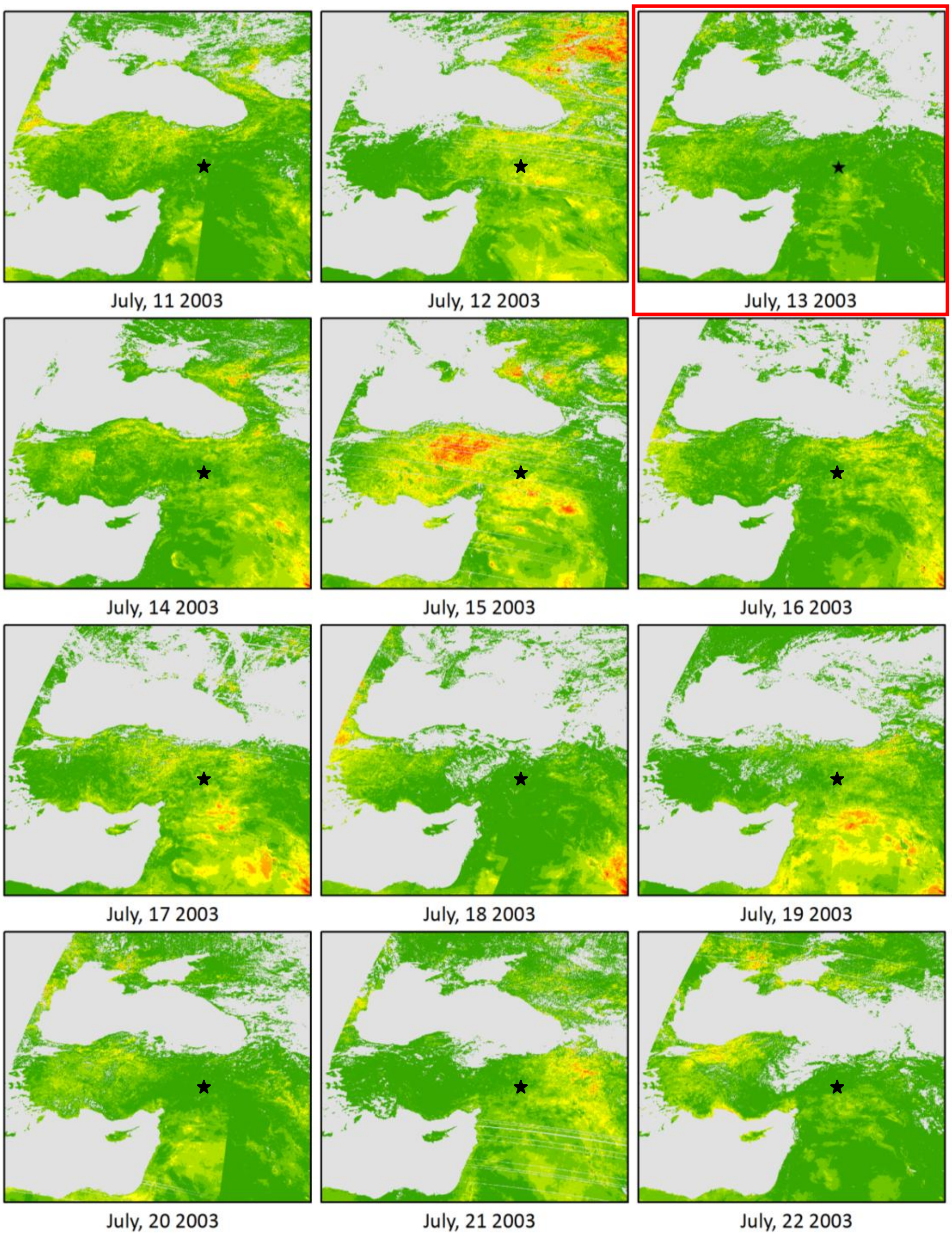

Figure 26: Spatial distribution of daytime LST differences comparing 2003 with the historical mean based on pixel values [July 11 – July 22] *Star icon indicates the epicenter of July 13, 2003 earthquake. Note that the red box indicates the day of the earthquake*

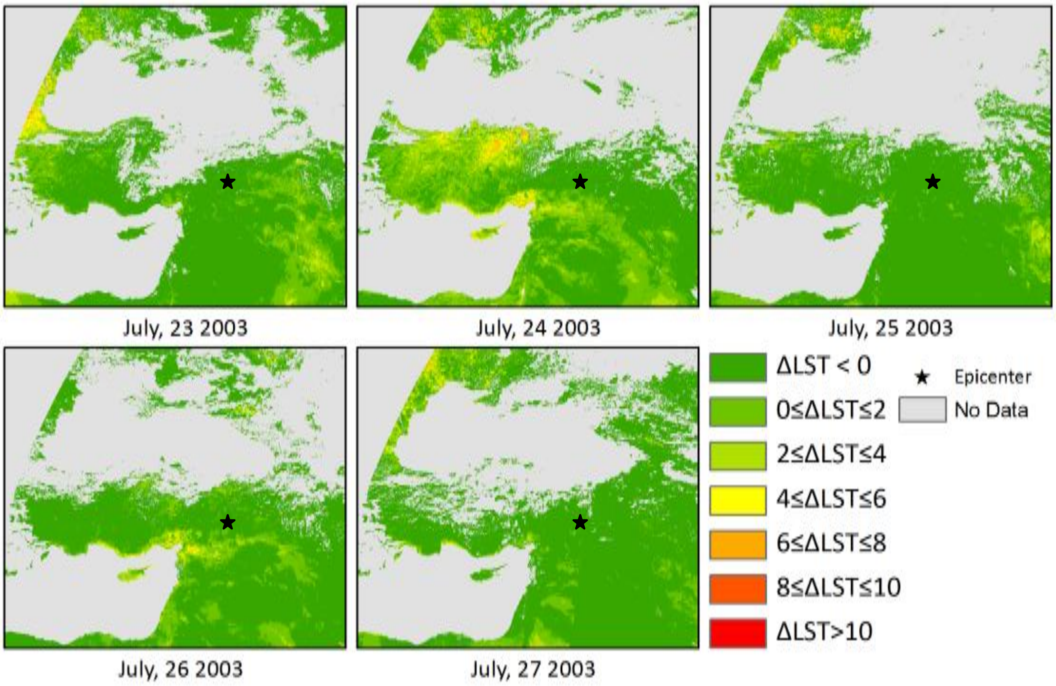

Figure 27: Spatial distribution of daytime LST differences comparing 2003 with the historical mean based on pixel values [July 23 – July 27] *Star icon indicates the epicenter of July 13, 2003 earthquake*

In the analysis of nighttime images it is observed that on the aforementioned days (July 3rd to July 6th) anomalous can also be seen however the intensity of the anomaly and the extent of the LST anomaly show different characteristics than the daytime images (Figure 28). For the days July 15th, July 17th, July 19th and July 21st where thermal anomaly is observed on the daytime images no thermal anomaly can be seen on the nighttime images (Figure 29). Since the intensity observed in the daytime is absent in the nighttime, it can be said that the Sun's irradiation during the day has considerable influence on the development of thermal anomaly which is detected by LST differencing of pixels.

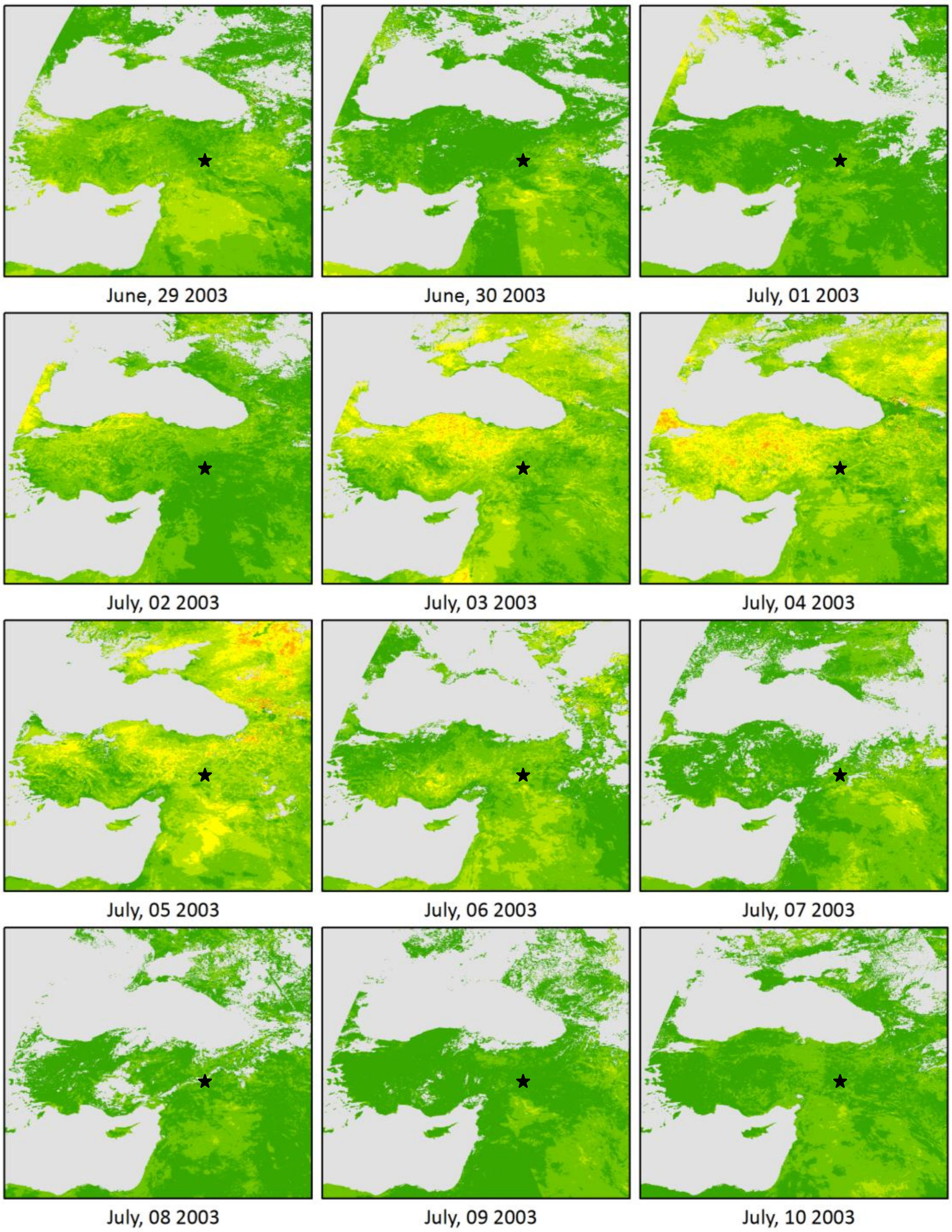

Figure 28: Spatial distribution of nighttime LST differences comparing 2003 with the historical mean based on pixel values [June 29 – July 10] *Star icon indicates the epicenter of July 13, 2003 earthquake*

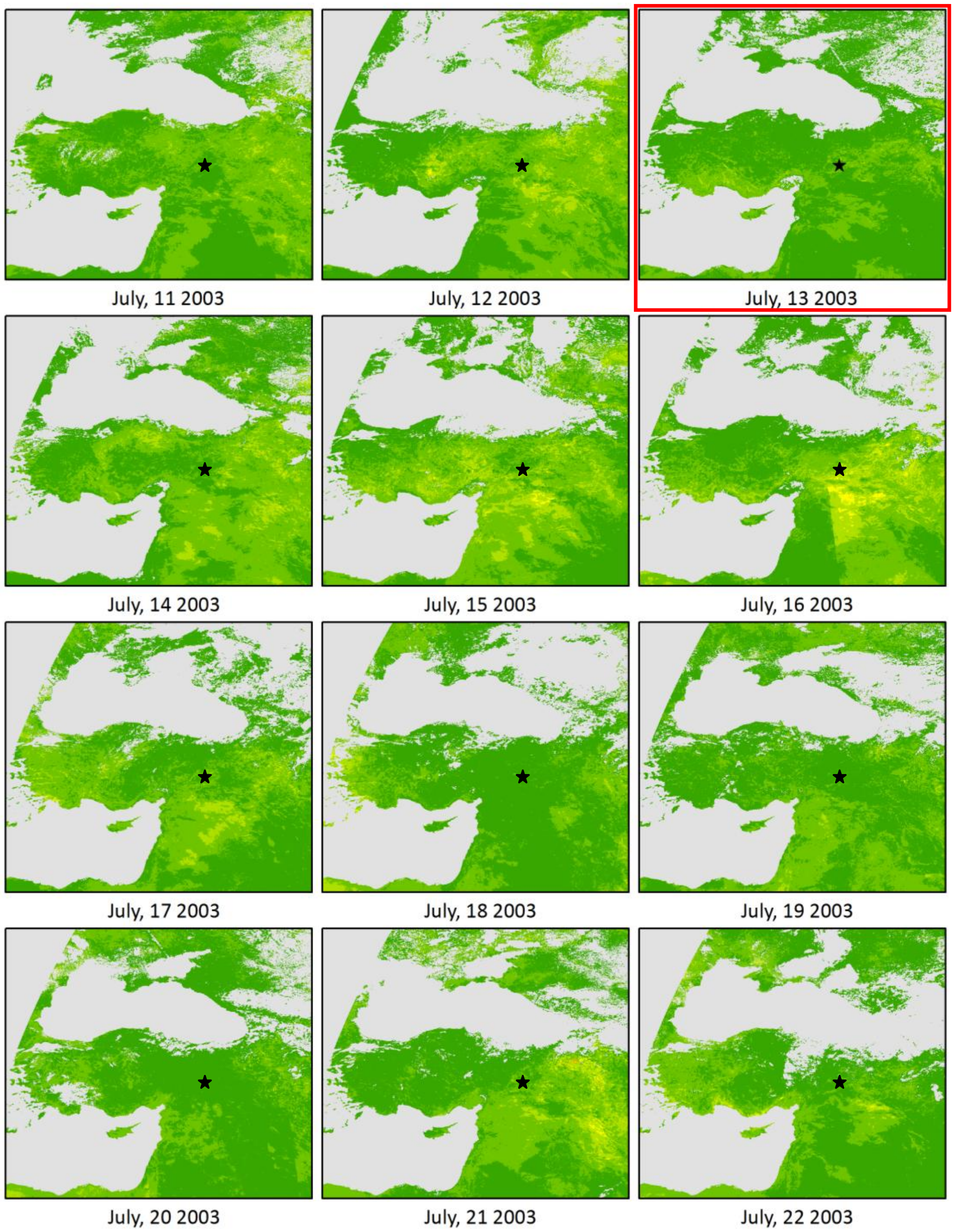

Figure 29: Spatial distribution of nighttime LST differences comparing 2003 with the historical mean based on pixel values [July 11 – July 22] *Star icon indicates the epicenter of July 13, 2003 earthquake. Note that the red box indicates the day of the earthquake*

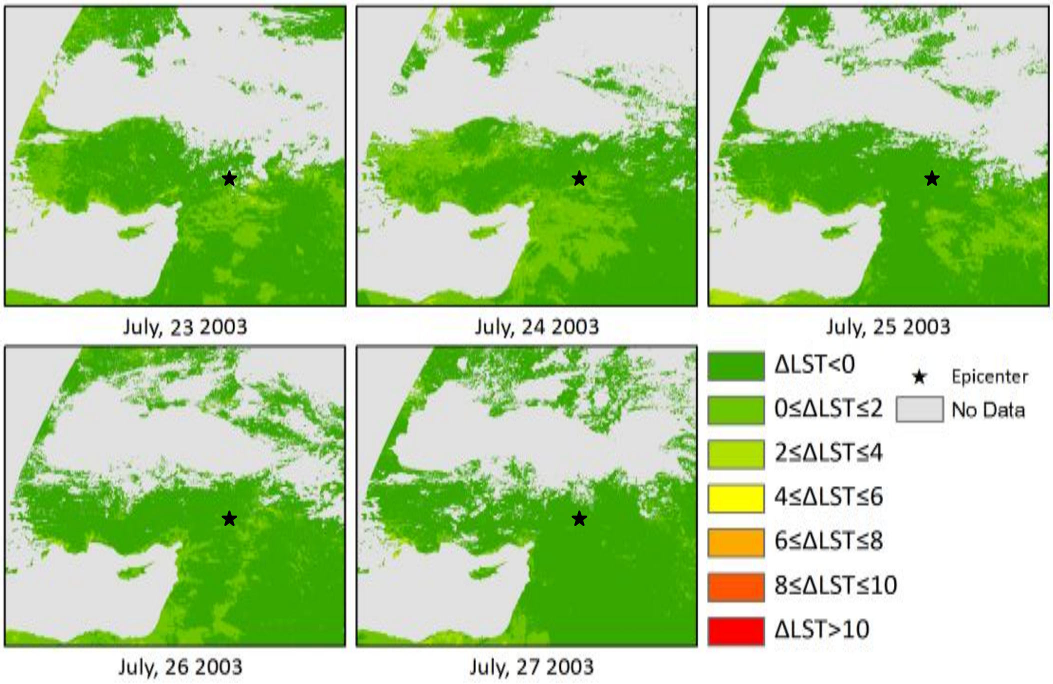

Figure 30: Spatial distribution of nighttime LST differences comparing 2003 with the historical mean based on pixel values [July 23 – July 27] *Star icon indicates the epicenter of July 13, 2003 earthquake*

Moreover, when the daytime and nighttime images representing the non-earthquake year are examined thermal anomalies are also seen. Similarly, the intensity of daytime anomalies is higher than the same of nighttime. The thermal anomalies of the non-earthquake year during the daytime are even more intense when it is compared with the ones of the earthquake year. For instance, anomalous pixels with 6 to 10°C can be seen between June 29th and July 17th on the daytime images of 2000 (Figure A1 and A2). On the following six days the thermal anomaly still exits but the intensity is slightly decreased. Then, starring with July 23rd until July 27th the anomalous pixels can be seen again with high intensities (Figure A3). The anomalous pixels that show positive thermal anomaly can be seen not only over the area of interest – South Eastern Turkey but also over far-out areas over the entire country and neighboring countries. Note that the figures regarding the non-earthquake year daytime and nighttime LST anomaly images can be found in Appendix A.1 and A.2.

4.5. Robust Satellite Technique (RST)

The reference images to be used for RST are generated as described in methods section. Following images are daytime reference images for June and July showing the time average and standard deviation for two months (Figure 31 and 32).Note that the nighttime reference images can be found in Appendix A.3 (Figure A7 and A8). By utilizing the reference images for month June and July in the RETIRA equation images that show the spatio-temporal change of R index are generated. As mentioned before RETIRA indices are divided into classes that show the variation of the pixel value from its normal/expected value.

Note that as described before the intervals for R index values are defined as $R_I \leq -3.5$, ≤ -3.0, ≤ -2.5, ≤ 2, $-2 < R_I < 2$, ≥ 2, ≥ 2.5, ≥ 3 and ≥ 3.5 in order not only to see the positive variability but also the negative variability of LST over space and time.

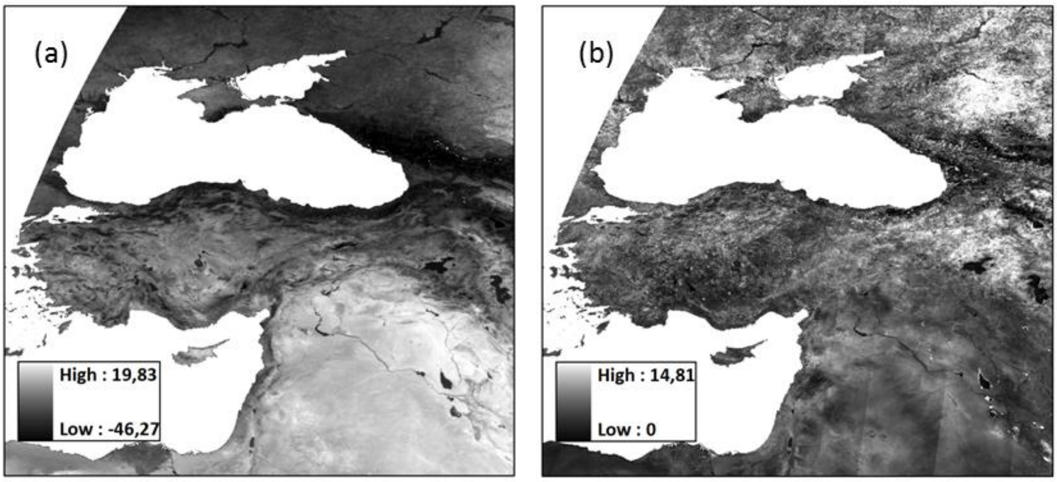

Figure 31: Daytime reference images (a) μΔLST(r) time average for month June and (b) σΔLST(r) standard deviation for month June computed over years (2000-2006)

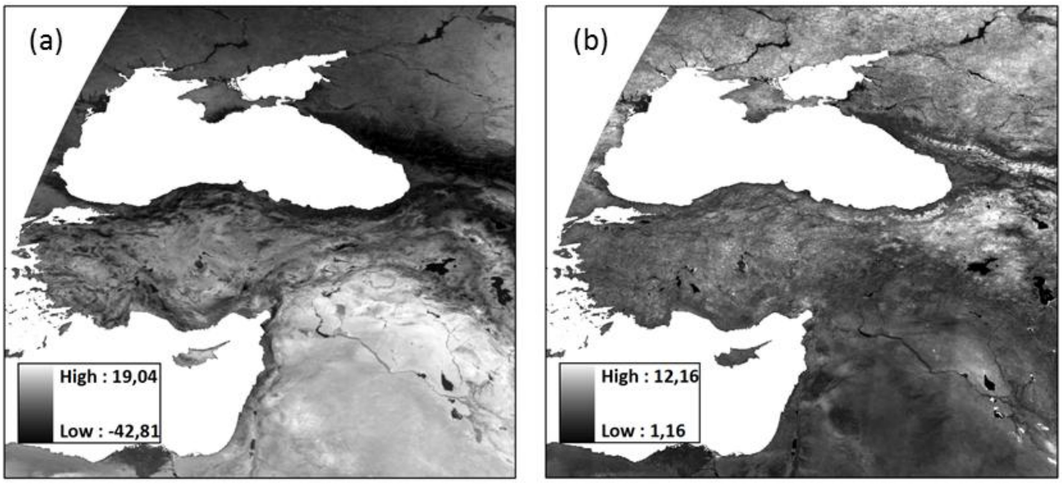

Figure 32: Daytime reference images (a) μΔLST(r) time average for month July and (b) σΔLST(r) standard deviation for month July computed over years (2000-2006)

As seen in the figures of daytime RETIRA index computation (Figure 33-35) anomalous pixels that indicates a positive variation can be seen on June 29th and soon after they disappears. On July 02nd until July 07th anomalous pixels affecting the region can be seen clearly over Eastern Balkans, Northern Turkey and Syria, Central Turkey and finally over Russia respectfully (Figure 33). Between July 7th and the day before the earthquake there is no anomalous pixel is observed. On July 12th anomalous pixels start to appear again over Russia with limited spatial distribution. Except the days July 15th, July 19th and July 21 there is no anomalous pixel affecting the region between July 13th and July 27th – the last day considered for the analysis These findings are consistent with findings of the previous method – LST differencing of pixels based on multiple years where anomalous pixels are observed affecting Central Turkey and Southern Russia on July 15th; Iraq on July 19th and Syria on July 21st with variable and limited spatial distribution (Figure 34). However, in a similar manner there is no convincing evidence that shows the direct link between the anomaly and the seismic activity.

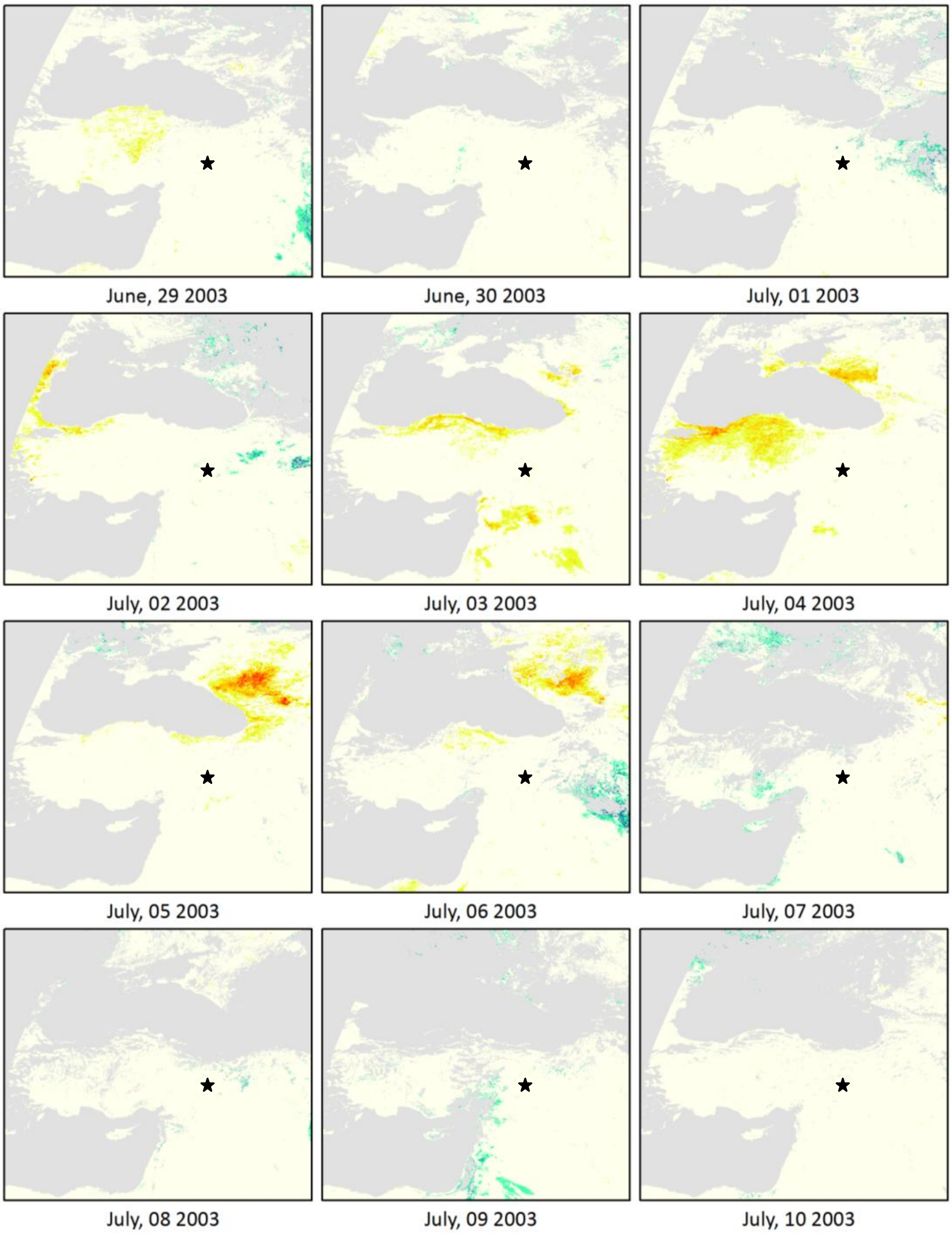

Figure 33: Results of daytime RETIRA index computation for earthquake year (2003) [June 29 – July 10] *Star icon indicates the epicenter of July 13, 2003 earthquake*

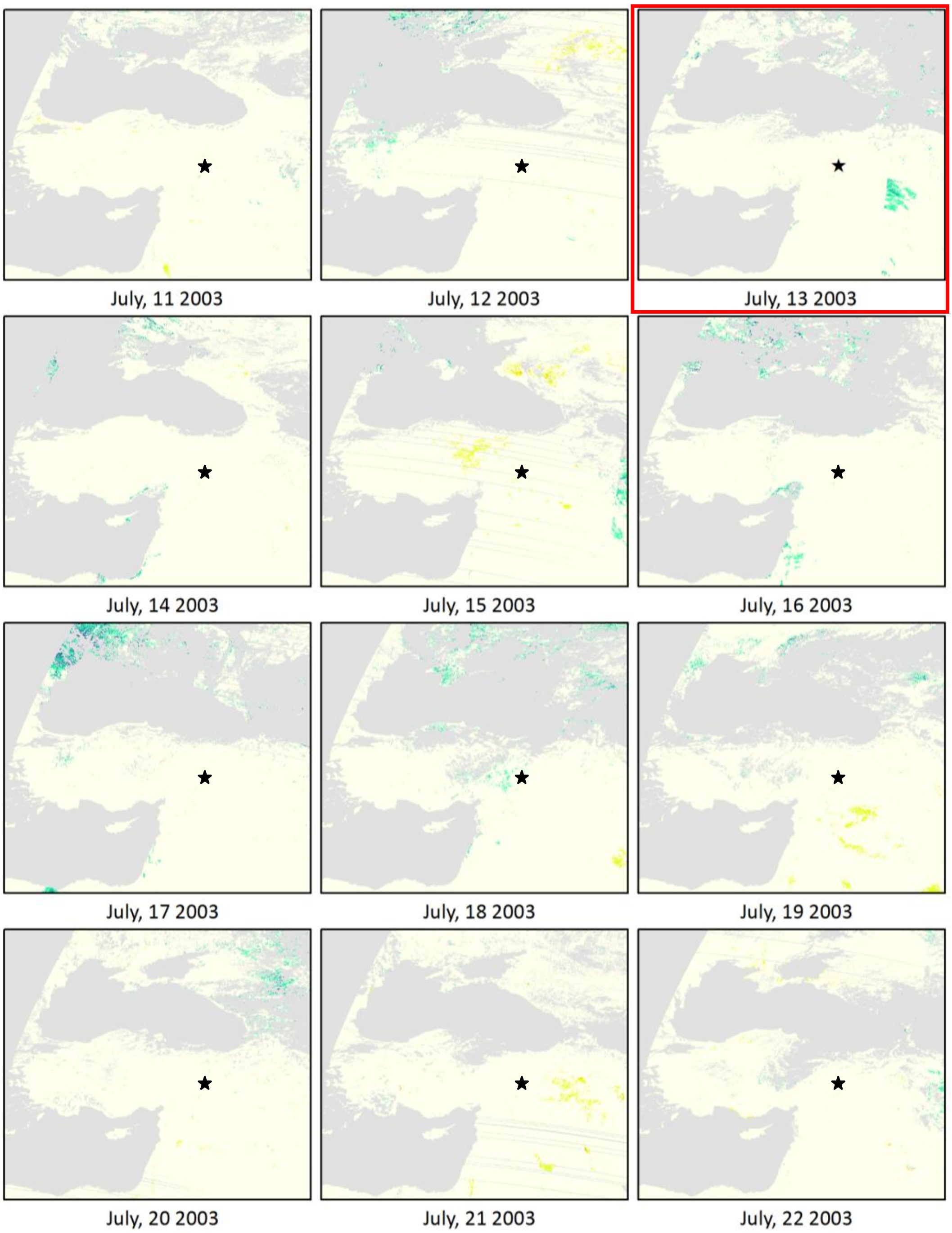

Figure 34: Results of daytime RETIRA index computation for earthquake year (2003) [July 11 – July 22] *Star icon indicates the epicenter of July 13, 2003 earthquake. Note that the red box indicates the day of the earthquake*

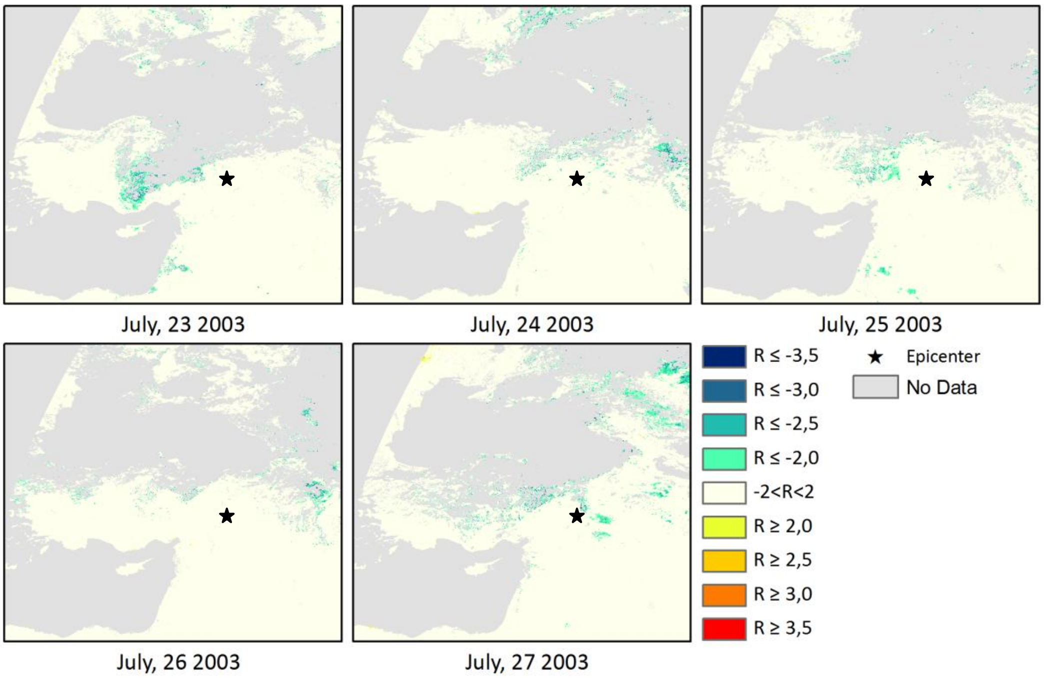

Figure 35: Results of daytime RETIRA index computation for earthquake year (2003) [July 23 – July 27] *Star icon indicates the epicenter of July 13, 2003 earthquake*

The nighttime RETIRA index computations show a bit different distribution pattern than daytime computations (Figure 36-38). The presence of anomalous pixels starts on June 29th and lasts until July 4th yet again with variable spatial distribution. However, anomalous pixels seen on July 5th and July 6th for the daytime computation are missing for nighttime computations (Figure 36). On June 29th, anomalous pixels are affecting North Western Turkey, Syria and Iraq. On June 30th and July 1st a very limited number of anomalous pixels are affecting Iraq and Eastern Balkans, respectfully. Between July 2nd and July 4th anomalous pixels of the region can be seen clearly which basically affect North Western Turkey and Central Turkey. Starting with July 4th the anomalous pixels fade away and on July 5th variable spatial distribution of anomalous pixels can only be seen in Central Turkey and South Russia. For the rest of the day until the end of the analysis no anomalous pixel is observed (Figure 37 and 38).

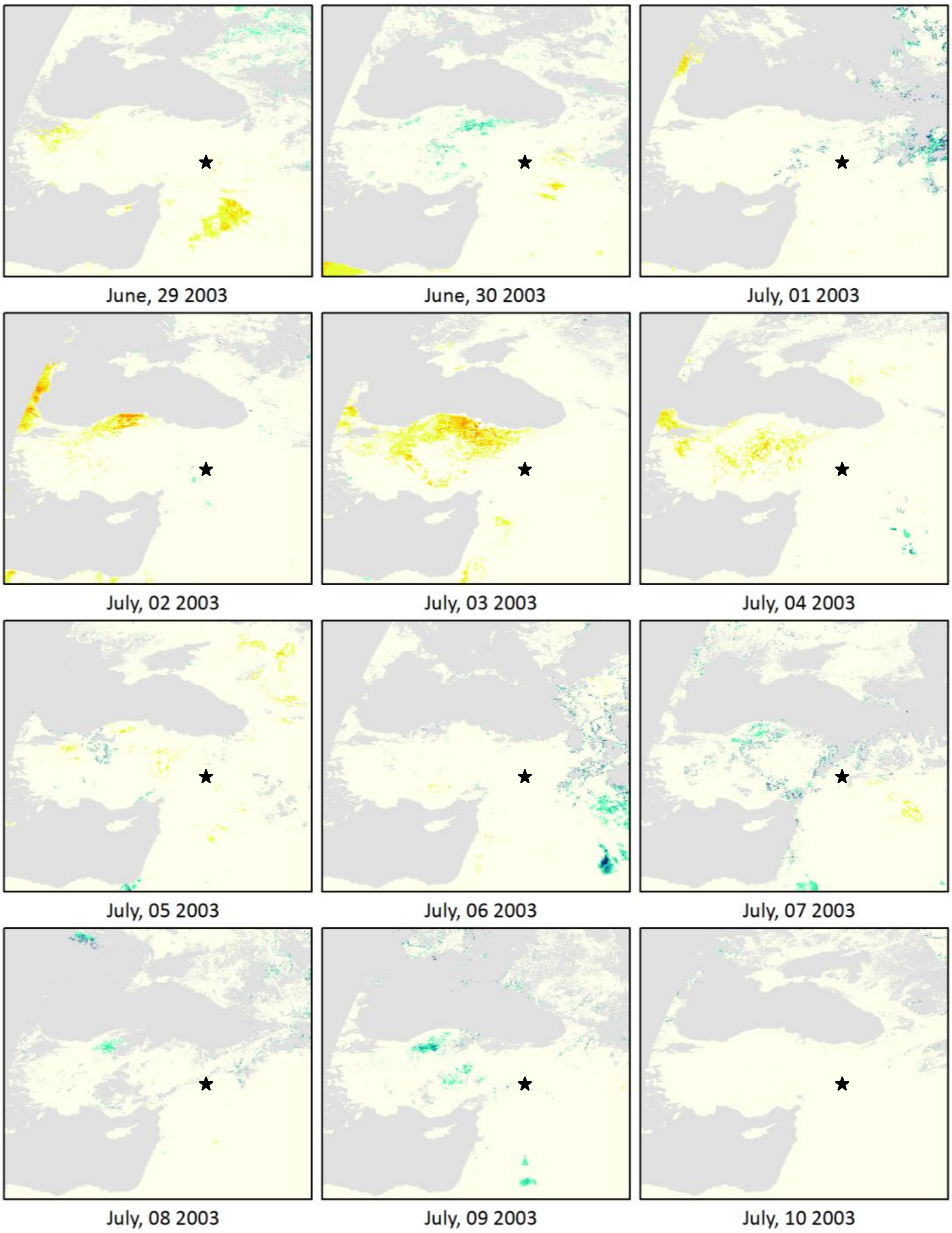

Figure 36: Results of nighttime RETIRA index computation for earthquake year (2003) [June 29 – July 10] *Star icon indicates the epicenter of July 13, 2003 earthquake*

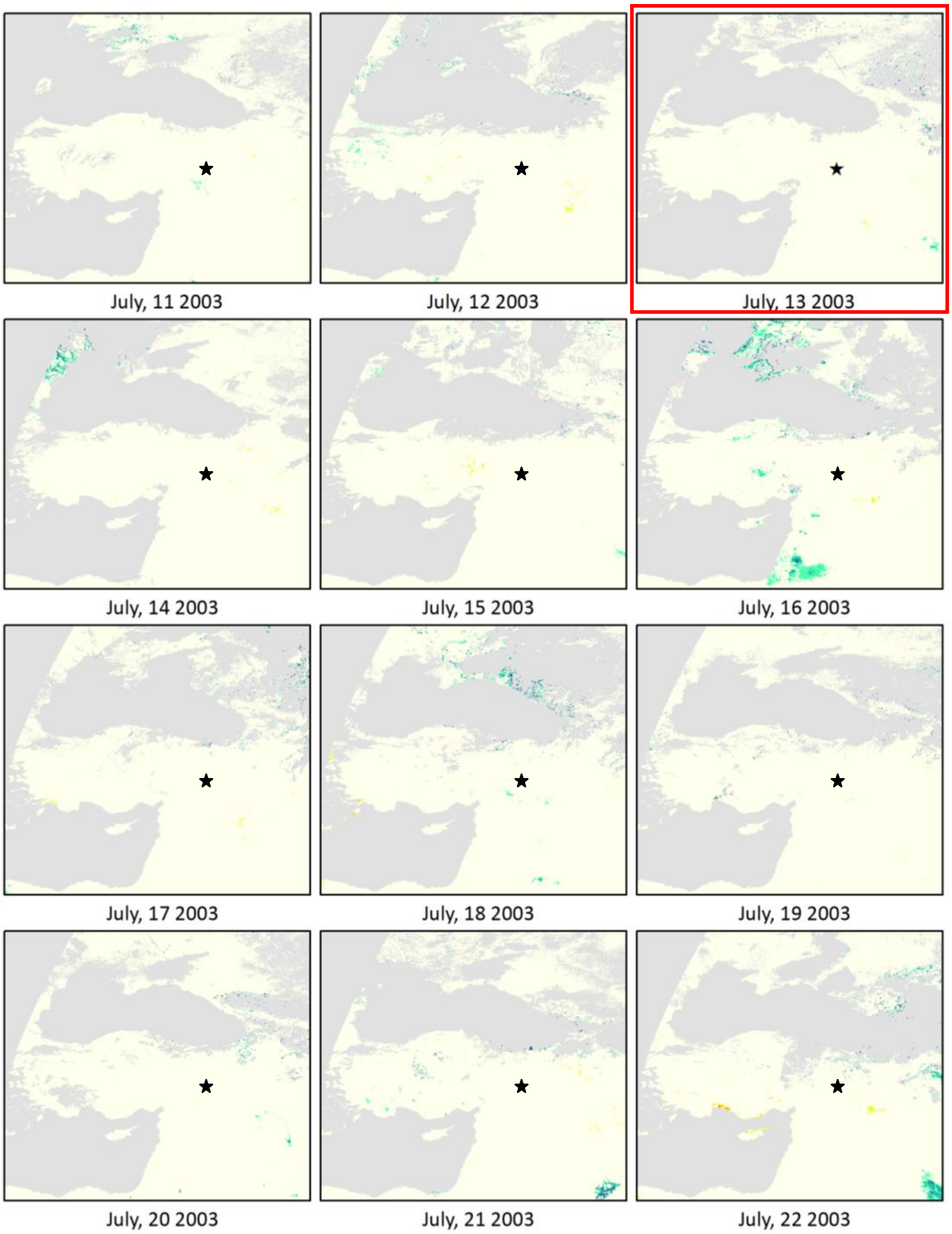

Figure 37: Results of nighttime RETIRA index computation for earthquake year (2003) [July 11 – July 22] *Star icon indicates the epicenter of July 13, 2003 earthquake. Note that the red box indicates the day of the earthquake*

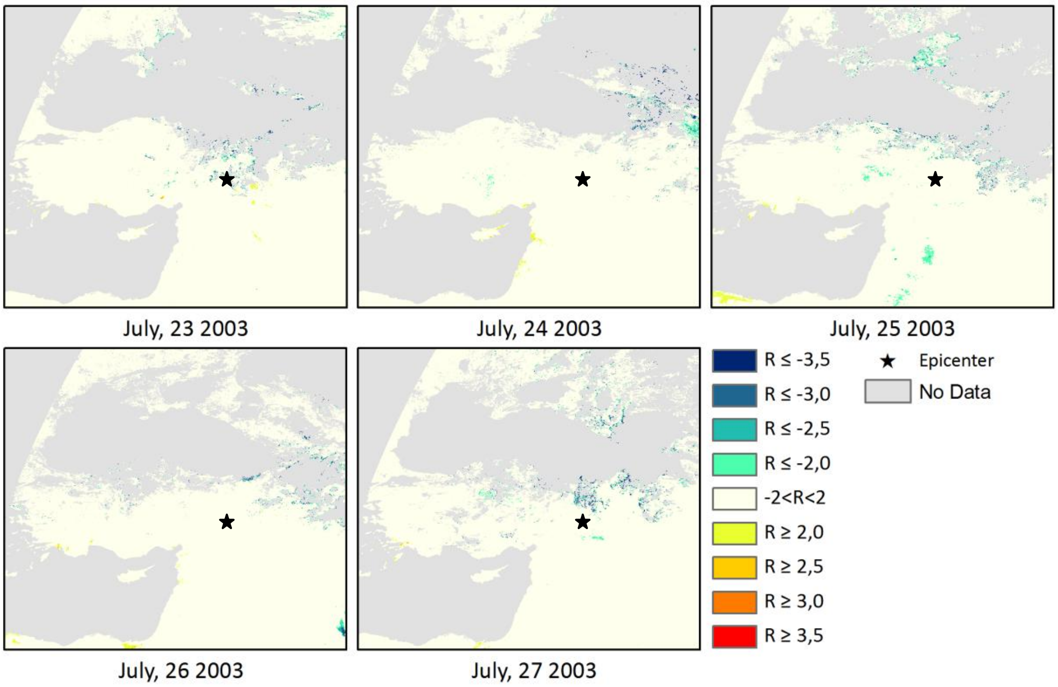

Figure 38: Results of nighttime RETIRA index computation for earthquake year (2003) [July 23 – July 27] *Star icon indicates the epicenter of July 13, 2003 earthquake*

As described before RETIRE index was computed for daytime and nighttime images of the year 2000 which represents the non-earthquake year.(Figure A9-A14) The figures showing the results can be found in Appendix A.4 and A.5. For the daytime computations it is clearly seen that between June 29th and July 17th anomalous pixels are observed with various intensities and spatial extent. Particularly, on July 9th and 13th anomalous pixels with high intensities affecting Western Turkey are highly visible (Figure A9 and A10). On July 12th, 14th, 15th and 17th anomalous pixels affecting Eastern Turkey can also be seen. Note that anomalous pixels are affecting Eastern Turkey on July 12th then Western Turkey on July 13th and on July 14th turns to Eastern Turkey again which reveals unsustainable results. Therefore, it can be said that environmental factors have also considerable influence on RST computations. Similarly, anomalous pixels with variable intensities and spatial extents are also observed for the nighttime computation which supports the aforementioned argument (Figure A12-A14).

5. Discussions and Conclusions

The objective of this study was to evaluate already suggested remote sensing method for detection of thermal anomalies prior to Malatya-Pütürge-Doğanyol earthquake. It was also aimed to compare the influence of different approaches on LST detection.

The first method used for the study was the LST differencing of spatial averages based on two years mainly the earthquake year and one of the previous non-earthquake years. In order to see the influence of the area on the analysis, spatial averages were calculated over five different areas. The method is a deductive method in its nature such that the epicenter is already known and the areas on which the spatial averages calculated are defined in accordance to the location of the epicenter. However, since the epicenters are not known for impending earthquakes as well as the possible areal extent where the anomaly can be observed prior to the earthquake the definition of the areas in order to calculate the spatial average would be tricky. If the area is defined too large the values of anomalous pixels will smooth out and also be affected by the values of far-out pixels which will prevent the average showing the characteristics of the area of interest. On the contrary, if the area is defined too small there is the possibility to miss out the anomalous pixels to be used for spatial averaging. Nonetheless, for this study it was observed that the areas used for the calculations with varying radii between 25km and 400km have a slight influence on the daily average LST calculations. The reason for that would be the fact that the temperature change affected the whole region commensurably. Furthermore, since the calculations are based on two years both the year of interest and the reference year used for differentiation have considerable influence on the calculations as seen in the results where LST anomaly can be seen between one earthquake year and one non-earthquake year as well as two non-earthquake years for the area of interest in this study. Additionally, the days on which LST anomaly is observed in daytime and nighttime observations were inconsistent for different pairs of years used for the analysis.

The second method used for this study was an extended version of the previous method in which instead of using two distinct years temporal means of the spatial averages of 4 years including the earthquake year were calculated over the same areas defined before. The idea of the calculation of temporal mean was to mitigate the individual influence of the reference year used for differentiation. By this the earthquake year and also the non-earthquake years could be compared independently. When it is compared with the previous method utilizing temporal mean as reference is more informative and representative for the region; therefore, it can be said that instead of using an individual year as reference, temporal mean would be more appropriate. The overall results, however, did not change except the decrease of the intensities of the observed LST anomalies. Similarly, LST anomalies or more precisely LST differences between the year of interest and the temporal mean could be detected consistently with this method using satellite data. On the other hand, when the method is utilized for the area of interest LST anomaly was observed between the earthquake year and the temporal mean, as well as between the non-earthquake years and the temporal mean for the same time interval. Since this method is only an extension of the first method all the observations mentioned for the previous method also stand for this method. Therefore, the definition of the areas is an issue for this method as well. As mentioned, since the epicenters are not known for earthquakes which have not occurred yet; it is not possible to define areas for spatial averaging for impending incidents. Therefore, LST differencing methods both based on two years and multiple years would not be informative and feasible for earthquake monitoring purposes.

In the third method, instead of spatial averages pixel values were directly utilized. Primarily, the historical temporal mean was calculated over 7 years of data for both daytime and nighttime. Then the values of the years of interest (2003 representing the earthquake year and 2000 representing the non-earthquake year) and the temporal mean were differentiated. Unlike the previous methods, the epicenter location is not needed for this method therefore it can be said that it has inductive and straightforward analysis approach. Only the satellite images that cover the area of interest are sufficient for the utilization of the method. Level of detail of information can also be preserved and the result is not affected by the size of the area of interest since the analysis is based on per-pixel values and no averaging is needed. Anomalous pixels can be seen on both daytime and nighttime images of earthquake year with varying intensities for Malatya-Pütürge-Doğanyol earthquake. However, the days that the LST anomalies are observed in daytime and nighttime analyses are not consistent and the intensities of anomalies vary from daytime to nighttime images. Furthermore, when the daytime and nighttime LST difference images of non-earthquake year (2000) were examined anomalous pixels were also observed in spite of the absence of seismic activity.

The last method used for this study is Robust Satellite Technique (RST) which utilizes RETIRA index calculated based on normal TIR response (Signal) and the natural variability of TIR response (Noise) ratio over time. In a similar manner with the previous method RST is also an inductive method however the total area for which RST is computed has also significance in this method. In order to calculate Signal and Noise values it requires the spatial averages of scenes for year of interest, all the years included in time average and standard deviation calculations. Therefore changing the area may change the outcome as the spatial average is likely to be changed as well. In other words, statistical significance of R index is sensitive to choice of both time period and the choice of study area. On the other hand, the nature of the method makes it applicable for different geographical locations and different sensors. One of the unclear issues regarding the method is the variability of thresholds and accepted ranges that show anomalous pixels. In general, the pixels having R index values ≥ 2, 2.5 or 3.0 are considered to be anomalous however the degree of anomaly is not defined in the literature. This issue becomes more complicated when comparing the daytime and nighttime values of R index. In this study, for both daytime and nighttime analysis anomalous pixels affecting the area of interest were observed for a few of days before and also after the earthquake. Negative anomalies are observed as common as positive anomalies. Although the days were consistent with the observations of previous methods in a similar manner with the previous methods the intensities observed in daytime and nighttime images are different as well as the days the anomalous pixels observed. Furthermore, anomalous pixels affecting the area of interest and neighboring areas were also observed for non-earthquake year (2000). Note that there is no earthquake magnitude more than 5 is reported within the time interval used for the analysis in the entire country.

Regarding the data used for the analysis, although the accuracy of MOD11A1 product is claimed to be ±1^{o}C in previous studies and quality assessment has been done before the image analysis, there are abrupt and unexpected changes between adjacent pixels which makes the values and the accuracy of the pixels questionable (Figure 25, [July 4th, July 6th]; Figure 26, [July 11th, July 18th, July 20th]; Figure 28, [June 30th], Figure 29, [July 16th]). These abrupt changes of pixel values manifest themselves as sharp boundaries on the image and can be found in some of the day and nighttime images. The reason for such errors might be related with the sensor itself, with the split window algorithm or more likely to be related with the algorithm used generating MOD11A1 products out of MOD11_L2 products.

When the results were examined only for the earthquake year, it is concluded that all four methods revealed LST anomalies in the area prior to the earthquake. In other words, regardless the approach and the method utilized LST anomaly could be detected before the earthquake. The observed LST anomalies are focused the days between July 3rd and July 6th 2003, 7 to 10 days before the earthquake. Therefore, at the first glance, based only on the analysis of the earthquake year it can be said that LST anomalies detected as earthquake precursor prior to Malatya-Pütürge-Doğanyol earthquake. This early interpretation based only on the analysis of the earthquake year, however, would be inadequate. Further observations showed that LST anomalies could also be seen after the occurrence of the Malatya-Pütürge-Doğanyol earthquake. Furthermore, when the results for non-earthquake year were examined regardless of the method LST anomalies were also observed for the same area for the equivalent time span. Since the LST anomalies are not unique for the year of the earthquake and were also seen for the non-earthquake year, it can be concluded that positive LST response in the earthquake year would be due to environmental factors rather than the occurrence of the Malatya-Pütürge-Doğanyol earthquake. Observing positive LST response for the non-earthquake year also supports this conclusion. Furthermore, positive LST responses for both earthquake year and non-earthquake year lose intensity from daytime to nighttime which also indicates that environmental factors are predominant on LST change. In brief, since there is no unique pattern of the LST anomaly for the earthquake year and no coherent evidence that shows that LST anomaly is caused by the stress accumulation prior to Malatya-Pütürge-Doğanyol earthquake, it can be said that LST anomaly is not directly related with the occurrence of the Malatya-Pütürge-Doğanyol earthquake.

It will not be irrelevant comment that if the LST of a particular region increases more than expected due to environmental factors such as increase of the Sun's irradiation, local air temperature, humidity, etc. all of the methods discussed above would reveal LST anomaly which is obviously not related with the occurrence of the earthquake. In other words, in spite of the absence of the earthquake in a particular region LST can increase and LST anomaly can be observed. Therefore using LST anomalies for earthquake monitoring might be inconclusive for such cases, which is the case for Malatya-Pütürge-Doğanyol earthquake. On the other hand, even if there is LST anomaly due to stress accumulation prior to earthquake, it might be suppressed/masked by the environmental factors. Therefore it can be said that regardless of the method utilized LST change detection based on satellite images can be affected by environmental factor, substantially. However, this phenomenon cannot be identified by satellite imagery. This property of LST anomaly also makes it unreliable for monitoring purposes. In addition to the aforementioned environmental factors, the study area (topography, geological setting, rock/soil type, etc.) and the time of the observation have considerable effect on the results as well as the intrinsic properties of the earthquake (i.e. magnitude, depth, etc.). For study area it can be said that area with low natural LST variability would be more appropriate for detection of LST change based on satellite thermal imagery. Regarding the time of the observation for the analysis nighttime images would be more appropriate since the effect of the Sun's irradiation is minimal during night.

Even though the results of the methods are quite similar the delivery formats of methods are discrete. The results of the first two methods are delivered in graphs which do not provide visual information in terms of spatial coverage and extent. On the other hand, remainder methods provide information visually comprehensible and self-explanatory in terms of spatial coverage and extent.

Unlike some of the studies in the literature which revealed direct relation between the occurrence of the earthquake and the LST anomaly, in this study it is found that the LST anomalies are not observed uniquely prior to the Malatya-Pütürge-Doğanyol earthquake and there is no coherent evidence found that shows LST anomalies observed are directly related with the occurrence of the earthquake. One of the possible reasons for such a diverse result would be the different characteristics of the earthquakes including magnitude, tectonic regime, focal mechanism and depth of the focus as well as the geological setting of the region including the rock and/or soil type and therefore internal properties of the rock and/or soil (i.e. heat capacity, thermal conductivity, etc.). Another possible explanation would be thermal anomalies due to seismic activities exist however suppressed or masked by other factors, mainly, obviously, by environmental factors. Furthermore, as mentioned before, most of the studies, except some, focused only on the year of the earthquake and the situations for non-earthquake year would have remained unresolved.

Land Surface Temperature change (LST anomaly) as a precursor prior to an earthquake is an incident dependent and unique manifestation of the stress accumulation for and only for the individual earthquake in a similar manner with foreshocks (as seismic precursor). In other words, LST change – if it occurs – has a unique pattern for an individual earthquake and directly related with the individual earthquake it precedes. This means LST change prior to an earthquake is not a potential but rather dynamic property for an earthquake which makes it incomparable between different incidents. Furthermore, as noted in the literature not all the earthquakes are preceded by a precursor (thermal and/or seismic) just like foreshocks (i.e. foreshocks might or might not be observed prior to the earthquakes) (Freund 2007; Saraf et al. 2009; Pulinets 2006). On the other hand, findings of this particular study also supports that not every LST anomaly is followed by an earthquake. Additionally, the explanations proposed for the mechanism of the precursors lack consistency which remains LST anomaly inconclusive as a precursor for impending earthquakes. Therefore, it is concluded that utilizing merely LST anomalies based on satellite images in order to monitor and forecast impending earthquakes would not be adequate and feasible. Note that in the literature all the studies regardless of the methods utilized are retrospective in their nature such that the studies were conducted after the earthquake. Therefore, time and date as well as the intrinsic properties of the earthquake are already known. In other words, there is no prudential study which has successful or promising forecasting results has been reported yet. It is also stated that based on the present knowledge and techniques in seismology it is still not possible to forecast seismic activities with precision in terms of time, location and magnitude (Saraf et al 2009). Unless the mechanism of the thermal precursors is very well understood, monitoring impending incidents by use of satellite thermal imagery does not seem to be conclusive and feasible in the near future.

5.1 Discussion on research questions

1. *Is there any LST anomaly prior to the Malatya-Pütürge-Doğanyol earthquake that can be detected by suggested remote sensing methods?*

   Land surface temperature anomalies were detected prior to the Malatya-Pütürge-Doğanyol earthquake by suggested remote sensing methods.
2. *Can the LST anomalies detected by the suggested remote sensing methods be due to the occurrence of Malatya-Pütürge-Doğanyol earthquake?*

Although the LST anomalies were detected before Malatya-Pütürge-Doğanyol earthquake there is no coherent evidence found that supports the direct link between the occurrence of the earthquake and LST anomaly. Since the observed LST anomalies are not unique for the year of earthquake and can also be observed in the absence of earthquake the LST anomaly cannot be directly related with the occurrence of the earthquake.

3. *How do different approaches of the suggested remote sensing methods affect the detection of LST anomalies?*

   The possible effects of individual methods have elaborately discussed in previous section.

4. *What are the strengths weaknesses of the suggested methods?*

   The strengths and weaknesses of different approaches of the suggested methods on LST anomaly detection is discussed in detail in the previous section.

5.2 Discussion on basic assumptions

1. *There exist LST anomalies prior to Malatya-Pütürge-Doğanyol earthquake which can be detected by suggested remote sensing methods.*

   According to the observations LST anomalies were detected by suggested remote sensing methods. Therefore, it can be said that the first assumption is validated.

2. *LST anomalies detected by suggested remote sensing methods are due to stress accumulation before Malatya-Pütürge-Doğanyol earthquake*.

   The LST anomalies are not observed uniquely prior to Malatya-Pütürge-Doğanyol earthquake and no coherent evidence could be found that shows a direct link between the stress accumulation and LST anomalies prior to Malatya-Pütürge-Doğanyol earthquake. Therefore, it can be said that the second assumption is confuted.

3. *Different approaches of suggested remote sensing methods do not affect the detection of LST anomalies.*

   With the results and discussions made different approaches of suggested methods affect the results of LST anomaly detection. Hence, it can be said that the third assumption is also confuted.

5.3. Limitations

1. Lack of in-situ validation was one of the biggest limitations for this study. Since the techniques are based only on the satellite data sets and thermal anomalies due to stress development before seismic activities is not well understood and identified yet validation of the techniques is still an issue.
2. The techniques mentioned and hence used for this study are based on multi-temporal analysis of satellite images. This multi-temporal analysis covers a wide time interval which varies from days to a few couple of weeks in one year and equivalent time interval over several years. Image acquisition for this time interval is not always possible throughout the year and over different years mainly because of climatological constraints such as cloud cover, bad weather conditions, etc.. Therefore, due to this issue applicability of remote sensing techniques for earthquake for earthquake monitoring is very limited. For instance, on Oct 23rd 2011, a highly destructive earthquake [M 7.3] struck city of Van (southeastern Turkey). Although it was a hot topic and it was intended to work on, due to the bad weather conditions satellite data was not available not only for 2011 but also for previous years for intended time span (fortnight before and after the earthquake).
3. Due to the time limitations for the study and the data availability the number of year utilized for the processing were limited to 4 for the first two methods and to 7 for the last two methods. Since the number of years prior to the year of the earthquake for the calculation of the temporal mean to be used as reference in the second method is limited only to 3 years (2000 – 2002) the year of the earthquake was also included in the temporal mean calculations although the possibility of bias on the calculations. However, when the temporal means including and excluding the earthquake year compared it is observed that the difference is negligible for the calculations (≤ 0.6 ^{o}C for nighttime observations and ≤ 1.0 ^{o}C for daytime observations) (Figure A15).
4. Although the accuracy of MOD11A1 was evaluated to be ± 1^{o}K and quality assessment has been done for all the images used for the analysis the accuracy of the LST values are questionable since some defects were observed on the images (i.e. unexpected and abrupt changes between adjacent pixels which follows a linear trend in the image).

5.4. Recommendation for future studies

1. Regarding the same earthquake and study area different algorithms in order to extract LST can be used as well as using different sensor data. Since the temperature calculations are based on emissivity values the better emissivity estimation means better temperature calculations. Therefore sensors with better radiometric resolution in TIR would help for better emissivity estimation which will lead more accurate LST calculation.
2. In addition to the mere LST values acquired from satellite images local parameters would be taken into account for LST anomaly detection analysis. These properties can be local air temperature, humidity, thermal inertia of the rocks, vegetation, ground and surface water presence, etc.
3. In most of the studies found in the literature information about the earthquakes were very limited. The focal mechanism and tectonic regime should also be taken into account as well as the parameters mentioned above since different mechanisms may affect the presence of thermal precursors prior to earthquakes.
4. As mentioned, yet the mechanism of thermal precursors is not very well understood and the possible explanations about the mechanism have not been accepted by scientific community. Until it is fully understood use of remote sensing for thermal precursor detection to be used for earthquake monitoring and forecast remains inconclusive. In order to help to understand the thermal precursor mechanism and reveal the similarities between earthquakes which were preceded by thermal precursors a model would be generated that covers as many earthquake as possible including all the effective parameters such as magnitude, focal depth, focal mechanism, tectonic regime, local environmental factors, rock/soil types, geological setting, etc. The results of the model would also give at least an insight about the direction of the future research and improvements.

Bibliography

AFAD. (2003). *Doğanyol (Keferdiz) Depremi-Malatya Basın Açıklaması.* Press Release, Bayındırlık ve İskan Bakanlığı-Afet İşleri Genel Müdürlüğü, Deprem Araştırma Dairesi Başkanlığı. [in Turkish]

Aliano, C.; Corrado, R.; Filizzola, C.; Genzano, N.; Pergola, N.; Tramutoli, V.;. (2008a). Robust TIR satellite techniques for monitoring earthquake actve regions: limits, main achievements and perspectives. *Annals of Geophysics, 51*(1), 303-318.

Aliano, C.; Corrado, R.; Filizzola, C.; Pergola, N.; Tramutoli, V.;. (2008b). Robust satellite techniques (RST) for the thermal monitoring of earthquake prone areas: the case of Umbria-Marche October, 1997 seismic events. *Annals of Geophysics, 51*(2/3), 451-459.

Becker, L.; Li, Z. -L.;. (1990). Towards a local split window method over land surfaces. *International Journal of Remote Sensing, 11*, 369-393.

Blackett, M.; Wooster, M. J.; Malamud, B. D.;. (2011). Exploring lans surface temperature earthquake precursors: A focus on the Gujarat (India) earthquake of 2001. *Geophysical Research Letters, 38*, L15303.

Carreno, E.; Capote, R.; Yague, A.; et al.;. (2001). Observations of thermal anomaly associated to seismic activity from remote sensing. *General Assembly of European Seismology Comission,Portugal*, 265-269.

Choudhury, S.; Dasgupta, S.; Saraf, A. K.; Panda, S. K.;. (2006). Remote sensing observations of pre-earthquake thermal anomalies in Iran. *International Journal of Remote Sensing, 27*(20), 4381-4396.

Coll, C.; Casellas, V.; Galve, J. M.; Valor, E.; Niclòs, R.; Sànchez, J. M.; et al. (2005). Ground measurements for validation of land surface temperatures derived from AATSR and MODIS data. *Remote Sensing of Environment, 97*, 288-300.

Filizzola, C.; Pergola, N.; Pietrapersota, C.; Tramutoli, A.;. (2004). Robust satellite techniques for seismically active areas monitoring: a sensitivity analysis on September 7, 1999 Athen's earthquake. *Physics and Chemistry of the Earth, 29*, 517-527.

Freund, F. (2002). Charge generation and propagation in igneous rocks. *Journal of Geodynamics, 33*, 543-570.

Freund, F. (2003). Rocks that crackle and sparkle and glow:strange pre-earthquake phenomena. *Journal of Scientific Exploration, 17*(1), 37-71.

Freund, F. (2007). Pre-earthquake signals-Part II: Flow of battery currents in the crust. *Natural Hazards and Earth System Sciences, 7*, 543-548.

Freund, F.; Keefner, J.; Mellon, J. J.; Post, R.; Takeuchi, A.; Lau, B. W.S.; La, A.; Ouzounov, D. (2005). Enhanced mid-infrared emission from igneous rocks under stress. *Geophysical Research Abstracts, 7*, 09568.

Geng, Q. (1985). *Scientia Sinica, B 28*, 323-336.

Genzano, N.; Alianno, C.; Filizzola, C.; Pergola, N.; Tramutoli, A.;. (2007). A robust satellite technique for monitoring seismically active areas: the case of Bhuj-Gujrat earthquake. *Tectonophysics, 431*, 197-210.

Genzano, N.; Aliano, C.; Corrado, R.; Filizzola, C.; Lisi, M.; Mazzeo, G.; Paciello, R.; Pergola, N.; Tramutoli, V.;. (2009). RST analysis of MSG-SEVIRI TIR radiances at the time of the Abruzzo 6 April 2009 earthquake. *Natural Hazards and Earth System Sciences, 9*, 2073-2084.

Gorny, V. I.; Salman, A. G.; Tronin, A. A.; Shillin, B. B. (1988). The Earth's outgoing IR radiation as an indicator of seismic activity. *Proceedings of Academy of Science,USSR*, *301*, pp. 67-69.

Hayakawa, M.; Molchanov, O. A.; Kodama, O. A.; Tanaka, T.; Igarashi, T. (2000). On a possibility to monitor seismic activity using satellites. *Advances in Space Research, 26*(6), 993-996.

Lisi, M.; Filizzola, C.; Genzano, N.; Grimaldi, C. S.L.; Lacava, T.; Marchese, F.; Mazzeo, G.; Pergola, N.; Tramutoli, V.;. (2010). A Study on the Abruzzo 6 April 2009 earthquake by applying the RST approach to 15 years of AVHRR TIR observations. *Natural Hazards and Earth System Sciences, 10*, 395-406.

Milne, J. (1913). *Earthquakes and Other Earth Movements* (6th Edition). London: Kegan Paul.

NASA. (2011). Land Processes Distributed Active Archive Center (LP-DAAC) MODIS Terra Data Pool. Available: ftp://e4ftl01.cr.usgs.gov/MOLT/MOD11A1.005/ Accessed on: Dec 10th, 2011.

Neteler, M. (2010). Estimating Daily Land Surface Temperatures in Mountainous Environments by Reconstructed MODIS LST Data. *Remote Sensing, 2*, 333-351.

Ouzounov, D.; Bryant, N.; Logan, T.; Pulinets, T.; Taylor, P.;. (2006). Satellite thermal IR phenomena associated with some of the major earthquakes in 1999-2003. *Physics and Chemistry of the Earth, 31*, 154-163.

Ouzounov, D.; Freund, F.;. (2004). Mid-infrared emission prior to strong earthquakes analyzed by remote sensing data. *Advances in Space Research, 33*, 268-273.

Özacar, A. A.; Zandt, G.; Gilbert, H.; Beck, S. L. (2010). Seismic images of crustal variations beneath the East Anatolian Plateau (Turkey) from receiver functions. *Geological Society, London. Special Publications*, *340*, pp. 485-496.

Panda, S. K.; Choudhury, S.; Saraf, S. K.; Das, J. D.;. (2007). MODIS land surface temperature data detects thermal anomaly preceeding 8 October 2005 Kashmir earthquake. *International Journal of Remote Sensing, 28*(20), 4587-4596.

Pergola, N.; Aliano, C.; Coviello, I.; Filizzola, C.; Genzano, N.; Lacava, T.; Lisi, M.; Mazzeo, G.; Tramutoli, V.;. (2010). Using RST approach and EOS-MODIS radiances for monitoring seismically active regions: a study on the 6 April 2009 Abruzzo earthquake. *Natural Hazards and Earth System Sciences, 10*, 239-249.

Pulinets, S. A. (2004). Ionospheric precursors of earthquakes: recent advances in theory and practical applications. *Terrestrial, Atmospheric and Oceanic Sciences, 15*(3), 413-435.

Pulinets, S. A. (2006). Space technologies for short-term earthquake warning. *Advances in Space Research, 37*, 643-652.

Pulinets, S. A.; Ouzounov, D.; Karelin, A. V.; Boyarchuk, K. A.; Pokhmelnykh, L. A.;. (2006). The physical nature of thermal anomalies observed before strong earthquakes. *Physics and Chemistry of the Earth, 31*, 143-153.

Qiang, Z.; Chang-gong, D.; Lingzhi, L.; Min, X.; Fengsha, G.; Tao, L.; Yong, Z.; Manhong, G.;. (1999). Satellite thermal infrared brightness temperature anomaly image - short-term and impending earthquake precursors. *Sci. China, 42*, 313-324.

Qiang, Z.; Kong, L. C.; Zheng, L. Z.; Guo, M. H.; Wang, G. P.; Zhao, Y.;. (1997). An experimental study on temperature increasing mechanism of satellite thermal-infrared. *Acta Seismologica Sinica, 10*(2), 247-252.

Qiang, Z.; Xiu-Deng, X.; Chang-Gong, D.;. (1991). Thermal Infrared anomaly-precursor of impending earthquakes. *Chinese Science Bulletin, 31*, 319-323.

Rawat, V.; Saraf, A. K.; Das, J.; Sharma, K.; Shujat, Y.;. (2011). Anomalous land surface temperature and outgoing long-wave radiation observations prior to earthquakes in India and Romania. *Natural Hazards, 59*, 33-46.

Salman, A.; Egan, W. G.; Tronin, A. A.;. (1992). Infrared remote sensing of seismic disturbances. *Proc. SPIE 1747*, (pp. 208-212).

Saraf, A. K.; Choudhury, S.;. (2005a). NOAA-AVHRR detects thermal anomaly associated with 26 January, 2001 Bhuj earthquake, Gujarat, India. *International Journal of Remote Sensing, 26*(6), 1065-1073.

Saraf, A. K.; Choudhury, S.;. (2005b). Satellite detects surface thermal anomalies associated with the Algerian earthquakes of May 2003. *International Journal of Remote Sensing, 26*(13), 2705-2713.

Saraf, A. K.; Choudhury, S.;. (2005c). SSM/I Applicaitons in studies of thermal anomalies associated with earthquakes. *International Journal of Geoinformatics, 2*(3), 197-207.

Saraf, A. K.; Choudhury, S.;. (2005d). Thermal Remote Sensing Technique in the Study of Pre-Earthquake Thermal Anomalies. *Journalof Indian Geophysics Union, 9*(3), 197-207.

Saraf, A. K.; Choudhury, S.; Panda, S. K.; Dasgupta, S.; Rawat, V.;. (2007). Does a Major Earthquake Precede a Thermol Anomaly. *International Journal of Geoinformatics, 3*(3).

Saraf, A. K.; Rawat, V.; Banerjee, P.; Choudhury, S.; Panda, S. K.; Dasgupta, S.; Das, J. D.;. (2008). Satellite detection of earthquake thermal infrared precursors in Iran. *Natural Hazards, 47*, 119-135.

Saraf, A. K.; Rawat, V.; Choudhury, S.; Dasgupta, S.; Das, J. (2009). Advances in understanding of the mechanism for generation of earthquake thermal precursors detected by satellites. *International Journaş of Applied Earth Observation and Geoinformation, 11*, 373-379.

Saraf, A. K.; Rawat, V.; Das, J.; Zia, M.; Sharma, K.;. (2011). Satellite detection of thermal precursors of Yamnotri, Ravar and Dalbandin earthquakes. *Natural Hazards*.

Snyder, W. C.; Wan, Z.;. (1998). BRDF models to predict spectral reflectance and emissivity in the thermal infrared. *IEEE Transactions on Gescience and Remote Sensing, 36*(1), 214-225.

Snyder, W. C.; Wan, Z.; Zhang, Y.; Feng, Y. -Z.;. (1998). Classsification-based emissivity for land surface temperature measuremen from space. *International Journal of Remote Sensing, 19*(14), 2753-2774.

Tan, O. (2004). *Kafkasya, Doğu Anadolu ve Kuzeybatı İran Depremlerinin Kaynak Mekanizması Özellikleri ve Yırtılma Süreçleri.* PhD Dissertation, İstanbul Teknik Üniversitesi/Fen Bilimleri Enstitüsü, Jeofizik Mühendisliği, İstanbul. [in Turkish]

Tramutoli, V.; Cuomo, V.; Filizzola, C.; Pergola, N.; Pietrapetrosa, C.;. (2005). Assessing the potential of thermal infrared satellite surveys for monitoring seismically active areas: the case of Kocaeli(Izmit) earthquake, August 17, 1999. *Remote Sensing of Environment, 96*, 409-426.

Tramutoli, V.; DiBello, G.; Pergola, N.; Piscitelli, S.;. (2001). Robust satellite techniques for remote sensing of seismically active areas. *Annals of Geofisica, 44*, 295-312.

Tronin, A. A. (1996). Satellite thermal survey-a new tool for the study of seismoactive regions. *International Journal of Remote Sensing, 17*, 1439-1455.

Tronin, A. A. (2000a). Thermal Satellite data for earthquake research. *IGARSS 2000, IEEE 2000 international geoscience symposium. Taking the pulse of the planet: the role of remote sensing in managing the environment.* Honolulu,HI.

Tronin, A. A. (2000b). Thermal IR satellite sensor data applicaiton for earthquake research in China. *International Journal of Remote Sensing, 21*(16), 3169-3177.

Tronin, A. A. (2006). Remote Sensing and earthquakes: A review. *Physics and Chemistry of the Earth, 31*, 138-142.

Tronin, A. A.; Hayakawa, M.; Molchanov, O. A.;. (2002). Thermal IR satellite data application for earthquake research in Japan and China. *Journal of Geodynamics, 33*, 519-534.

Wan, Z. (1999). *MODIS Land-Surface Temperature Algorithm Theoretical Basis Document (LST ATBD) Version 3.3.* University of California, ICESS, Santa Barbara.

Wan, Z. (2008). New refinements and validation of MODIS Land-Surface Temperature/Emissivity products. *Remote Seninsing of Environment, 112*, 59-74.

Wan, Z. (2009). *Collection-5 MODIS Land Surface Temperature Products Users' Guide.* University of California, ICESS, Santa Barbara.

Wan, Z., Zhang, Y., Zhang, Y. Q., Li, Z. L. (2004). Quality Assessment and validation of the global land surface temperature. *International Journal of Remote Sensing, 25*, 261-274.

Wan, Z.; Dozier, J.;. (1996). A generalized split-window algorithm for retrieving land-surface temperature from space. *IEEE transactions on Geoscience and Remote Sensing, 34*, 892-905.

Wan, Z.; Zhang, Y.; Zhang, Y. Q.; Li, Z. L.;. (2002). Validation of the land-surface temperature products retrieved from Moderate Resolution Imaging Spectroradiometer data. *Remote Sensing of Environment, 83*, 163-180.

Wu, G.; Zhu, F.; Zhong, Y.; Xia, H.;. (1982). Hai Cheng Earthquake in 1975. *Seismological Publishing House, 220*.

Wu, J. (1980). *Seismology and Geology, 2*, 65-78.

APPENDICES

A.1 Daytime results of LST differencing of pixels for non-earthquake year (2000)

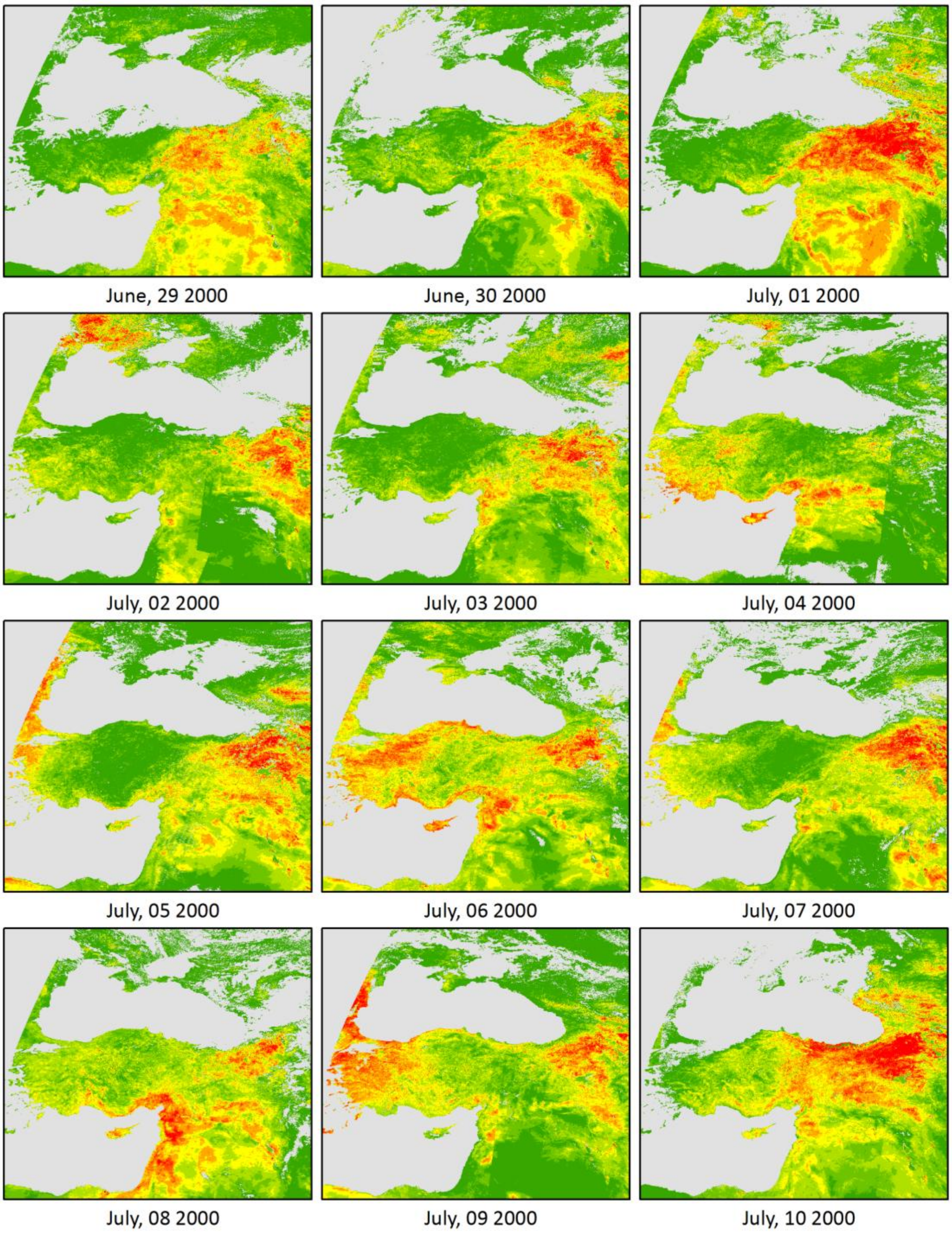

Figure A 1: Spatial distribution of daytime LST differences comparing 2000 with the historical mean based on pixel values [June 29 – July 10]

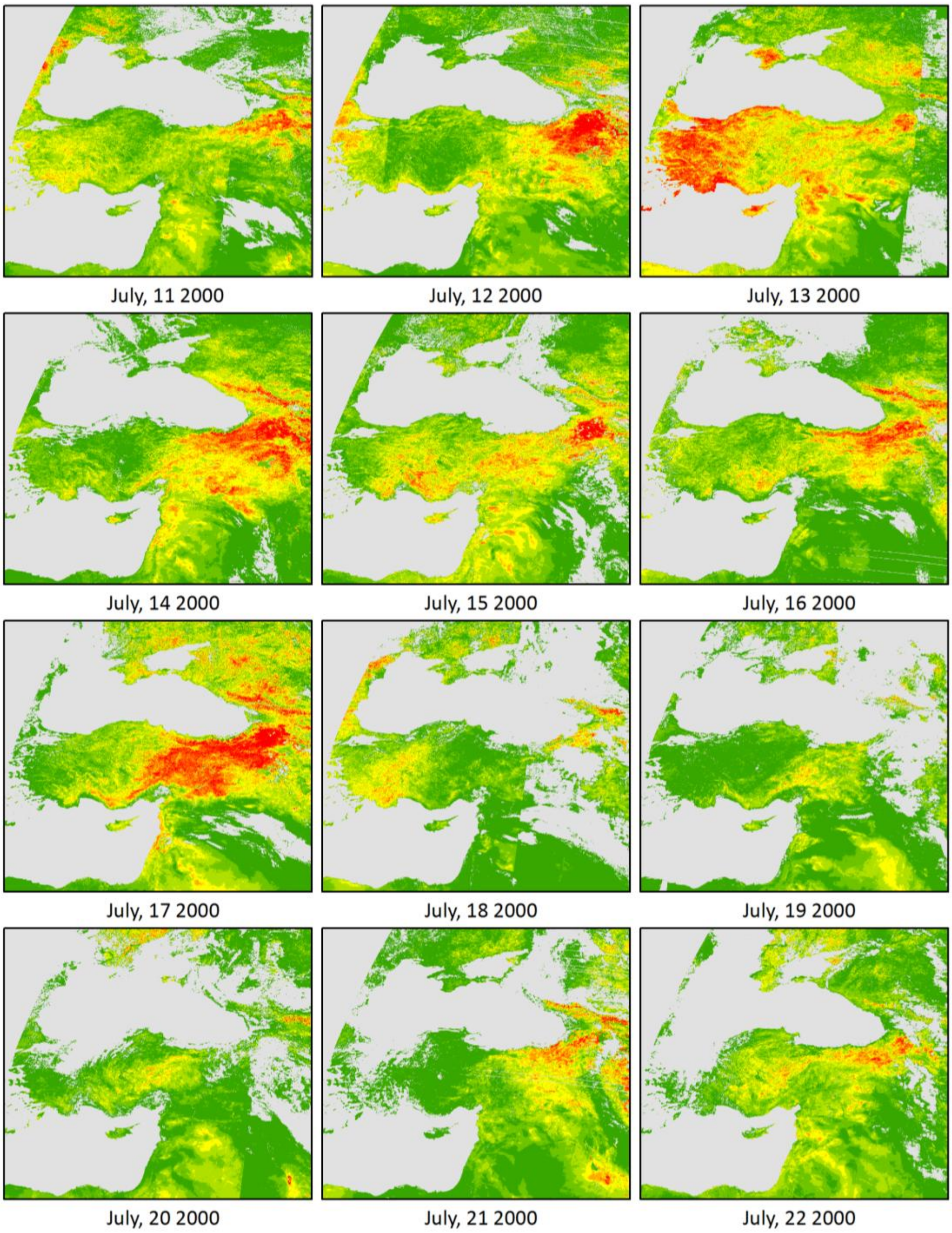

Figure A 2: Spatial distribution of daytime LST differences comparing 2000 with the historical mean based on pixel values [July 11 – July 22]

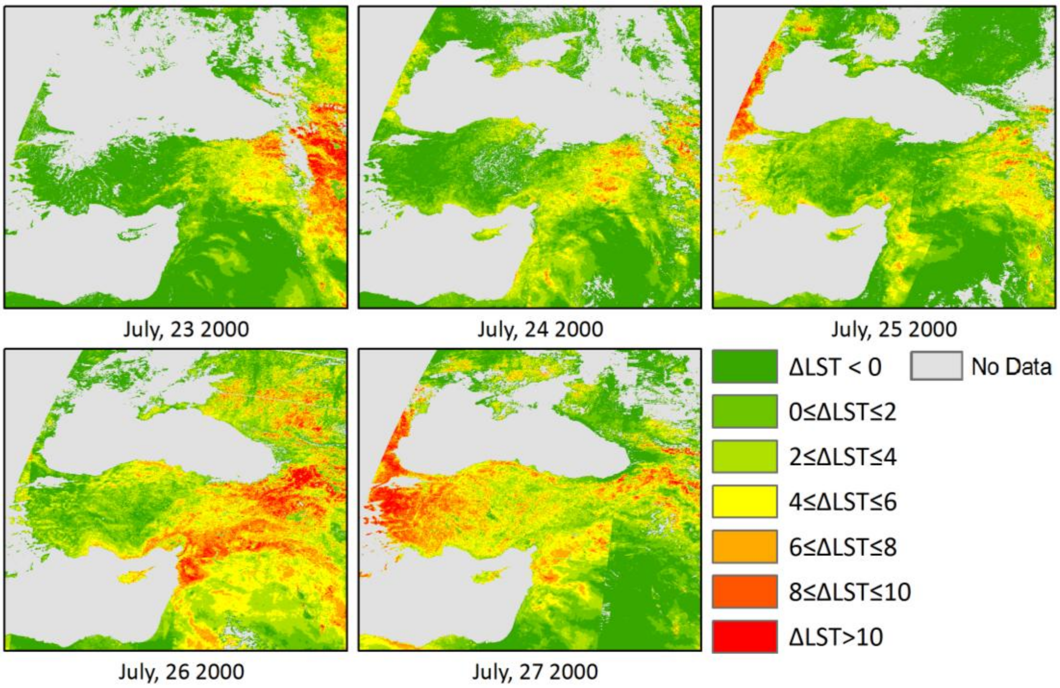

Figure A 3: Spatial distribution of daytime LST differences comparing 2000 with the historical mean based on pixel values [July 23 – July 27]

A.2 Nighttime results of LST differencing of pixels for non-earthquake year (2000)

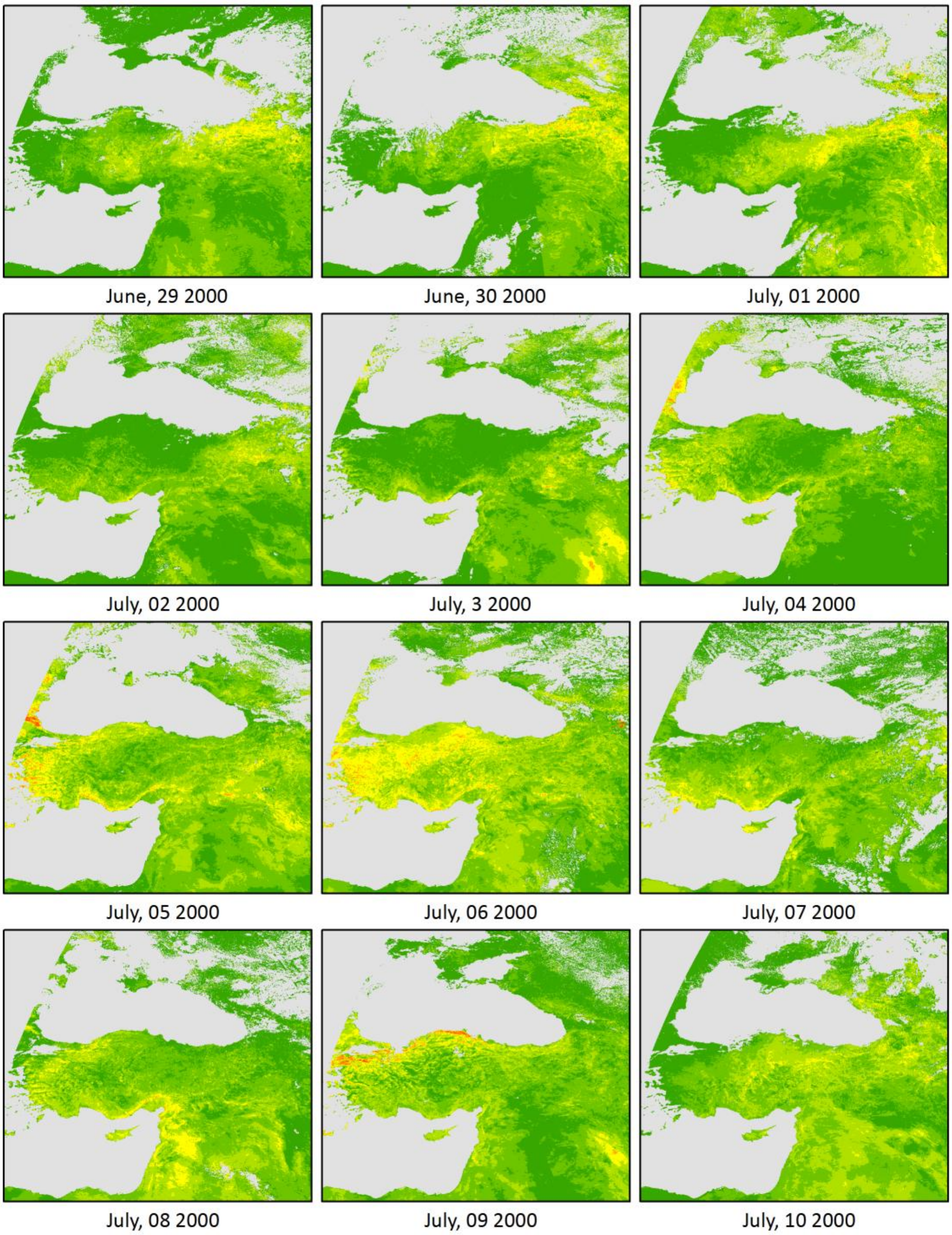

Figure A 4: Spatial distribution of nighttime LST differences comparing 2000 with the historical mean based on pixel values [June 29 – July 10]

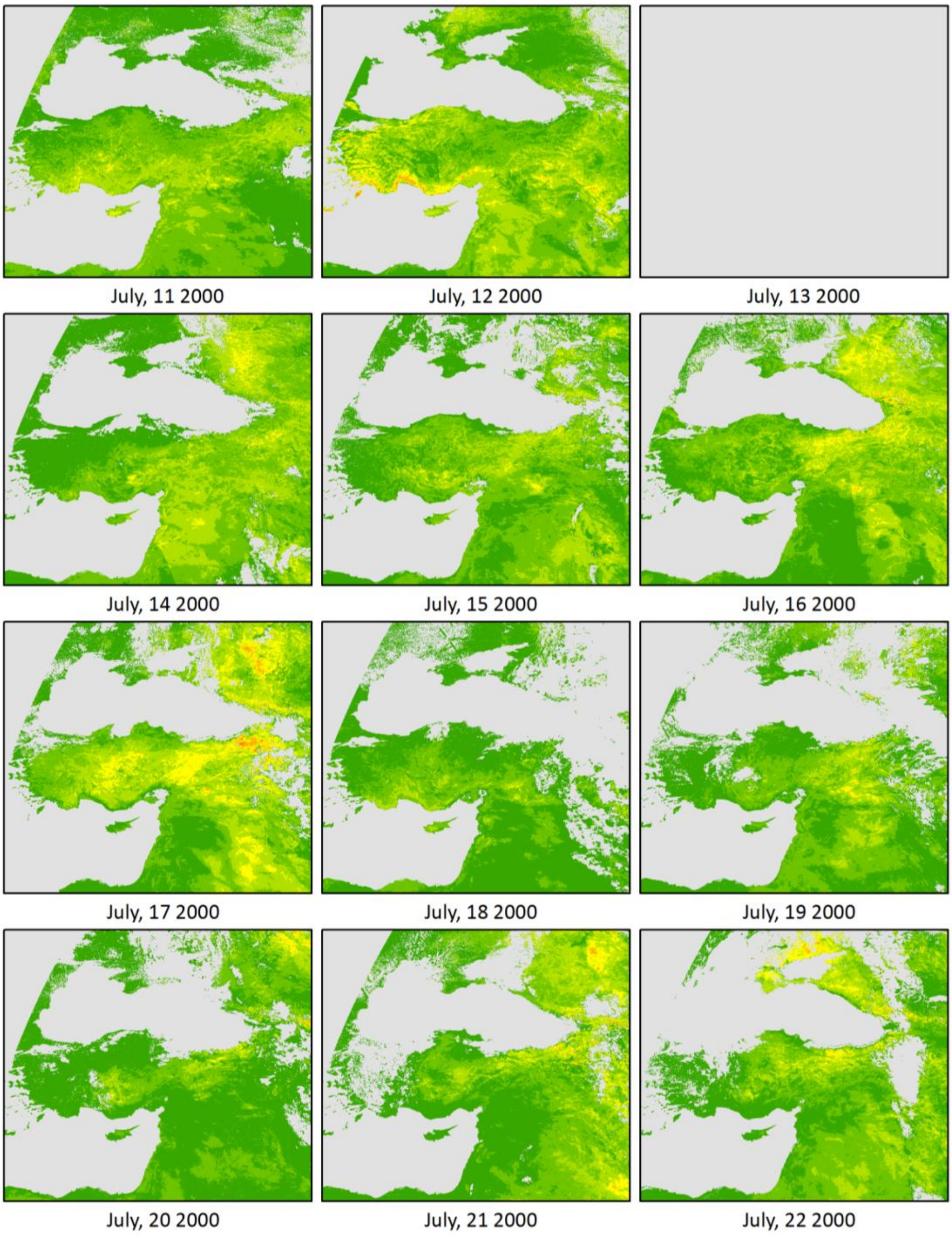

Figure A 5: Spatial distribution of nighttime LST differences comparing 2000 with the historical mean based on pixel values. [July 11 – July 22] *Note that on July 13, 2000 LST nighttime image is not available*

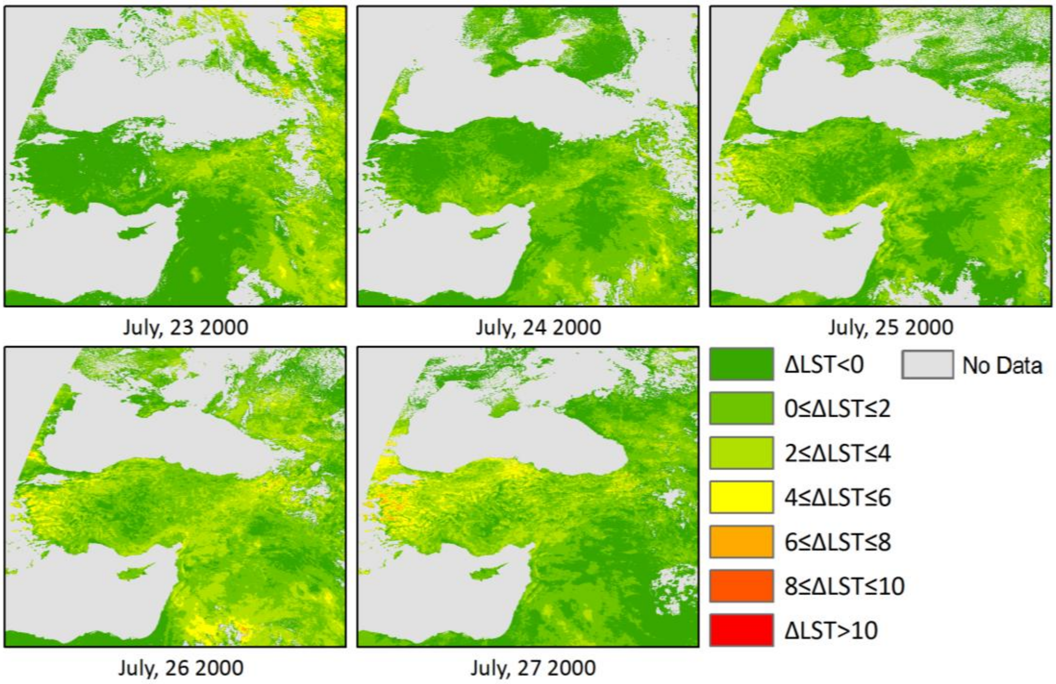

Figure A 6: Spatial distribution of nighttime LST differences comparing 2000 with the historical mean based on pixel values [July 23 – July 27]

A.3 Nighttime reference images for Robust Satellite Technique

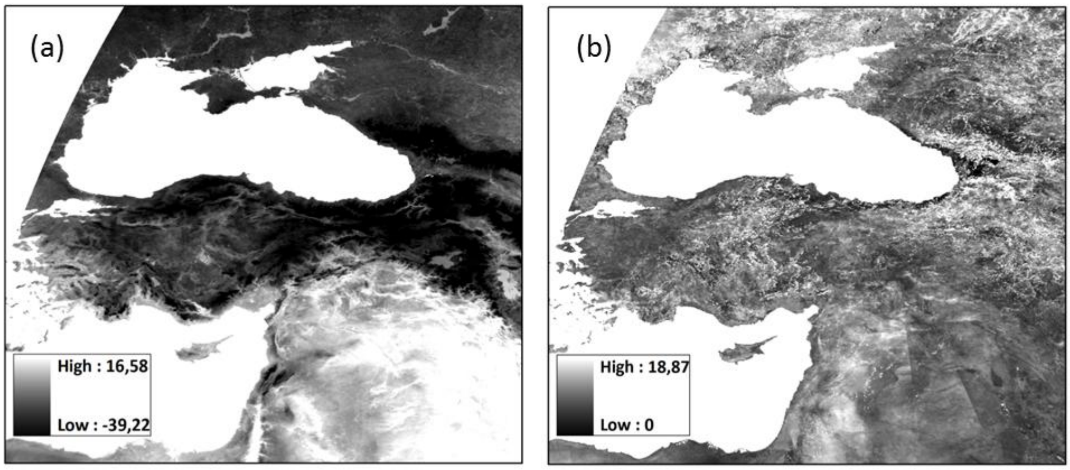

Figure A 7: Nighttime reference images (a) μΔLST(r) time average for month June and (b) σΔLST(r) standard deviation for month June computed over years (2000-2006)

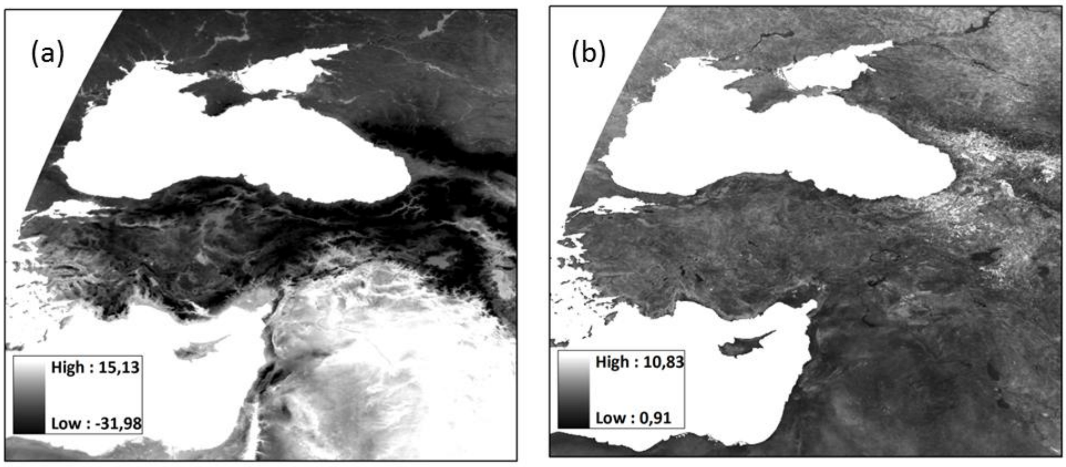

Figure A 8: Nighttime reference images (a) μΔLST(r) time average for month July and (b) σΔLST(r) standard deviation for month June computed over years (2000-2006)

A.4 Results of daytime RETIRA index computation for non-earthquake year (2000)

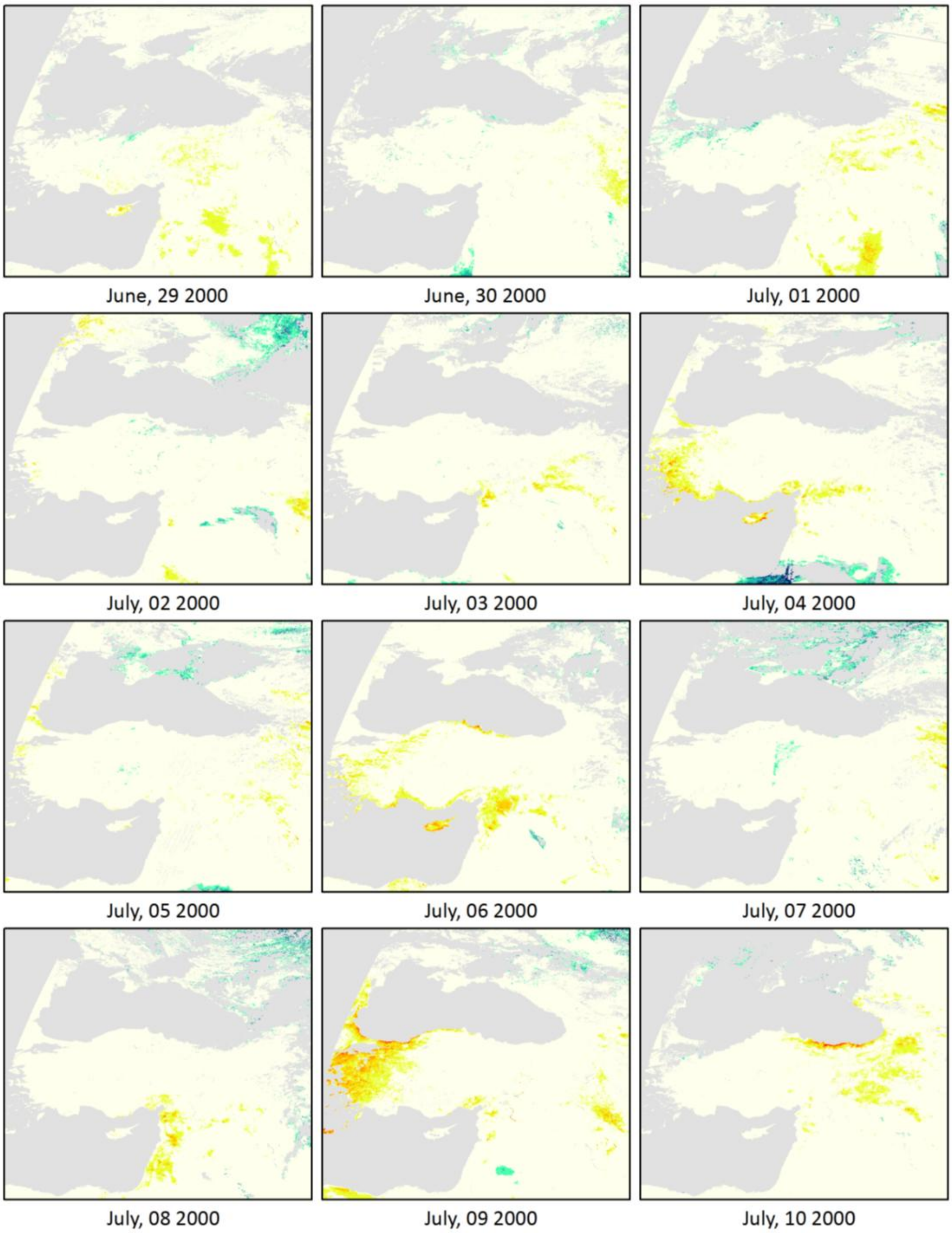

Figure A 9: Results of daytime RETIRA index computation for non-earthquake year (2000) [June 29 – July 10]

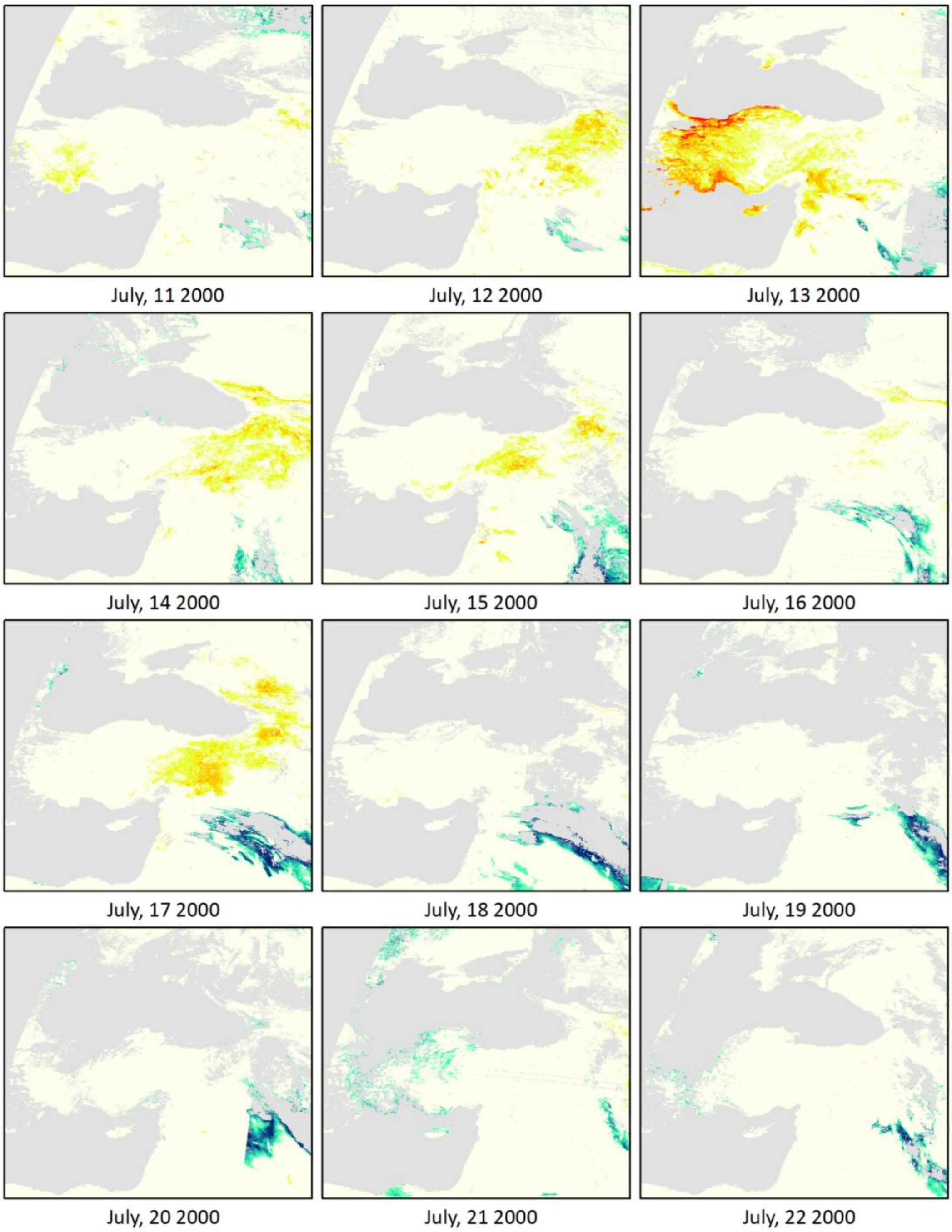

Figure A 10: Results of daytime RETIRA index computation for non-earthquake year (2000) [July 11 – July 22]

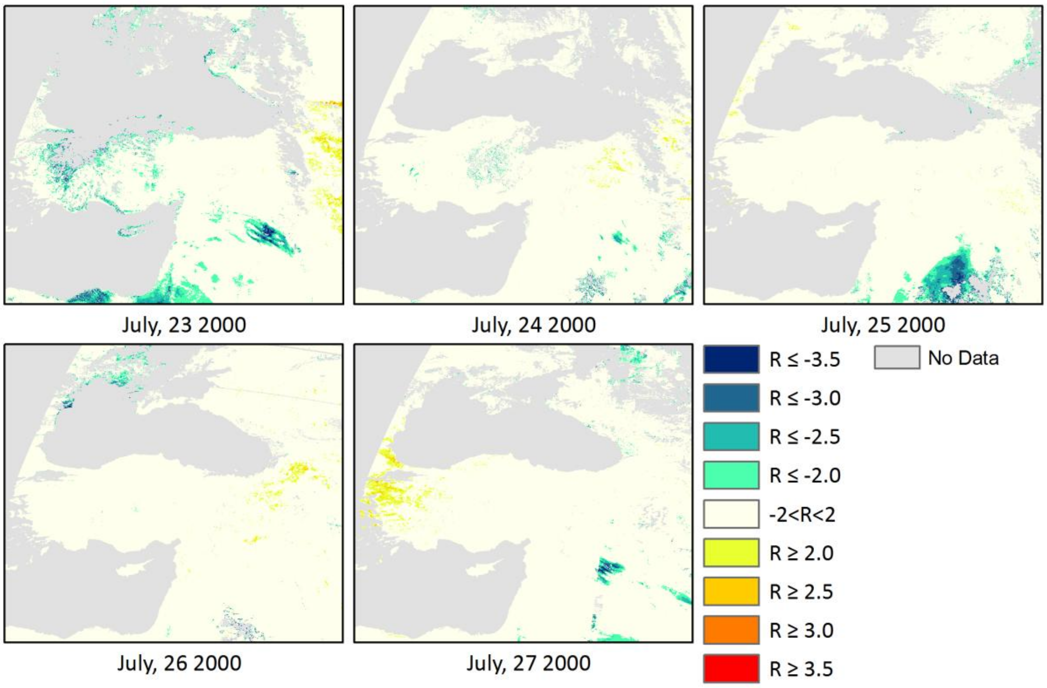

Figure A 11: Results of daytime RETIRA index computation for non-earthquake year (2000) [July 23 – July 27]

A.5 Results of nighttime RETIRA index computation for non-earthquake year (2000)

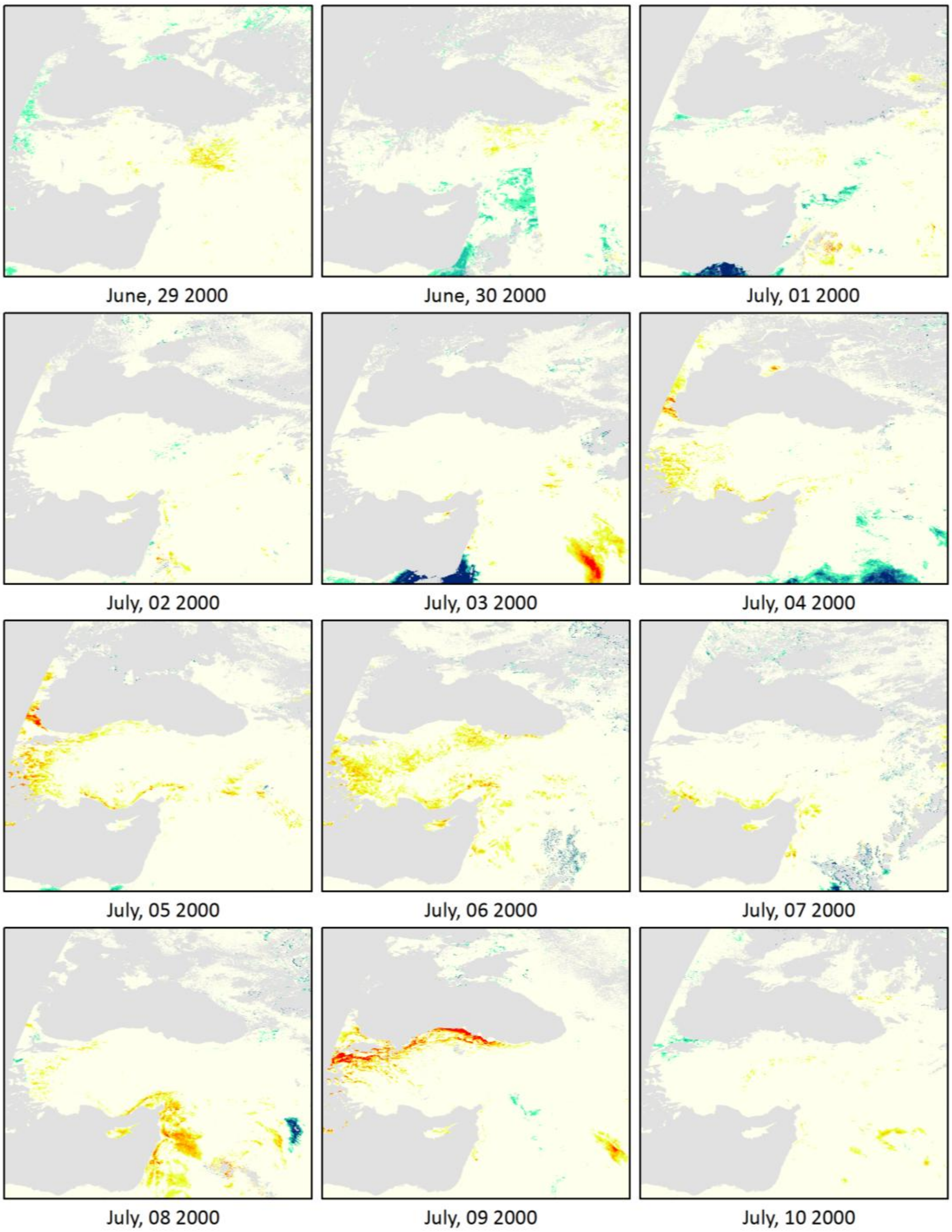

Figure A 12: Results of nighttime RETIRA index computation for non-earthquake year (2000) [June 29 – July 10]

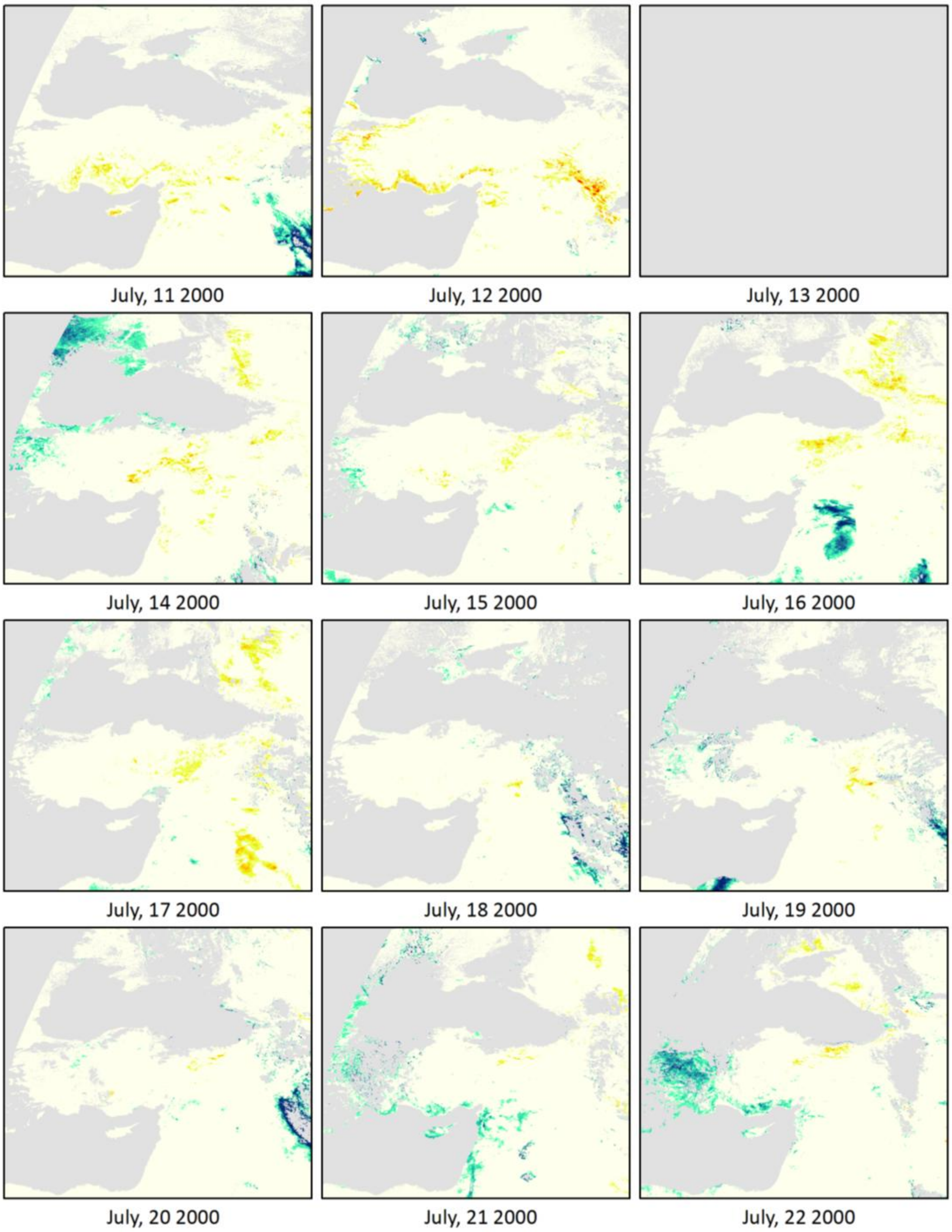

Figure A 13: Results of nighttime RETIRA index computation for non-earthquake year (2000) [July 11 – July 22]
Note that on July 13, 2000 LST nighttime image is not available

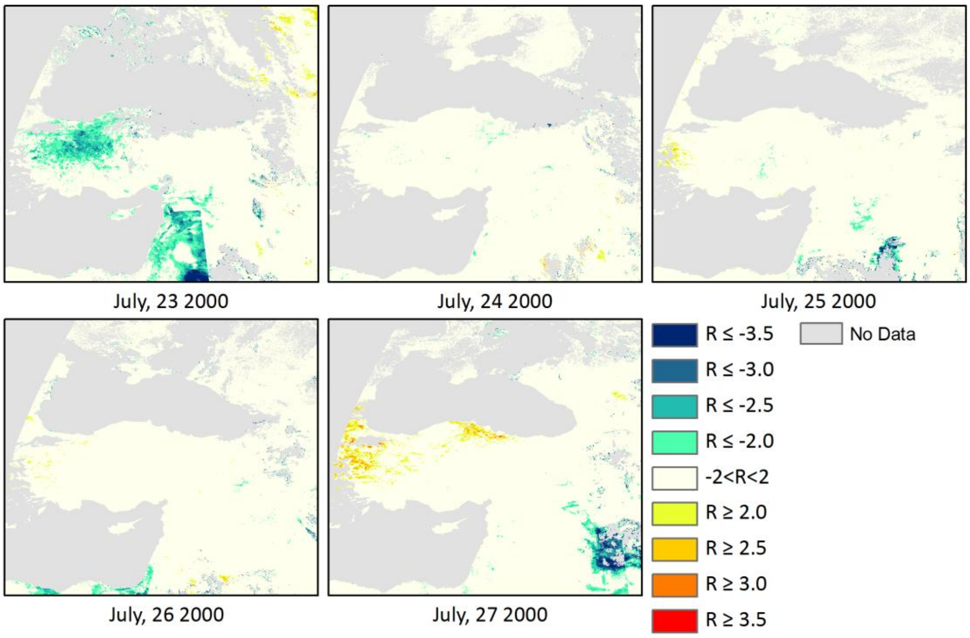

Figure A 14: Results of nighttime RETIRA index computation for non-earthquake year (2000) [July 23 – July 27]

A.6 Comparison of temporal means calculated including and excluding earthquake year.

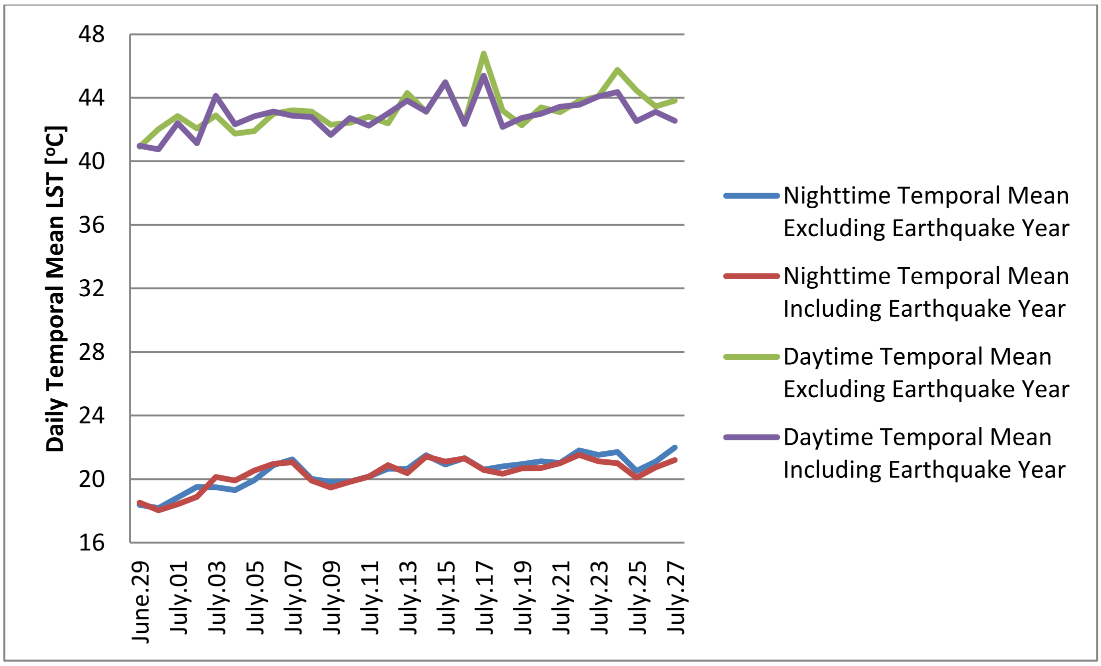

Figure A 15: Daytime and Nighttime temporal means calculated including and excluding earthquake years over the area r=400km around epicenter